Intelligent ISFET sensory system for water quality monitoring

Chen, Deyu

2009

Chen, D. (2009). Intelligent ISFET sensory system for water quality monitoring. Doctoral thesis, Nanyang Technological University, Singapore.

https://hdl.handle.net/10356/18689

https://doi.org/10.32657/10356/18689

NANYANG TECHNOLOGICAL UNIVERSITY

AN INTELLIGENT ISFET SENSORY SYSTEM FOR WATER QUALITY MONITORING

CHEN DEYU

SCHOOL OF ELECTRICAL AND ELECTRONIC ENGINEERING

2009

AN INTELLIGENT ISFET SENSORY SYSTEM FOR WATER QUALITY MONITORING

CHEN DEYU

School of Electrical and Electronic Engineering

A thesis submitted to the Nanyang Technological University
in fulfillment of the requirement for the degree of
Doctor of Philosophy

2009

ACKNOWLEDGMENTS

It is my pleasure to express my sincere gratitude and appreciation to my supervisor, Associate Professor Chan Pak Kwong. It was he who chose this promising topic for my Ph.D. research work, and he also provided me with good training and conductive research environment. His never ending flow of ideas, unerring intuition and infectious enthusiasm give me a very rewarding path. His concern and insight have helped me grow far beyond the boundaries of academic research. In particular, I want to thank Prof. Chan for much needed encouragement over the past years, and for his admirable integrity.

I also grateful acknowledge to Associate Professor Tse Man Siu for his guidance on device and process on this research work. I am also grateful to Fan Xian Ping, a PhD graduate of Prof. Chan. My progress would not have been so smooth if not for her unselfish assistance, the helpful discussions and valuable suggestions.

I would like to give special thanks to the technical staff in MFF Laboratory and CICS Laboratory, for the uncountable help they had given me during these years. They provided me great assistance when I have problems with the workstations and on the electronic workbench.

Finally, I would like to acknowledge my parents, my wife and my other family members, for being there whenever I need them and always putting their highest priority on my education. Their love, encouragement and support have played an important role in the successful completion of my education at NTU.

ABSTRACT

This thesis presents a new intelligent ISFET sensory system dedicated to a precision pH sensory function as well as long-term monitoring capability without being jeopardized by temperature and drift fluctuations in the water-quality monitoring environment. The research leads to the information of a new ISFET behavior-SPICE model for ISFET sensor simulation, a new non-saturation based ISFET interface circuit, a new saturation-based ISFET interface circuit, a novel ISFET nonlinear temperature compensation method, a novel ISFET drift and slow pH response compensation method, a new dynamic current mirror for use in temperature compensation and a microcontroller-based ISFET sensory system that realizes the proposed temperature and drift compensation technique for precision pH sensing in long-term monitoring at different temperatures. The ISFET interface circuit has been fabricated in TSMC CMOS 0.25 μm process technology. The Si_3N_4-gate ISFET sensor is based on the D+T Microelectrónica, A.I.E (CNM), Spain. The proposed intelligent ISFET sensory system, including the sensor, interface IC, microcontroller and support circuits, has been validated by the experiments at a single 3.3V supply. It exhibits a maximum accuracy error of 0.02 pH at 23^{o}C and 0.05 pH at 40^{o}C with dual compensation. The compensation results show a maximum time drift of 0.003 pH/hour (0.166 mV/hour) at 23^{o}C and an average temperature drift of 0.00049 pH/hour/^{o}C (0.0245 mV/hour/ ^{o}C) for a reference temperature increase from 23^{o}C to 40^{o}C, with the value of the pH solution ranging from 4 to 9 in six-hourly measurements. These measured results outperform those of the reported drift reduction techniques, suggesting that the ISFET sensory system using novel compensation is able to provide significant immunity against temperature change, time drift and temperature drift, which are favorable towards robust measurements in environmental monitoring applications.

TABLE OF CONTENTS

TABLE OF CONTENTS

TABLE OF CONTENTS

TABLE OF CONTENTS

TABLE OF CONTENTS

List of Figures

LIST OF FIGURES

LIST OF FIGURES

List of Tables

LIST OF TABLES

CHAPTER I

INTRODUCTION

1.1 Background

Regular monitoring of the pH value of a water resource and sewage discharge is a necessary task for an over-developed environment. Although pH does not necessarily indicate a particular kind of water pollution, it is closely related to the survival of aquatic life. The normal range of pH in surface water systems is 6.5 to 8.5 and of groundwater systems is 6 to 8.5. Water with a pH lower than 6.5 is acidic, soft or corrosive and contains elevated levels of toxic metals, thus posing a health risk. Although water with a pH higher than 8.5 or so-called hard water does not pose a health risk, it can cause aesthetic problems [1]. Therefore, the pH value is one of the most important indicators in environmental regulations for sewage water discharged from plant involved in the manufacturing process. At water treatment plants, water from rivers and lakes is disinfected with chlorine; impurities are settled out and filtered. Finally, they are removed with the aid of an agglutinating agent. During this process, the pH of the water is maintained at a value appropriate to the action of the chlorine and the agglutinating agent. Therefore, water should be neutralized through the addition of alkaline before it is supplied to homes, commercial and public facilities. Sewage-treatment plants do not only measure the pH at each processing steps, but also measure the pH adjustment of pH to optimize the bacterial activity in sludge when the activated-sludge method and treatment of

generating bubbles from the active agent is utilized. pH measurement is also widely used in the area of biomedical, food industry, and agricultural fields.

1.2 Motivations

Since the birth of the glass electrode in 1909 by Habert and Klemensiewicz [2] and the development of the first glass-electrode pH meter in Japan in 1950, the glass-electrode pH meter is now widely used in the measurement of pH. Recently, the Ion-Selective Field Effective Transistor (ISFETs) have recently emerged as important sensing devices for pH measurement in the areas of environmental monitoring applications, analytical chemistry and biomedical applications since their introduction in the pioneering work of P. Bergveld in 1970 [3]. The ISFET is, in fact, a MOSFET with the gate connection separated from the chip in the form of a reference electrode inserted in electrolyte which is in contact with the gate insulator material - the hydrogen sensitivity layer. With further advances in semiconductor technology [4]-[8], the ISFET sensors have appreciable advantages over traditional glass-electrode pH sensors on the basis of their small size, robustness (they are unbreakable), faster response time, simplicity of fabrication and low cost. This allows for the construction of a relatively cheap portable pH measurement instrument for regular monitoring of the water pH value of water in the field [9]-[13]. Advances in semiconductor technology have led to the emergence of ISFET sensors as the standard measurement tool. Despite the fact that development of the ISFET sensor has spanned over 30 years [14], however, some non-ideal effects of ISFET sensors have often been observed. Typical examples include time-invariant nonlinear temperature dependence on various pH values [15]-[23], time variant

fluctuation arising from the drift mechanism [24]-[32] and slow pH response [33]-[36]. All of these undesirable properties severely impede the accuracy of the ISFET sensor in long-term monitoring applications.

Over the last 30 years, research efforts have involved the development of the mechanism of hydrogen-sensitive properties of the sensing membrane exposed to the electrolyte [37]-[44]. Based on these pivotal studies, a sophisticated physical-chemical model has been developed and introduced into SPICE [45] version 2G (University of California, Berkeley, CA, USA), yielding a modified version called BIOSPICE for simulating ISFET and ISFET-based micro-systems [46]-[56]. Although it has the capability to fully characterize the behavior of the ISFET, its complexity as well as user-unfriendliness hinders its ability to be widely applied. The ISFET Macro-SPICE model [54], [56] compatible with HSPICE was developed later. However, its application remains limited due to the difficulty of extracting many electrochemical parametervs. Meanwhile, the two published ISFET modeling approaches are regarded as being highly complex and having a lack of flexibility for the Sensor System on Chip (SSOC) design. A new ISFET modeling is therefore required in order to alleviate the problems associated with the pre-existing ones. This is the primary focus of this research work. Followed by the modeling issue, many types of readout interface circuit for ISFET sensors have been reported for pH measurement [57]-[73]. Most of these published circuit configurations with ISFET device nonzero body bias would not only affect linearity through bulk modulation, but would also introduce an undesirable temperature-dependent effect. The ISFET sensors have also been integrated with the telemetry system

to be applied to the monitoring of water pollution [13], as illustrated in Fig. 1.1. Investigations on temperature compensation for ISFET have been addressed in recent efforts [58] - [60], [62]- [64], [73]-[79]. However, in most of their applications, the temperature characteristic of the ISFET device is stabilized at a particular pH or in a narrow pH range, which are not suitable for environmental applications with a broader range of both pH values and temperature values. For a broader range of pH values, the temperature coefficient ($T.C$) of the electrochemical component is also a function of pH value [15], [18]. More importantly, the ISFET temperature characteristic tends to exhibit nonlinear behavior. This increases the motivation to solve the tangible issues encountered by ISFET sensors for a broader pH range in conjunction with a wider temperature range. Simultaneously, other research efforts [80]-[84] have been conducted on drift compensation techniques. Unfortunately, of all the methods, they require a thermo-stable condition to avoid cross-coupling of the temperature effect on the ISFET. Therefore, the key research work of this thesis is to investigate and develop an intelligent ISFET measurement system with a dedicated hardware design incorporating software algorithms that not only provides a precision pH sensing function but also simultaneously performs smart compensation in terms of temperature and drift so as to allow for low-cost solutions for long-term environmental monitoring applications.

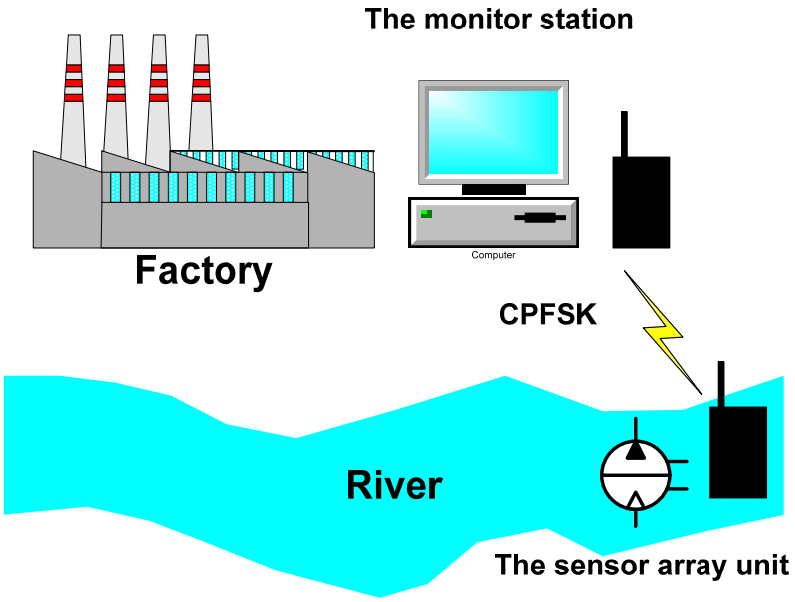

Fig. 1.1 Application of the water pH monitoring system using ISFET-based measurement system [13]

1.3 Major Contributions of this Thesis

This thesis performs the fundamental work required for the investigation of the behavior of the ISFET sensor, including its working mechanism, thermal property, time-dependent drift and slow pH response. Based on the previous pivotal studies, the study conducts a modeling as well as the characterization of the ISFET device followed by a study of different types of ISFET interface circuits and of different methodologies of ISFET temperature compensation as well as the drift compensation techniques. The achievements of this research can be summarized as follows:

(1) Propose a new ISFET Behavior-SPICE model for ISFET sensor simulation.

(2) Propose a new non-saturation based ISFET interface circuit.

(3) Propose a new saturation based ISFET interface circuit

(4) Propose a novel ISFET nonlinear temperature compensation method.

(5) Propose a novel ISFET drift and slow pH response compensation method.

(6) Propose an intelligent ISFET sensory system that realizes the proposed temperature and drift compensation technique for precision pH sensing in long-term monitoring at different temperatures.

1.4 Organization of the Thesis

This thesis is divided into eight chapters. Chapter I introduces the background of the thesis, including the motivations and applications. Chapter II presents the theory of operational mechanism of the ISFET. Chapter III reviews the prior-art ISFET models. This is then followed by a presentation of a new Behavior-SPICE ISFET model based on the hybrid-model approach that enhances the simplicity and ease of usage for sensor circuit simulations. Chapter IV focuses on the ISFET interface circuits, consisting of a review of the published circuits and a proposal for two new interface circuits. Chapter V reviews the current methods of ISFET temperature compensation and time-variant drift compensation. A novel ISFET nonlinear temperature compensation method and a novel ISFET drift and slow pH response compensation method are then proposed. Chapter VI presents the implementation of an intelligent ISFET sensory system which comprises system hardware architecture as well as the smart compensation software algorithm. Chapter VII discusses the simulation and measurement results of the proposed ISFET interface circuits together with a comparison of simulation results with prior-art interface circuits. The measurement results of the proposed temperature compensation and proposed sensory system using smart compensation for long-term pH monitoring are also

presented to prove the effectiveness of the proposed methods. This is then followed by the concluding remarks and future works in Chapter VIII.

CHAPTER II

ISFET SENSOR

2.1 Background

The *pH* measurement is used in a wide variety of applications: wastewater treatment, the food industry, agriculture and biomedical fields. *pH* is a measure of the acidity or alkalinity of a solution (also called a solute or electrolyte). It states the relative quantity of hydrogen ions (H^+) and hydroxide ions (OH^-) contained in a solution on a scale of 0 to 14, where the greater the concentration of H^+ ions, the more acidic the solution and the lower the *pH* value. In this relationship, pH is defined as the negative logarithm of hydrogen ion activity.

$$pH = -\log[H^+] \tag{2.1}$$

Since it is the hydrogen ion that is responsible for acidity and alkalinity, the abbreviation "*pH*" stands for the "potential of hydrogen". The neutral point of pH=7 actually indicates the presence of equal concentrations of free hydrogen and hydroxide ions. This study focuses on the measurement of hydrogen ions, H^+ of the electrolyte. Multiple ions sensing technique can be extended from the techniques and methods developed in this work.

2.2 Operation Mechanism of ISFET Sensor

2.2.1 Electrical Characteristics of the ISFET Device

The ISFET (Ion-Selective Field Effect Transistor), first introduced by Bergveld in 1970 [3] and developed to measure hydrogen ions and a variety of other ions,

is a solid-state device that combines the ion-sensitive properties of a sensing membrane with the field-effect characteristics of a MOSFET (Metal Oxide Silicon Field Effect Transistor), as shown in Fig. 2.1.

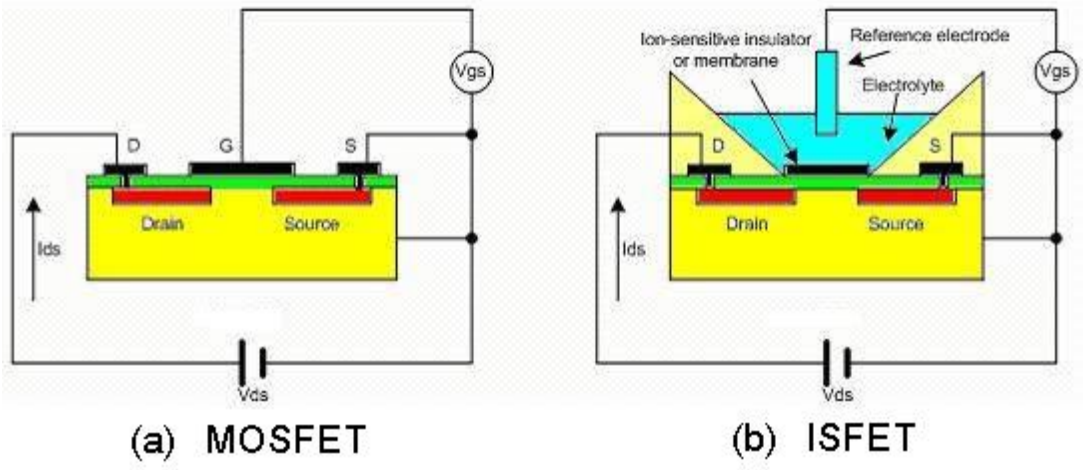

Fig. 2.1 Comparison of MOSFET and ISFET structure

The basic principle underlying the MOSFET [85]-[89] is the control of a current flowing between the drain and source terminals of the MOSFET by a voltage applied between the gate source (V_{GS}). The MOSFET gate is now commonly made of polycrystalline silicon (polysilicon, or poly for short) and formed on top of the gate insulator, a thin layer of silicon dioxide (SiO_2), typically growing on the silicon substrate material, insulating the gate from the substrate. However, in the case of the ISFET, the poly-gate is removed from the silicon surface and replaced by a reference electrode inserted in an electrolyte. The electrolyte is in direct contact directly with the ISFET gate insulator which is selectively sensitive to the H^+ concentration of the electrolyte. Most insulators have ion binding sites on their surface that thermodynamically

dissociate ions to or *accept ions* from the solution with respect to the ion concentration in the electrolyte. The kind of ion that interacts with insulator surfaces is normally a proton. If protons are dissociated from the insulator surface, the negative charges are left behind at the insulator and shift its potential in a negative direction relative to the solution. At the interface between the insulator and the solution, there is an electric potential difference that depends on the concentration of H^+ of the electrolyte. If the pH value of the electrolyte changes, which means its H^+ concentration changes, the potential of the gate changes, leading to a modulation of the drain current. Conversely, the drain current can be kept constant by changing the potential applied to the reference electrode to counteract the change in the drain current, which is commonly employed in practical ISFET interface circuit designs. In this way, the value of the gate-to-source voltage of the ISFET, V_{GS} is the usual measurement of an ISFET-based *pH* measurement system for the *pH* or *pH* change.

As the ISFET has a similar structure to the MOSFET as shown in Fig. 2.1, one can begin with the I_{DS}-V_{GS} transfer characteristic of the ISFET, which is derived from the electrochemical theory and semiconductor theory of the MOSFET, with an indication of key process model parameters and their definitions. Then, the time-invariant thermal characteristic of ISFET and the time-variant behaviors, including drift and slow pH response, are described to provide useful insights into as well as to understand their impact on the ISFET sensing device. The operation principle of ISFET has been studied in [38]-[44]. Like the

standard MOSFET [85]-[89], the I_{DS}-V_{GS} transfer characteristic for a long-channel ISFET operating in a non-saturation region can be expressed as

$$I_{DS} = \mu C_{OX} \frac{W}{L}\left[\left(V_{GS} - V_{th(ISFET)}\right)V_{DS} - \frac{1}{2}V_{DS}^2\right] \tag{2.2a}$$

In a saturation region, the drain-source current of the ISFET is

$$I_{DS} = \frac{1}{2}\mu C_{OX} \frac{W}{L}\left(V_{GS} - V_{th(ISFET)}\right)^2 \tag{2.2b}$$

where C_{ox} in MOSFET is the capacitance of oxide per unit area. Note that in an ISFET, it is the effective capacitance of oxide in series with a sensitivity layer of silicon nitride (Si_3N_4) in the ISFET device employed in this project. μC_{ox} is the process transconductance parameter and W/L is the device aspect ratio. V_{GS} is the gate-source voltage in ISFET when defining the metal connection of the reference electrode as a remote gate of ISFET in Fig. 2.1. It can be observed that the major difference between the MOSFET and ISFET is in their threshold voltage. The ISFET threshold voltage [14] combined with the MOS transistor counterpart which includes the body effect in a four-terminal device [89], can be unified as follows:

$$V_{th(ISFET)} = V_{th\_chem} + V_{th\_mos} \tag{2.3}$$

or

$$V_{th(ISFET)} = E_{\mathrm{Re}f} + \Delta\varphi^{lj} - \psi_{eo} + \chi^{sol} + \left[\frac{-\Phi_{Si}}{q} - \frac{Q_{OX} + Q_{SS} + Q_B}{C_{OX}} + 2\varphi_f + \gamma\left(\sqrt{2\varphi_f + V_{SB}} - \sqrt{2\varphi_f}\right)\right] \tag{2.4}$$

with $V_{th\_chem} = E_{\mathrm{Re}f} + \Delta\varphi^{lj} - \psi_{eo} + \chi^{sol}$ (2.5)

and

$$V_{th\_mos} = \frac{-\Phi_{Si}}{q} - \frac{Q_{OX} + Q_{SS} + Q_B}{C_{OX}} + 2\varphi_f + \gamma\left(\sqrt{2\varphi_f + V_{SB}} - \sqrt{2\varphi_f}\right) \quad (2.6)$$

where V_{th_chem} denotes the chemical portion of ISFET threshold voltage. E_{Ref} is the potential of the Ag/AgCl reference electrode and is defined as [15], [18]:

$$E_{\mathrm{Re}f} = E_{abs} + E_{rel} \quad (2.7)$$

Here, E_{abs} is the normalized hydrogen potential [15], [18], which is temperature independent. The value of this parameter has been found to be 4.7V [15]. E_{rel} is the potential of the Ag/AgCl reference electrode relative to a hydrogen electrode, which is temperature-dependent and has a typical value of 0.205V at room temperature [15]. $\Delta\varphi^{lj}$ is the potential drop between the reference electrode and the solution, which has a typical value of 3mV [15]. ψ_{eo} is a chemical input parameter that is a function of the solution *pH*, whereas χ^{sol}, having a typical value of 50mV [15], is the surface dipole potential of the solvent that is independent from the pH. The combined $-\psi_{eo} + \chi^{sol}$ item is now defined as V_{chem} to represent the potential between the electrolyte and the insulator. Regarding the ISFET-based MOS threshold voltage V_{th_mos}, the terms in (2.6) are similar to that of the standard MOSFET threshold voltage, except for the absence of the gate metal work function. It does not actually disappear, but is "burried" by the definition of E_{abs} in the term of E_{Ref} as defined in (2.7) [14].

In (2.6), Φ_{Si} is the work function of the silicon; Q_{OX} is the accumulated charge in the oxide; Q_{SS} is the accumulated charge in the oxide-silicon interface; Q_B is the depletion charge in the silicon; φ_f is the Fermi potential. The first three terms represent the threshold voltage at zero body-to-source bias while the

fourth term denotes the presence of the body effect with the condition that $V_{SB} \neq 0$. It should also be mentioned that the n-type ISFET is mostly used for its low-drift and high mobility properties [76]. Hence, in the application of an integrated micro-system where the ISFET sensor and interface circuit are fabricated in the same die, the source-to-bulk potential of ISFET plays a crucial role in circuit performance when referencing the apparent body effect item in (2.4).

2.2.2 Mechanism of ISFET H^+ Sensitivity described by the Site-binding and Gouy-Chapman- Stern Model

Based on the above analysis on the operation of the ISFET, it is obvious that almost all the efforts to explain the operational mechanism of ISFET have been devoted to the elucidation of the chemical input parameter, ψ_{eo}, which is the only parameter that is a function of the solution *pH* value. The general explanations of the electrolyte-insulator interface model are based on the theory of the site-binding model and the Gouy-Chapman-Stem model [37], [39], [42].

The site-binding model describes the charging mechanism of an oxide as the equilibrium between the surface sites and the H^+ ions in the bulk of the solution. It assumes that the surface of the insulator has ionizable sites that directly interact with the electrolyte to either release or bind hydrogen ions. It has been pointed out that the surface of the silicon nitride (Si_3N_4) insulator contained both amphoteric and basic sites [40], [47]. The amphoteric sites are of the *SiOH* group resulting from the oxidation of the surface of the silicon nitride and the basic sites are the primary amine sites that remain on the silicon

nitride surface after oxidation [40]. A set of equations has been well-derived in [47] to fully characterize the Electrolyte-Insulator-Semiconductor (EIS) structure with two kinds of binding sites for Si_3N_4:

$$SiOH_2^+ \xleftrightarrow{K_a} SiOH + H_S^+ \qquad K_a = \frac{[SiOH][H_S^+]}{[SiOH_2^+]} = \frac{\theta_0}{\theta_+}[H_S^+] \tag{2.8}$$

$$SiOH \xleftrightarrow{K_b} SiO^- + H_S^+ \qquad K_b = \frac{[SiO^-][H_S^+]}{[SiOH]} = \frac{\theta_-}{\theta_+}[H_S^+] \tag{2.9}$$

$$SiNH_3^+ \xleftrightarrow{K_{N+}} H_S^+ + SiNH_2 \qquad K_{N+} = \frac{[SiNH_2][H_S^+]}{SiNH_3^+} = \frac{\theta_{N0}}{\theta_{N+}}[H_S^+] \tag{2.10}$$

Here, H_S^+ is the concentration of the protons on the surface of insulator whose relation to the bulk concentration of H_B^+ in the solution is given by the Boltzmann equation:

$$H_S^+ = H_B^+ \exp\left(-\frac{q\psi_{eo}}{kT}\right) \tag{2.11}$$

where $[SiOH_2^+]$, $[SiOH]$, $[SiO^-]$, $[SiNH_2]$and $[SiNH_3^+]$ are the number of sites per unit area, while K_a, K_b, K_{N+} are the dissociation constants for the chemical reactions at the insulator interface. θ_0, θ_-, θ_+, θ_{N0}, θ_{N+} are yielded by the normalization condition [47]:

$$\theta_+ + \theta_- + \theta_0 = \frac{N_{sil}}{N_S} \tag{2.12}$$

$$\theta_{N+} + \theta_{N0} = \frac{N_{nit}}{N_S} \tag{2.13}$$

$$\theta_0 + \theta_+ + \theta_- + \theta_{N+} + \theta_{N0} = 1 \tag{2.14}$$

where N_{sil}, N_{nit}, N_S are the numbers of silanol sites, primary amine sites and the total number of available binding sites per unit area, respectively. The charge density of the surface sites σ_0 on the insulator is given by [47]:

$$\theta_+ + \theta_{N+} - \theta_- = \frac{\sigma_0}{qN_S} \tag{2.15}$$

Combining the above equations gives:

$$\frac{\sigma_0}{qN_S} = \left(\frac{[H^+]_S^2 - K_a K_b}{[H^+]_S^2 + K_a [H^+]_S + K_a K_b} \right) \frac{N_{sil}}{N_S} + \left(\frac{[H^+]_S}{[H^+]_s + K_{N+}} \right) \frac{N_{nit}}{N_S} \tag{2.16}$$

The relationship between the *pH* value and potential of the electrolyte-insulator interface can be built by combining the above equations based on the site-binding model. The following equations derived from the Gouy-Chapman-Stern theory describe the insulator surface potential as a function of the charge density σ_d in the diffuse layer and the ion concentration C_0 in the solution [47].

$$\psi_{eo} = -\frac{2kT}{q} \sinh^{-1}\left[\frac{\sigma_d}{8\varepsilon_w kTC_0} \right] - \frac{\sigma_d}{C_h} \tag{2.17}$$

where ε_w is the permittivity of the solution and C_h is the capacitance of the Helmholtz layer.

2.2.3 A Simple Theory of the ISFET pH Sensitivity

Instead of expressing the insulator-electrolyte potential, ψ_{eo}, as a complicated equation in (2.17), Hal and Eijkel [41] created a simple theory of the pH sensitivity of the ISFET, which is the change of ψ_{eo}, on a change of the bulk pH, with the intrinsic buffer capacity β_{int} and the differential capacitance C_{dif} as key parameters. This theory is derived using the site-binding model, but is

valid for all theories that describe the charging of an insulator-electrolyte interface as a result of interactions taking place on specific sites at the surface [41].

$$\frac{\partial \psi_{eo}}{\partial pH} = -2.303 \frac{kT}{q} \alpha \tag{2.18}$$

$$\text{with } \alpha = \frac{1}{\left(2.303 kTC_{dif} / q^2 \beta_{\text{int}}\right) + 1} \tag{2.19}$$

where α is a dimensionless sensitivity parameter with a value varying between 0 and 1 depending on β_{int} and C_{dif}. β_{int} symbolizes the surface buffer capacity, e.g. the ability of the oxide surface to deliver or take up protons, while C_{dif} is the differential double-layer capacitance, whose value is mainly determined by the ion concentration of the bulk solution. Equation (2.19) shows that only in the case where α approaches 1, the maximum Nernstian sensitivity of approximately 58.2mV/pH (when T=20°C) can be obtained. For oxides that have a value α<1, a *sub-Nernstian* response can be expected. It was shown in the expression of α in (2.19) that α=1 could be reached for oxides with a large value of the surface buffer capacity β_{int} and a low value of the double-layer capacity C_{dif}. This theory can explain why ISFET sensors with different sensitive material have different pH sensitivities.

2.3 Nonidealities of Sensor

Although the ISFET sensor was invented more than 30 years ago, it is still common to observe many nonideal effects in ISFET sensors. Typical examples include time-invariant nonlinear temperature dependence, time-variant fluctuation arising from the drift mechanism and a slow pH response. All of

these undesirable properties would severely impede the accuracy of the ISFET sensor in long-term continuous monitoring applications. With reference to the earlier pivotal studies [35] as well as taking into account of the ISFET temperature dependence, the ISFET output signal variation,ΔV can be generalized in the following form:

$$\Delta V = \frac{\partial V}{\partial pH}\Delta pH\left[1-\sum_{i=1}^{n}\varepsilon_i \exp\left(-\frac{t}{\tau_i}\right)\right]+\frac{\partial V}{\partial t}dt+\frac{\partial V}{\partial T}dT \qquad (2.20)$$

where $\partial V/\partial pH$ is the pH sensitivity of the ISFET, which has already been described in (2.18). ΔpH is the amplitude of the pH-step signal introduced. ε_i and τ_i are the normalized amplitude and time constant of the corresponding exponential term i. From (2.20), it can be seen that the time-variant variables come from (i) the bracket term that represents the slow pH response of the ISFET sensor and (ii) the drift term $(\partial V/\partial t)\times dt$ that represents the change in output over time. The time-invariant term $(\partial V/\partial T)\times dT$ denotes the change in output with a change in temperature. Therefore, it is necessary to understand the nonideal behavior of the ISFET sensor from the previous works.

2.3.1 ISFET Temperature Characteristic

Several investigations [15]-[23] have demonstrated that the ISFET exhibits thermal instability. The temperature characteristic of the ISFET is a complex function pertaining to the reference electrode, electrolyte-insulator potential and MOS transistor. It can be expressed as:

$$T.C_{total} = T.C.R. + T.C.F. + T.C.I. \qquad (2.21)$$

where $T.C_{total}$ is the total temperature coefficient of ISFET. *T.C.R.* is the temperature coefficient of the Ag/AgCl reference electrode with a filling of 3.5M KCL, saturated with AgCl. For any given temperature value, T_1, the E_{ref} defined in (2.7) can be extended as [18]:

$$E_{\mathrm{Re}f}(T_1) = E_{abs} + E_{\mathrm{Re}f}(T_0) + \left(\frac{dE_{\mathrm{Re}l}}{dT}\right)(T_1 - T_0) \tag{2.22}$$

where T_0 is the room temperature. It has been investigated by [15] that E_{abs} is temperature independent. Thus, the *T.C.R* is equal to $\frac{dE_{\mathrm{Re}l}}{dT}$, which has been reported by [15], [18] with a typical value of 0.14mV/°C. *T.C.F.* is the temperature coefficient of the MOS structure of the ISFET. Owing to the ISFET is a chemical sensor based on the MOSFET technology, and the temperature characteristics of *T.C.F* are similar to that of the conventional MOSFET. Based on the device physics [85], [89], two parameters are mainly responsible for the temperature characteristics of MOS transistor: one is the mobility while the other is the threshold voltage. For any given temperature, T_1, they are modeled as follows:

$$\mu(T)|_{T=T1} = \mu(T_0)\left(\frac{T_1}{T_0}\right)^m \tag{2.23}$$

$$V_T(T)|_{T=T1} = V_T(T_0) + K_{VT}(T_1 - T_0) \tag{2.24}$$

where T_0 is the absolute reference temperature (note that the absolute room temperature is taken as a reference) and m is a constant, with typical values between -1.9 and -2.2 [90], depending on the doping concentrations of silicon. K_{VT} is the temperature coefficient of the threshold voltage, usually between -0.5mV/°C and -3.0mV/°C [90].

The third term in (2.21), *T.C.I.*, is the temperature coefficient of the electrolyte-insulator interface potential. This phenomenon can be explained with reference to the equations of mechanism of the ISFET H^+ sensitivity described in Section 2.2, where the parameters such as the dissociation constants, K_a, K_b, K_{N+}, and the electrolyte surface dipole potential, χ^{sol} are all temperature dependent [15], [18]. It can also be observed from (2.18) and (2.19) that the potential of the electrolyte and sensitive insulator is not only pH dependent but also temperature dependent. *T.C.I.* has also been found to be a function of pH value [15]-[18], [20], [21], [23]. It has been indicated in (2.18) that the slope of $d\psi_{eo}/dT$ is negative. The higher the pH value, the larger is the temperature coefficient[18], [20]. It may vary from 0.64mV/°C to 1.1mV/°C as the pH increases from 4 to 10 [18]. Obviously, all the factors described above will eventually make the ISFET temperature compensation in a measurement of the pH range more complicated.

2.3.2 The ISFET Time-variant Characteristic

Apart from time-invariant thermal instability, the ISFET also suffers from time-variant effects, which include drift and slow pH response. Several investigations [24]-[36] have been carried out to characterize and model the behaviors of these two effects, providing useful insight into their mechanisms. The drift in Si_3N_4-gate ISFET is characterized by a relatively slow, monotonic temporal change in the threshold voltage, which occurs over a period of several hours and is postulated to be associated with relatively slow conversion of the silicon nitride surface to a hydrated SiO_2 or oxynitride layer [26]. This

hydration will cause the variation of effective insulator capacitance due to different dielectric constants of the hydrated layer and nitride layer, which would lead to a decrease in the overall insulator capacitance over time. As a result, the threshold voltage of ISFET would monotonically increase over time. According to Jamasb's physical model [24]-[26] on the drift characteristics, with reference to (2.4), the drift of the ISFET threshold voltage can be expressed as

$$\Delta V_{th(ISFET\_Drift)}(t) = -(Q_{OX} + Q_{SS} + Q_B) \times \left(\frac{\varepsilon_n - \varepsilon_{HL}}{\varepsilon_n \varepsilon_{HL}} \right) x_{HL}(t) \qquad (2.25)$$

where ε_n and ε_{HL} are the dielectric constants of nitride and the hydrated layer. x_{HL} is the thickness of the hydrated layer. It can be observed from (2.25) that the drift is directly proportional to the thickness of the hydrated layer. Nevertheless, the value of the drift is independent from the ISFET biasing condition [26].

Besides the ISFET drift, the ISFET slow pH response, which is about 3%-7% of the total pH response [35], is another time-variant parameter. It is postulated that this slow response behavior can be interpreted in terms of a surface model [30], [33], in which a portion of the surface sites located under the surface reacts very slowly to the diffusion of ions in the insulator to the site. It can be very slow, even across small distances. The behavior of this slow response effect has been modeled in the first bracket term of equation (2.20). Contrary to the drift effect, the amplitude of the ISFET slow pH response as well as its polarity is also determined by the amplitude and polarity of the input pH-step signal, ΔpH [82]. Although these two time-variant nonidealities of ISFET are triggered by different mechanisms, the variation on the ISFET output caused by

these two effects overlaps in the time domain. For instance, if there is a negative step in the input pH signal, the variation on the ISFET output contributed by the slow pH response is negative, which counteracts with that contributed by the drift effect. Using the ISFET readout circuits as described in the next section, the output signal that is essentially equivalent to the gate-to-source voltage, V_{GS} of the ISFET, would be the appropriate signal to demonstrate the drift and slow pH response of the ISFET. As illustrated in Fig. 2.2, the V_{GS} of ISFET in pH7 solution without any pH step applied is monitored to be increasing in a temporal monotonic manner, whereas the V_{GS} of the ISFET could decrease when a negative pH step is applied as shown in Fig. 2.3.

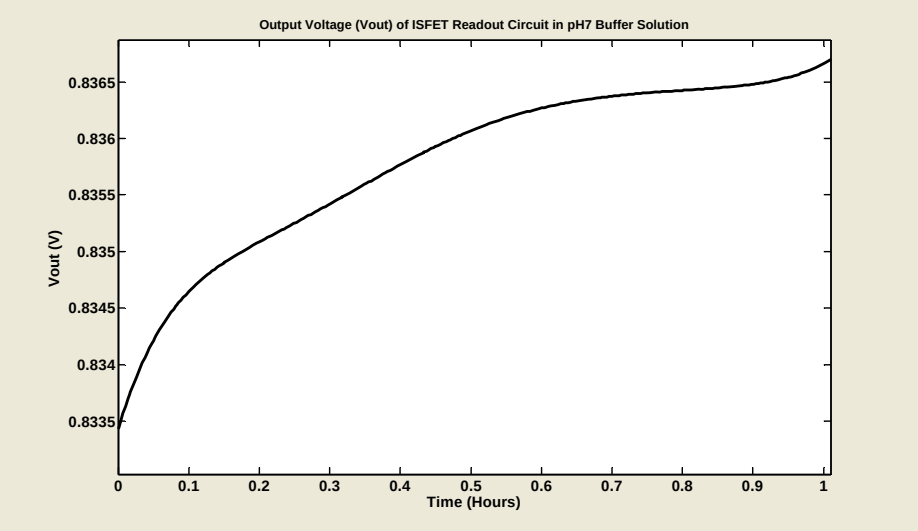

Fig. 2.2 Exemplary Drift Output (Without Initial Drift) Based on Monitoring of V_{GS} of ISFET in pH7 solution

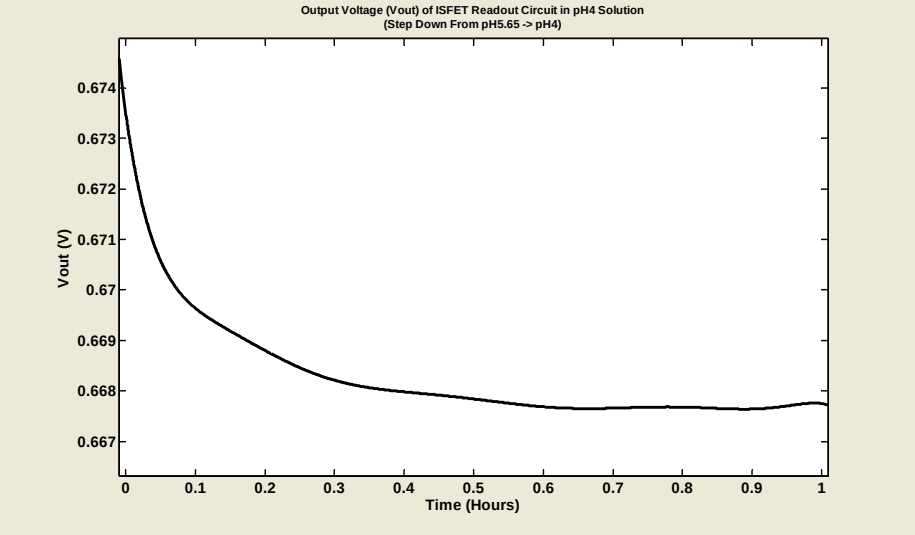

Fig. 2.3 Exemplary Output (Without Initial Drift) Based on Monitoring of V_{GS} of ISFET when pH solution steps from pH5.65 to pH4

As a final remark on the comprehensive observation of the practical characteristics of the ISEFET sensor, the use of intelligent electronic means to compensate for the nonideal effects of the sensor is another promising way of enhancing the performance of the standard ISFET sensor in a sensory system design apart from sensor technology improvement. In order to achieve the ultimate objectives, the presentation in this thesis follows the research task sequence of modeling for sensor circuit simulation, interface circuits, compensation techniques and the application of the smart compensation technique in conjunction with a circuit, system and software algorithm for intelligent sensory system design.

CHAPTER III

ISFET SENSOR MODELING

3.1 An Overview of ISFET Models

Computer-aided design in the form of simulation programs, such as SPICE [45] originally developed designing and simulating electronic circuits, can be adapted to simulate the field-effect-based ISFET in association with its interface circuit. Therefore, the approach to developing computer models of the ISFET device based on the SPICE electronic circuit analysis program is necessary for designing the ISFET-based interface circuit. A generalized physical model that includes two kinds of binding sites described in Chapter II has been proposed for ISFET devices [48]. The physical model composed by complicated equations is built into a modified version of the electronic circuit simulation program SPICE, called BIOSPICE [51]. This Built-in model is later evolved through a hybrid-modeling approach and called the ISFET Macro-SPICE model [54] [56] in HSPICE: it involves some simplification without a loss in accuracy. Ease of usage and simplification can be further improved by the introduction of a new ISFET Behavior-SPICE model in this study. It comprises a simplified behavior model that describes the ISFET pH sensitivity in a chemical portion on the basis of Hal and Eijkel's theory [41] using the highly-flexible mixed-signal Verilog-A language [91] and a simplified SPICE LEVEL 3 [88] model for the MOS device portion of the ISFET.

3.2 The ISFET Built-in Model

The built-in model is a sophisticated physical-chemical model that fully characterizes the ISFET behavior. The Sergio Martinoia research group introduced models of ISFET to the SPICE version 2G (University of California, Berkeley, CA, USA) as physical-chemical built-in models [47]-[53]. This approach yields a modified version of the original SPICE-2G, called BIOSPICE, where 14 static parameters [47]-[51] that can be specified by a user of the BIOSPICE in the *.MODEL* statement to characterize the ISFET static behavior, are added to the MOSFET static model parameters. [47].

Although this built-in model approach permits the fully characterization of the behavior of the ISFET with different sensitive insulators and takes into account of some of the nonideal effects such as the effect of temperature on the characteristics of the ISFET over user-defined pH and temperature ranges [50], [51], it suffers from some drawbacks that limit its scope for wide application [54]. For example: (i) it requires the availability of the program source and (ii) it requires a deep knowledge of the code subroutines and structures, compiling the whole program when a new model has to be implemented or when modifications to the models have to be made. Thus, these requirements prevent the broad usage of such a tool for designing ISFET-based integrated interface circuits.

3.3 The ISFET Macro-SPICE Model

To order to overcome these drawbacks, Sergio Martinoia proposed a more general and user-friendly macro ISFET chemical model by incorporating the

ISFET MOS device model [54] that is compatible with many commercial SPICE versions such as HSPICE. It is proposed that the ISFET can be separated into two fully uncoupled portions: an electronic portion, the MOSFET, which is the starting structure of the ISFET and an electrochemical portion, the electrolyte-insulator interface. Based on this definition, the HSPICE sub-circuit block, together with its external connections for the ISFET macro model, is depicted in Fig. 3.1(a) [54] while the equivalent electric circuit of the ISFET structure is depicted in Fig. 3.1(b) [54]. The two series capacitances C_{Helm} and C_{Gouy} in Fig. 3.1(b) are the equivalents of the Helmholtz and Gouy-Chapman Capacitance, which have already been developed by the site-binding theory and the electrical double-layer theory described in the previous section. The equations for the charge density and electrolyte-insulator potential are also derived from the site-binding model and the Gouy-Chapman-Stern model, which are provided by [54].

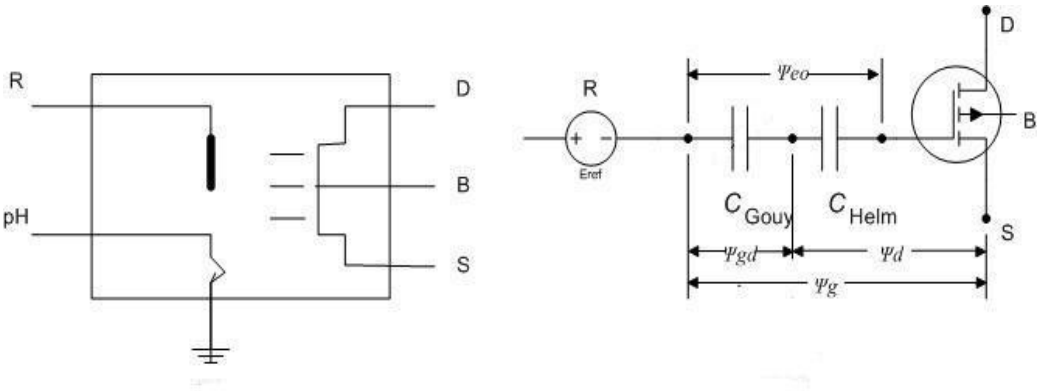

(a) (b)

Fig. 3.1 (a) HSPICE sub-circuit block and its external connections for the ISFET macro model. R= Reference electrode; D=Drain; S=Source; B=Bulk; pH=solution pH value

(b) Equivalent electric circuit of the ISFET structure [54]

It should be noted that in order to facilitate implementation in the CAD tool and to avoid the convergence issue in the numerical calculations based on (2.17), the alternative electrolyte-insulator potential ψ_{eo} [54] can also be expressed as follows:

$$\psi_{eo} = \frac{1}{C_{eq}}\left[\left(\frac{\left[H^+\right]^2 \exp\left(-\frac{2\psi_{eo}}{V_T}\right) - K_a K_b}{\left[H^+\right]^2 \exp\left(-\frac{2\psi_{eo}}{V_T}\right) + K_a\left[H^+\right] \exp\left(-\frac{\psi_{eo}}{V_T}\right) + K_a K_b}\right) N_{sil} + \left(\frac{\left[H^+\right] \exp\left(-\frac{\psi_{eo}}{V_T}\right)}{\left[H^+\right] \exp\left(-\frac{\psi_{eo}}{V_T}\right) + K_{N+}}\right) N_{nit}\right] \tag{3.1}$$

Therefore, the electrolyte-insulator potential ψ_{eo} can be represented by a voltage-dependent voltage source in HSPICE, which is connected in series to the MOSFET. It has been verified that the assumption of the model partition into an electronic portion and an electrochemical portion do not affect the accuracy of using such a macro model approach [54].

3.4 The ISFET Behavior-SPICE Model

Although the Macro-SPICE model has demonstrated its advantages of being a more general and user-friendly approach than the Built-in model in BIOSPICE, there are still many electrochemical parameters that must be extracted as indicated in (3.1); the procedures for extracting the electrochemical model parameter values are complicated and these model parameters are difficult to optimize. This study presents a simplified ISFET behavior-SPICE model on the basis of Hal and Eijkel's theory [41]. As described in equations (2.18), only one of the key parameters, α, the dimensionless sensitivity parameter with a value

that varies from 0 to 1, is required to describe the electrochemical portion of the ISFET. Similar to the Macro-SPICE model described in the previous subsection, it consists of a chemical portion and a MOS transistor, as shown in Fig. 3.2. Herewith, the MOS transistor is modeled by a simplified version of the MOS Level 3 empirical model (SPICE LEVEL3) [88]. Further details pertaining to the device characterization of the SPICE model for ISFET are discussed separately in Section 3.5.

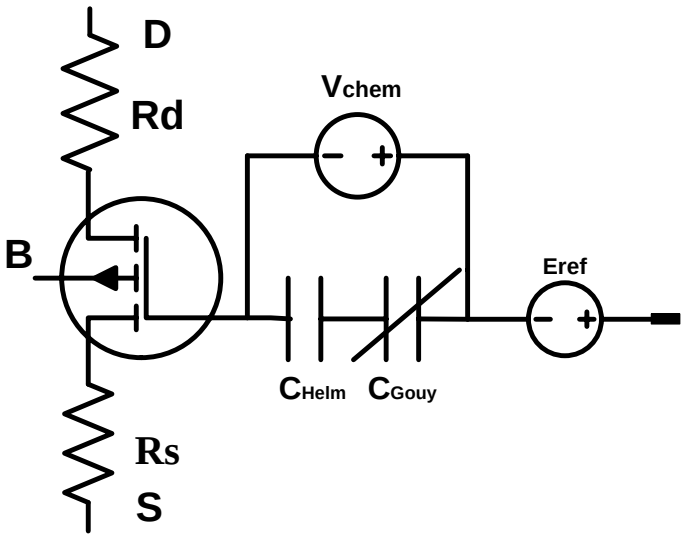

Fig. 3.2 ISFET Modeling Components

In the chemical portion, two voltage sources E_{ref} and V_{chem} are connected in series to denote the voltage components of the chemical threshold voltage of the ISFET in (2.5). V_{chem} consists of two potentials $-\psi_{eo}+\chi^{sol}$, in which χ^{sol} is a constant with respect to the pH value, and ψ_{eo} is the only chemical parameters that is responsible for the ISFET pH sensitivity. The pH sensitivity of ψ_{eo}, which is defined as the change in ψ_{eo} with respect to a change in the pH value of the solution $\partial\psi_{eo}/\partial pH$, has already been explained by Hal and Eijkel's

theory as described in equations (2.18) and (2.19). By integrating (2.18), the pH sensitivity parameter ψ_{eo} can be obtained as follows:

$$\psi_{eo} = -2.303\frac{kT}{q}\alpha \times pH + C \tag{3.2}$$

where C is a constant. Therefore, the voltage source V_{chem} becomes:

$$V_{chem} = 2.303\frac{kT}{q}\alpha \times pH + \left(\chi^{sol} - C\right) \tag{3.3}$$

where the first term is pH-dependent and the constant terms in parentheses are pH-independent. Finally, the drain-and-source diffusion resistor R_d and R_S are added to take into account the fact that a typical ISFET has a longer source and drain diffusion area than its MOSFET counterparts [62]. The Verilog-A language [91] was employed in this project for modeling the chemical portion of the proposed simplified ISFET model as illustrated in Fig. 3.2, which includes V_{chem} and V_{ref} and the two series capacitances C_{Helm} and C_{Gouy}. The Verilog-A language is derived from Verilog HDL for the description of high-level analog behavior. Furthermore, the Verilog-A has been embedded in the Cadence environment, which relaxes the complexity while simulating the ISFET interface circuit, which contains the ISFET behavior model. Furthermore, the employment of Verilog-A language for the modeling is also compatible with a future Sensor System on Chip (SSOC) design. The most critical parameter of the chemical portion of the ISFET behavior model is the pH-sensitivity parameter α in (3.2), which can be extracted by measuring the ISFET threshold voltages in solutions with different pH values. Theoretically, the value of the constant C is determined by the value of pH_{pzc} (point zero of charge). Many previous research studies [92]-[93] have made an efforts to

investigate the value of this parameter, but no coincident conclusions have yet been reached. In general, the value of parameter C in (3.2) can be treated as a DC offset term in the ISFET sensor. It is not harmful to the overall system accuracy because it can be nulled during system calibration and measurement procedures. Indeed, from the sensor simulation point of view, the combined value of the constant (χ^{sol} − C) in (3.3) can be extracted from the experimental results in the form of a fitting constant parameter for modeling the ISFET sensor offset.

3.5 Methodology of Device Characterization of ISFET SPICE Model Parameters

The parameters of ISFET would be extracted from the electrical transfer characteristics in different pH buffer solutions. For the electrical transfer characteristics, as with the existing ISFET micro-models [54], the SPICE MOSFET model is adapted to the MOS portion of the ISFET. Although the BSIM models have the capability to provide the precision modeling of the transistor, the very limited data provided by the manufacture of the ISFET sensor employed in this project hinder the acquisition of BSIM model parameters. On the other hand, the LEVEL1 SPICE model is not accurate enough. Therefore, a simplified version of the MOS Level 3 [88] empirical model is employed in this project.

Most of the parameters related to the short channel effect are allowed to be neglected due to the fact that the ISFET normally has a wide gate width (W) and a long gate length (L). Thus, the I_{DS}-V_{GS} characteristics of the MOS

transistor operating in a linear region (and a strong inversion region) can be described by the following equation:

$$I_{DS} = \mu_S C_{OX} \frac{W}{L}\left[(V_{GS} - V_{th})V_{DS} - \frac{1}{2}V_{DS}^2\right] \tag{3.4}$$

where μ_S represents the dependence of mobility on the gate electric field and is equal to:

$$\mu_S = \frac{\mu_0}{1+\theta(V_{GS} - V_{th})} \tag{3.5}$$

where μ_0 is the surface mobility with zero gate electric field and θ is the mobility modulation coefficient. In this study, the information on the parameters, W, L and C_{OX} have not been provided by the ISFET device manufacturer, so it is not possible to individually extract those parameters, but they can be lumped together as one parameter, β_0 that is, $\beta_0 = \mu_0 C_{OX}\frac{W}{L}$ for the purpose of extraction. As the only difference between the ISFET and MOSFET in (3.4) is the threshold voltage, equation (3.5) can also be applied to the ISFET by simply replacing V_{th} with V_{th_ISFET} in (2.4). As a result, there are three parameters to be extracted. They are V_{th_ISFET} , β_0 and θ. Similar with the standard MOSFET parameter extraction procedure, the parameters of ISFET are extracted from its I-V curves, which are measured by the micro-probing station and the semiconductor parameter analyzer. The only difference is that the characterization of the ISFET should be carried out in different standard buffer solutions. The details of the ISFET I-V curve measurement and the parameters extraction would be described in Chapter VII of Results and Discussions.

3.6 Comparison with Prior-Art Models

In order to demonstrate the technical merit of the proposed ISFET Behavior-SPICE model, Table 3.1 presents a comparison of features with those of the prior-art models. The proposed ISFET Behavior-SPICE model overcomes the major drawbacks encountered by the prior-art models. Due to its simplicity and the fact that there are only three empirical electrochemical parameters to be extracted in characterization, the improved model is a cost-effective solution for ISFET research work as well as for the development of ISFET products for commercial application. Although the prior-art work on the ISFET Macro-SPICE model can be compatible with the system design, the proposed ISFET Behavior-SPICE model demonstrates even higher flexibility due to the employment of the Verilog-A language in its behavior model. This is mainly because Verilog-A is developed for use in analog-mixed signal design environments, with powerful description scripts for ease of modeling. It can link a transistor-level simulator for realistic simulation with sensor circuits and systems. Moreover, it is also easy to add in extra features to describe the physical phenomenon of the device to the behavior model such that the chemical-based behavior model becomes as realistic as real physical devices. Although the current modeling work addresses the basic and necessary modeling parameters in a preliminary development stage, there is strong potential to extend the proposed model to a more sophisticated one, which fits the need for ISFET technology products with stringent requirements.

Table 3.1 Comparison of proposed ISFET Behavior-SPICE model with prior-art models

Item	ISFET Built-in Model BIOSPICE [47]-[51]	ISFET Macro-SPICE Model [54]	Proposed ISFET Behavior-SPICE Model
Program Source	Not available	Available	Available
Electrochemical Parameters	14 Physical-Chemical Parameters	14 Physical-Chemical Parameters	3 Empirical Parameters
Ease of Parameters Extraction	Complicated	Complicated	Simple
User-Friendly	No	Yes	Yes
Compatibility with SSOC Design	No	Yes	Yes
Flexibility	Low	Moderate	High

Chapter IV

ISFET Interface Circuits

4.1 Introduction

The basic function of the ISFET interface circuit aims at detecting the change in the ISFET threshold voltage that reflects the variation of the pH value in the solution. Many research works [57]-[73] have exploited different circuit architectures of interface circuits, which usually play a role in translating the pH values to voltage domain presentation, with the goal of obtaining good sensitivity as well as linearity. As the transfer characteristics (I_D/V_{GS}) of the ISFET devices are essentially those of the FET substructure that is utilized, so far there are three different ways of detecting pH value of the solution. If the applied gate bias potential (via reference electrode) is fixed, then the changes in the chemical ambient would directly modulate the ISFET threshold voltage, which in turn controls the device drain current, I_D. The second method is to maintain the drain current at a constant value by using the negative feedback loop to control the potential of the reference electrode. Consequently, the output signal can be read from the reference electrode. The third way is to keep the drain current constant and apply a fixed voltage to the reference electrode, thus allowing for the modulation of the ISFET threshold voltage to be read from the source terminal of the ISFET. The latter two methods are commonly employed in current ISFET signal processing technology. However, it is common to observe that circuits with a non-zero body bias would not only affect linearity through bulk modulation, but also introduce an undesirable temperature

dependent effect. Finally, the ISFET sensing device can be designed to operate in a non-saturation region or in a saturation region.

4.2 A Review of Triode-Based ISFET Interface Circuits

The ISFET can work successfully in both non-saturation and saturation region. In this section, several representative ISFET interface circuits with the ISFET device configured to operate in non-saturation region are reviewed.

4.2.1 ISFET as a Source Follower (ISFET-SF)

One of the representative interface circuits reported in previous research studies [13], [61]-[62], [74], [82] is that the ISFET can be configured as a non-saturated based source follower structure, as depicted in Fig. 4.1. Since the ISFET is biased in the linear region, the drain current I_{DS} to the first order have been provided in Chapter II and rewritten as follows:

$$I_{DS} = \mu C_{OX} \frac{W}{L}\left[\left(V_{GS} - V_{th(ISFET)}\right)V_{DS} - \frac{1}{2}V_{DS}^2\right] \tag{4.1}$$

With reference to Fig. 4.1, the ISFET is biased with a constant drain-source voltage V_{DS} clamped by the outputs of two amplifiers. Simultaneously, a constant drain current I_{DS} is established via the current sink I_{S2}. Since the gate of the ISFET is defined by a reference voltage, any change in the pH of the solution is translated into the electrolyte-insulator potential of the ISFET, which is reflected in the ISFET source terminal potential as follows:

$$V_S = V_{ref} - \frac{I_{S2}}{\mu C_{OX}(W/L)I_{S1}R} - \frac{I_{S1}R}{2} - V_{th(ISFET)} \tag{4.2}$$

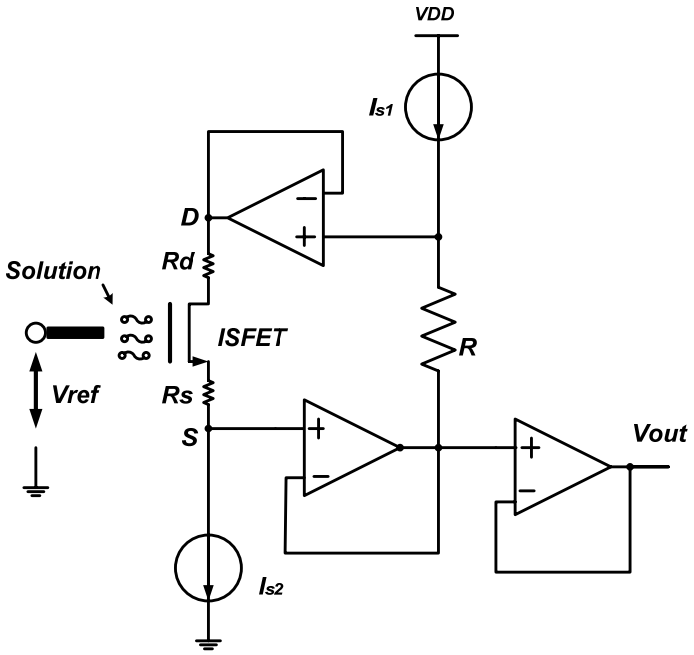

Fig. 4.1 ISFET Interface circuit configures the ISFET as a source follower [61]

For ideal offset-free op-amps, the output is obtained as $V_{out}=V_S$. It has been shown that the variation in the ISFET threshold voltage, $V_{th(ISFET)}$ caused by the variation in the pH value of the solution, can be measured directly from the source terminal of the ISFET sensor. However, in a standard n-well CMOS technology where all the devices are shared in a common substrate, not only does $V_{th(ISFET)}$ vary with pH value, but it is also a function of the body effect in the ISFET. This can be observed from the definition of the ISFET threshold voltage in (2.4). Here it is reproduced as:

$$V_{th(ISFET)} = E_{REF} + \Delta\varphi^{lj} - \psi_{eo} + \chi^{sol} + \left[\frac{-\phi_{Si}}{q} - \frac{Q_{OX}+Q_{SS}+Q_B}{C_{OX}} + 2\varphi_f + \gamma\left(\sqrt{2\varphi_f + V_{SB}} - \sqrt{2\varphi_f}\right)\right] \tag{4.3}$$

As can been seen from (4.3), the output voltage in the source terminal in (4.2) could be nonlinear to the input pH signal with respect to the regulation of the

source-body voltage, V_{SB}. Besides the body effect, other second-order effects include the ISFET drain and source diffusion resistances. This stems from the fact that the area surrounding the gate is completely covered with protecting and insulating layers and no metal contacts can exist in the vicinity of this region. Therefore, the ISFET usually has a longer source and drain diffusion area than the corresponding MOSFET for the electrical contact to the drain and source terminals, which could result in R_d and R_S having a resistance up to 100Ω [62] or above, depending on the process technology and device design. Thus, when incorporating these resistances, the output of the interface circuit can be approximated as follows:

$$V_{out} = V_{ref} - \frac{I_{S2}}{\mu C_{OX}(W/L)\left[I_{S1}R - I_{S2}(R_d + R_S)\right]} - \frac{I_{S1}R - I_{S2}(R_d + R_S)}{2} - V_{th(ISFET)} \tag{4.4}$$

Here, the second term and third terms are quiescent dc biasing voltages that have offset error terms arising from a dc voltage drop on the drain and source diffusion resistor. Apart from the static terms, V_{out} is still a function of the threshold of the ISFET, $V_{th(ISFET)}$ from ac variation point of view. Furthermore, another nonideal effect is that of the offset voltage introduced by the three operational amplifiers (op-amps). It should be noted that the offset for each op-amp may not be identical in its practical realization. Integrated op-amps with identical designs may have better offset matching characteristics. Although the offset voltage of an op-amp is chemically insensitive, its temperature dependent behavior will contribute to an additional error and temperature sensitivity of the interface circuit.

4.2.2 ISFET with a Constant V_S and I_{DS} (ISFET-CVCI)

The variation in the ISFET threshold voltage caused by the pH variation can also be read from the reference electrode, as shown in Fig. 4.2 [65]. The drain-source voltage and the source voltage of the ISFET are set by the current source I_{BIAS} and the resistors R_{DS} and R_{REF}. The output of the amplifier, *Op2*, drives the reference electrode. The ISFET threshold voltage will changes with the pH value of solution, but the feedback mechanism of the circuit would keep the drain current constant by regulating the voltage applied to the reference electrode, which is regarded as the output voltage of the ISFET interface circuit. Since the voltage of the ISFET source terminal is clamped by the operational amplifier Op2, the influence of the body effect on the output pH sensitivity is weak even in one-chip implementation. This can be explained with the aid of the equation of the ISFET threshold voltage in (4.3). As the voltage of the source terminal is clamped by Op2, the source-body bias potential, V_{SB}, is able to remain constant. Therefore, the value of $\gamma\left(\sqrt{2\varphi_f + V_{SB}} - \sqrt{2\varphi_f}\right)$ in (4.5) is independent of the ψ_{eo}, which would be proportional to the variation in the pH value. Thus, the ISFET threshold voltage is the only function of ψ_{eo}. This is verified by the simulation results discussed later in Chapter VII. It is important to note that, although this constant source-body bias would not affect the linearity of the interface circuit, it would introduce an additional temperature-dependent component that makes the ISFET temperature compensation more complicated.

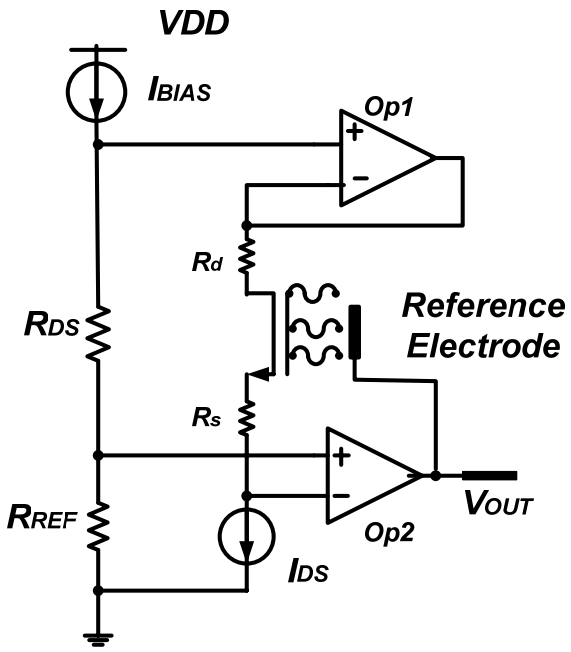

Fig. 4.2 Constant V_S and I_{DS} interface circuit [65]

Taking into account the drain and source resistances, the output voltage of the circuit is obtained as follows:

$$V_{out} = \frac{I_{DS}}{\mu C_{OX}(W/L)\left[I_{BIAS}R_{DS} - I_{DS}(R_d + R_S)\right]} + I_{BIAS}R_{REF} + \frac{I_{BIAS}R_{DS} - I_{DS}(R_d + R_S)}{2} + V_{th(ISFET)} \tag{4.5}$$

As can be observed from (4.5), the output consists of the dynamic term $V_{th(ISFET)}$ that links to the pH value and several static terms arising from biasing parameters and nonideal transistor parameters.

4.2.3 ISFET Operational Transconductance Amplifier (ISFET-OTA)

Many research studies have investigated the use of an ISFET sensing device and a MOSFET to form the differential input stage of a CMOS operational amplifier [58]-[60], [63]-[65] . A representative circuit is illustrated in Fig. 4.3. It is a modified symmetrical OTA that incorporates a PMOS source follower to

form an ISFET buffer. The ISFET and its buffer circuitry are integrated into one process so as to enable a more stable operation. By introducing the bootstrap transistors T2a and T2b, using the same technology as T1a and T1b with a Pt (platinum) gate, the drain-source voltage over transistors T1a and T1b are kept constant. For correct operation, the drain-source current of the ISFET is kept constant as well. Any variation in the threshold voltage between the two input transistors T1a and T1b at the differential input stage caused by a variation in the pH value in the test solution will appear at the output. The ISFET is biased in the linear region by an external bias V_{set} and the voltage at the solution-insulator interface is denoted as V_{chem}. The PMOS source follower (formed by transistors T5 and T6) is added to match the input and output voltage swing and also to lower the output impedance. The output voltage can be expressed as

$$V_{Out} = V_{set} + V_{th\_T1b} - V_{th\_T1a} + V_{OS} \tag{4.6}$$

where V_{OS} is the offset voltage, which is chemically insensitive but temperature sensitive. The solution-insulator interface voltage, V_{chem}, is contained in the threshold voltage, V_{th_T1a}, of the ISFET transistor. The offset voltage is composed of a random mismatch component and a systematic mismatch component. The random mismatch component constitutes (i) the mismatch of a differential transistor pair in the form of transistor gain ($\beta = \mu C_{OX} W / L$) and threshold voltage, (ii) the mismatch of current sources and (iii) the mismatch of current mirrors. On the other hand, the systematic mismatch component arising from the circuit design can be minimized, making the random mismatch the dominant mismatch term. In addition to the above-mentioned mismatch effects,

the value of V_{set} should also be carefully set such that both transistors T1a and T1b operate at the correct biasing point.

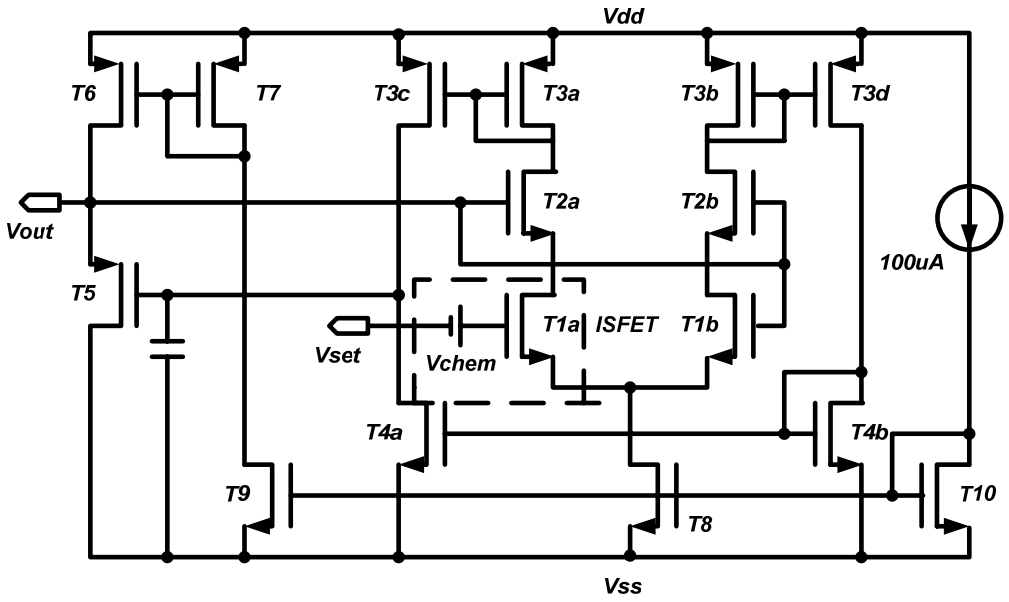

Fig. 4.3 Transistor schematic of the modified ISFET OTA [64]

4.3 A Review of Saturation-Based ISFET Interface Circuits

A technique of a complementary ISFET/MOSFET pair (CIMP) [68] has been recently reported for the monolithic implementation of ISFET sensors, as shown in Fig. 4.4. The principle can best be described by assuming a CMOS pair with non-shorted gates (this structure is also known as a Quasi-Inverter), in which one of the n-channel MOSFETs is replaced by an n-channel ISFET. It should also be noted that the ISFET can work in a saturation region. Fig. 4.4(a) shows the direct gate feedback configuration called CIMP-DGF. The drain current of the ISFET is kept constant. The op-amp is used to preserve a constant V_{ds} bias in n-ISFET and p-MOSFET and apply a feedback signal to the reference electrode. Alternatively, Fig. 4.4(b) shows the indirect gate feedback

configuration, called CIMP- IGF, in which the reference electrode is constantly biased and the drain current is made variable by means of negative feedback such that the variation in the measured pH value is translated into the output voltage.

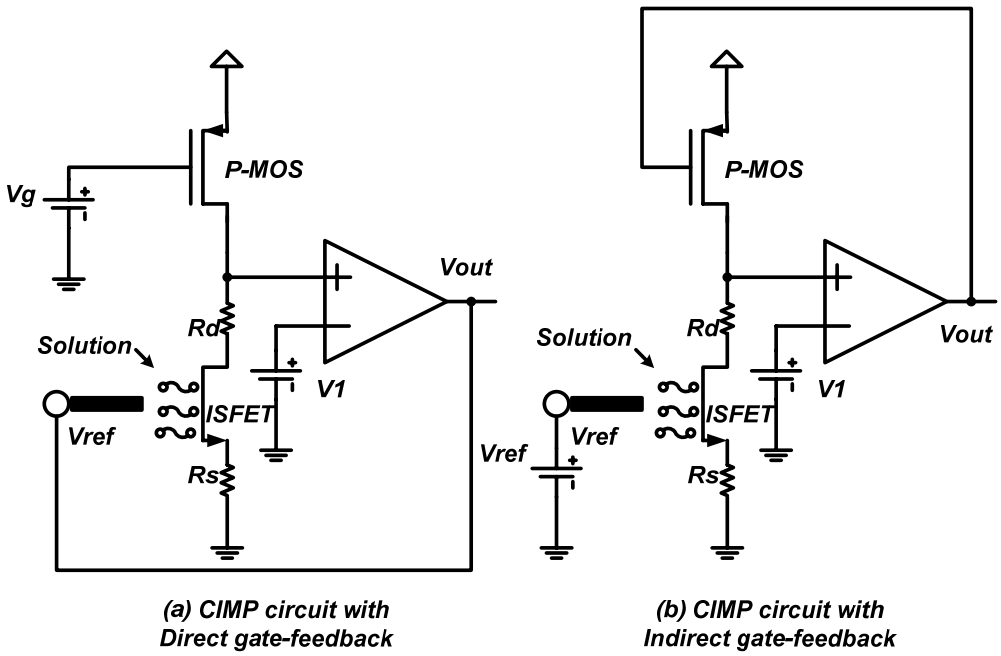

Fig. 4.4 Direct and Indirect Gate-feedback ISFET Interface Circuits [69]

Consider the ISFET operating in a saturation region, the drain current to the first order has been provided in Chapter II and is repeated here as follows:

$$I_{DS} = \frac{1}{2}\mu C_{OX}\frac{W}{L}\left(V_{GS} - V_{th(ISFET)}\right)^2 \tag{4.7}$$

where $A = \frac{1}{2}\mu C_{OX}\frac{W}{L}$ (4.8)

and $\alpha = A_{p-MOSFET} / A_{n-ISFET}$ (4.9)

Hence, the output of CIMP-DGF in Fig. 4.4(a) can be obtained by assuming the ideal amplifier:

$$V_{out} = \sqrt{\alpha}\left(V_{GS\_pMOSFET} - V_{th\_pMOSFET}\right) + V_{th(ISFET)} = K1 + V_{th(ISFET)} \tag{4.10}$$

This leads to the result that the change in the output is the only function of the change in the ISFET threshold voltage:

$$\Delta V_{out} = \Delta V_{th(ISFET)} \tag{4.11}$$

In the case of the CIMP-IGF in Fig. 4.4(b), the circuit output can be obtained as follows:

$$\Delta V_{out} = \Delta V_{th(ISFET)} / \sqrt{\alpha} \tag{4.12}$$

Compared to the CIMP-DGF, the ac output voltage of the CIMP-IGF is not only dependent on the pH variation of the test solution but also on the dimension and process parameters of the ISFET and PMOS current source device. With reference to (4.8) and (4.9), the effective mobility (μ_S) of these two devices will change with the gate-source voltage, which means that the value of $\sqrt{\alpha}$ is difficult to keep constant with different biasing conditions of the ISFET and PMOS. Therefore, it would exhibit a different level of sensitivity as well as nonlinear gain sensitivity when compared with that of the CIMP-DGF circuit.

4.4 New ISFET Interface Circuits

4.4.1 Non-Saturation Based ISFET Voltage-V Current-I (ISFET-VI) Interface Circuit

The schematic of the proposed ISFET interface circuit is shown in Fig. 4.5. The basic principle of the ISFET interface circuit is that the drain current is kept constant by counteracting the change in the drain current via a change in the potential applied to the reference electrode. Consider the circuit

implementation: the ISFET operating in a non-saturation region is biased by a constant current I_B and claimed by a constant voltage V_{ds} through a super transistor formed by a transistor *M2* and an op-amp *Op1* with a biasing voltage V_B. The circuit uses *Op1* in a negative feedback loop to control the gate-source voltage of transistor *M2*. If the *Op1* is ideal, the negative feedback loop adjusts the gate of the transistor *M2* until the voltage difference between the two amplifier inputs is zero. In other words, the drain-source voltage of the ISFET is driven to equal V_B. In practice, the amplifier *Op1* is not perfect, which means that the drain-source voltage of the ISFET will deviate from V_B by a small amount in a form of a lumped offset contributed by *Op1*. Such a nonideal dc parameter comes from the foundation offset as well as finite gain error of the op-amp. However, it can be viewed as a systematic offset from the viewpoint of the ISFET system and can be cancelled during the ISFET calibration in solution of different standard pH values. The details of the calibration procedure are demonstrated in later chapters. The ISFET-VI circuit, like a VI converter structure, behaves in the form of dynamic VI conversion with a constant current *I* forcing through an ISFET sensing element but with a dynamic voltage *V* being established through the gate-source voltage of an ISFET element to reflect the change in pH value. Such a dynamic balance is locked through a source follower in a feedback structure. The output of the source follower or the gate voltage of the ISFET, which is the reference electrode of the ISFET, is forced to settle to a value determined by the pH value of the solution in which the ISFET is immersed. Finally, the source follower also functions as a voltage buffer for driving the next stage of electronics. This provides an economical means of

driving circuit design whilst avoiding the op-amp design which introduces an additional offset to the ISFET system. The feedback mechanism of the ISFET-VI circuit can be explained in the following example. Consider an increase in the ISFET threshold voltage $V_{th(ISFET)}$ due to an increase in pH change; the feedback phenomenon is observed as follows:

1) The drain current I_d initially decreases. Since the ISFET is arranged in a common-source structure with a super transistor cascode active load, the drain voltage of *M2* would increase in response to the excitation. The change in drain voltage is then coupled to the common-drain (source follower) configuration formed by transistor *M1* and current source I_o.
2) As a result, the output of the source follower, which is the source terminal of *M1* serving as the reference electrode (gate) of ISFET, rises to increase the gate-source voltage (V_{gs}) of the ISFET such that I_d increases to counteract the action of excitation.
3) The I_d returns to the value set by the current source I_B through the feedback action.

As a final remark, the process flow can be summarized in the following way:

$pH \uparrow \Rightarrow \Delta V_{th(ISFET)} \uparrow \Rightarrow I_d \downarrow \Rightarrow V_{M2\_drain} \uparrow \Rightarrow V_{M1\_source} \uparrow \Rightarrow V_{gs} \uparrow \Rightarrow I_d \uparrow$

and vice versa for the opposite case of a decrease in the ISFET threshold voltage $V_{th(ISFET)}$ due to a decrease in pH change.

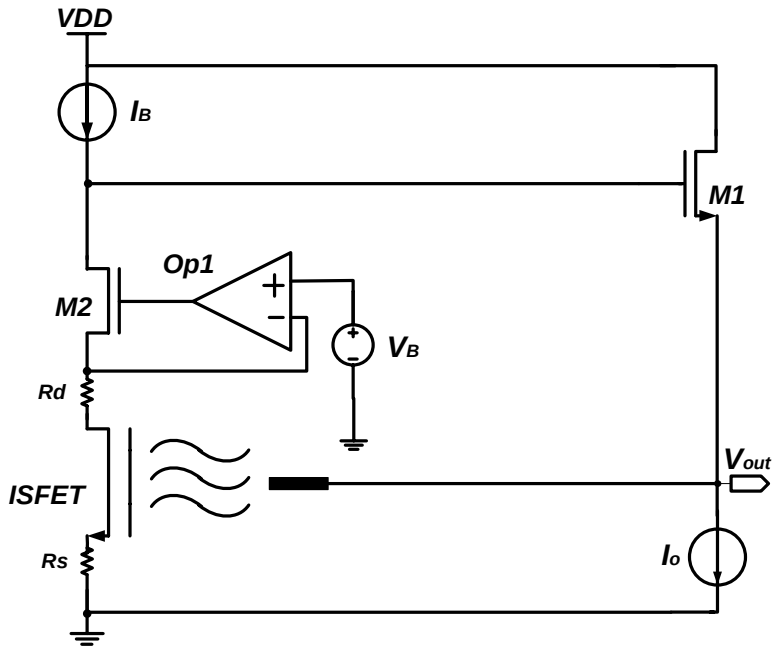

Figure 4.5 Schematic of the proposed non-saturated ISFET interface circuit

According to the expression of the ISFET drain current I_{DS} in (4.1) for small V_{ds} and including the drain and source resistance, R_d and R_S, the output of the proposed interface circuit can be approximated as follows:

$$V_{out} = V_{gs} \cong V_{th(ISFET)} + \frac{I_B}{\mu C_{OX}\frac{W}{L}\left[V_B - I_B\left(R_d + R_S\right)\right]} + \frac{V_B - I_B\left(R_d + R_S\right)}{2} \qquad (4.13)$$

Here, the second term is defined as a quiescent dc biasing voltage at the equilibrium state of the feedback circuit. The bandgap reference circuit as well as the external reference resistor with a high precision (1%) can be utilized to generate a constant V_B and I_B so as to reduce the variation due to process, temperature and supply. The third term is a dc biasing component that has a residual dc error caused by the drain and source diffusion resistor. Therefore, V_{out} becomes a function of the threshold voltage of ISFET, $V_{th(ISFET)}$, which is linearly propositional to the pH value of the buffer solutions. By grounding the

ISFET's source and bulk terminals, the body effect dc does not alter the sensitivity, whereas the voltage drop across the source diffusion resistor may be negligible as long as the product $I_B R_S$ is minimized in the design. Meanwhile, the temperature-dependent body effect contributes a few percentages to the total *T.C.* of the temperature-uncompensated output, which is insignificant. The methodology of temperature compensation is discussed in the next chapter.

4.4.2 Saturation-Based ISFET Level-Shifted Diode (ISFET-LSD) Interface Circuit

On the basis of the non-saturation based ISFET interface circuit discussed in the previous section, a new ISFET interface circuit, called the ISFET-LSD, can be devised for classification in the second category. The simplified schematic is depicted in Fig. 4.6. It comprises an ISFET device operating in saturation region via a constant current source I_B and a level shifter, realized by a source follower consisting of the transistor *M1* and the current source I_O, in a feedback arrangement to form a level-shifted diode-like ISFET structure.

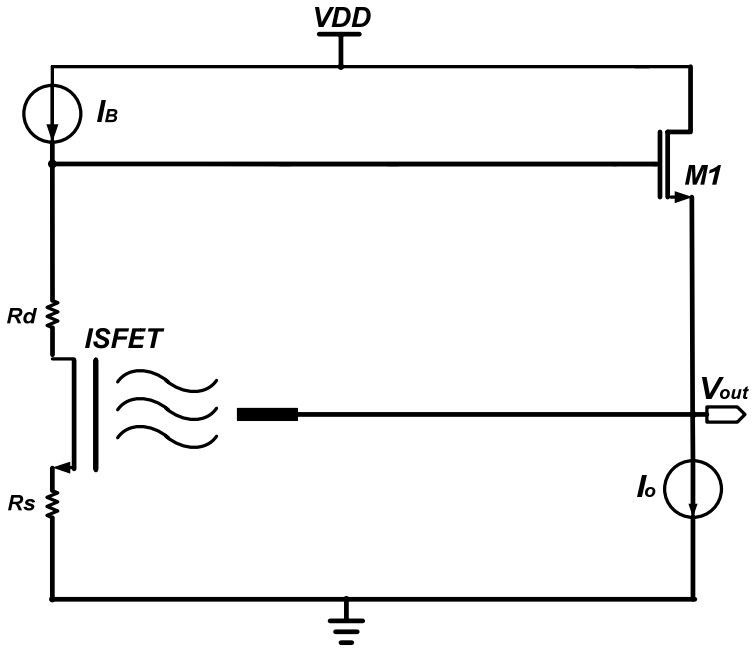

Fig. 4.6 Simplified schematic of the proposed saturation-based ISFET interface circuit

As described above, the target of the ISFET interface circuit is to detect the variation in the pH value of the solution by measuring the change in the ISFET threshold voltage via its gate-source voltage (V_{GS}). The circuit structure in Fig. 4.6 is similar to the proposed ISFET interface circuit discussed in the previous subsection but has a simpler structure. With the elimination of the op-amp component and stable drain current characteristics regardless of the varying drain-source voltage for a long channel saturation-based ISFET, the offset is further reduced in the ISFET-LSD circuit.

In the proposed configuration of the ISFET interface circuit, the V_{GS} of the ISFET becomes self-biased through a source follower in a feedback loop. The operation is explained as follows. When passing a constant current through the ISFET, the V_{GS} of the ISFET must be established to fulfill the biasing condition. As the gate of the ISFET is tied to the source of the transistor *M1*, a floating dc will be developed in the gate of *M1* due to the V_{GS1} (gate-source voltage of

transistor *M1*) being established by I_O. Any change in the ISFET's V_{GS} will shift the V_{GS1} dynamically in the source follower. Therefore, the output of the interface circuit or the reference electrode voltage of the ISFET is forced to settle at a value determined by the pH value of the solution in which the ISFET is immersed. Although the shift in V_{GS1} may be caused by the variation in the drain-source voltage of the ISFET, the effect of the channel length modulation may be negligible due to the long channel length of the ISFET device. As with the non-saturation ISFET-VI interface circuit, the source follower also performs as an economical voltage buffer for driving the next stage electronic circuit. This is advantageous because of the elimination of an op-amp-based buffer. According to (2.2b) and (2.4), when an ISFET is operating in saturation region, the output of the proposed interface circuit can be derived as:

$$V_{out} = V_{gs} = V_{th(ISFET)} + \sqrt{\frac{2I_B}{\mu C_{OX}\left(\frac{W}{L}\right)}} + I_B R_S \tag{4.14}$$

where the second term is defined as a quiescent dc biasing voltage arising from the gate-overdrive bias, and the third term is a dc component caused by the voltage drop across the source diffusion resistor (R_S). Nevertheless, it can be negligible as far as the product $I_B R_S$ is minimized in the design. Therefore, the output V_{out} becomes the only function of the threshold voltage of the ISFET $V_{th(ISFET)}$, which is linearly proportional to the pH value of the solution. With the grounding of the ISFET's source and bulk terminal, the body effect dc does not alter the sensitivity but the temperature-dependent body effect contributes few percentages [73] to the total *T.C.* of the temperature-uncompensated output, which is insignificant. This new self-adjusted V_{GS} ISFET sensing circuit fulfills

the first step of the basic sensing function while meeting the requirement of simplicity and almost eliminating the temperature-dependent body effect item. The second step for temperature compensation is discussed in the following chapters.

4.5 Summary

The basic principle of the ISFET interface circuit for pH measurement has been described in this chapter. In addition the representative ISFET interface circuits such as the ISFET-SF, ISFET-CVCI, ISFET-OTA, CIMP-DGF and CIMP-IGF that have previously been published were critically reviewed. Then, a new non-saturation based ISFET-VI interface circuit and a new saturation-based ISFET-LSD interface circuit have been proposed. Both circuits have demonstrated the significant advantage of insensitivity to the body effect. Therefore, the pH sensitivity of the output of the interface circuit well reflects the pH sensitivity of the ISFET sensor. Moreover, their intrinsic simple structures reduce the circuit components as well as the circuit sensitivity and provide an economical buffer design. The ISFET-LSD, which is regarded as the simplest structure among all the interface circuits, is demonstrated with smart compensation for the ISFET sensory system design in later chapters.

CHAPTER V

COMPENSATION TECHNIQUES

As studied in Chapter II, the nonideal effects existing in the ISFET would severely impede the accuracy of the ISFET sensor in application of long-term monitoring. Therefore, the compensation technique becomes one of the critical design tasks in the ISFET-based measurement system. The nonideal effects in the ISFET sensors can be classified into time-variant fluctuation arising from the drift mechanism, slow pH response and time-invariant temperature dependence on various pH values. The total ISFET output signal variation, ΔV, has well been generalized in equation (2.20), which is repeated here to illustrate the composite effect:

$$\Delta V = \frac{\partial V}{\partial pH}\Delta pH\left[1-\sum_{i=1}^{n}\varepsilon_i \exp\left(-\frac{t}{\tau_i}\right)\right]+\frac{\partial V}{\partial t}dt+\frac{\partial V}{\partial T}dT \qquad (5.1)$$

Therefore, this chapter critically reviews the previous research studies on ISFET temperature compensation as well as drift compensation. Then, a novel ISFET temperature compensation method is proposed with detail analysis. Later, this is followed by a proposal of a novel compensation method for ISFET time-variant nonideal effects.

5.1 A Review of Temperature Compensation Techniques

The last term in (5.1), represents the variation of output as function of temperature. It has been investigated in Chapter II that the temperature characteristics of the ISFET can be divided into three major components: the

reference electrode (*T.C.R.*); the electrolyte-insulator interfacial potential (*T.C.I.*) and the MOS structure of ISFET (*T.C.F*). The composite temperature effect greatly limits the performance of ISFET sensors and leads to unacceptable results in critical measurements. Therefore, one of the essential features of the signal processing circuit is to support temperature compensation scheme. Herewith, the ISFET temperature compensation techniques are reviewed followed by the introduction of a new temperature compensation methodology along with its detailed second-order analysis.

Research efforts have been spent on various ISFET temperature compensation techniques [58]-[60], [62]-[64], [66], [69], [73]-[74], [76]-[79] along with interface circuit design. In earlier study [74], the thermal stability of an ISFET is improved when it is biased in an experimental determined athermal operating point. However, as described in Chapter II, the athermal operating point of the ISFET varies in buffer solutions with different pH values due to the pH-dependent of the *T.C.I* described in (2.21). This standalone constant biasing method would not be effective for temperature compensation in a wide pH range. Other major research efforts [58]-[60], [62]-[64], [76] have focused on the configuration of the hybrid differential-pair amplifiers, which are commonly known as the ISFET operational amplifiers and appear in various circuit elements or method combinations: *A)* the differential pair of ISFET/MOSFET [58]-[59],[63]-[64]; *B)* the differential pair of ISFET/MOSFET incorporating a p-n junction diode [76]; *C)* the differential pair of ISFET/REFET [77]; and *D)* the differential pair of ISFET/ISFET with different materials for different pH sensitivities [60], [62], [69].

5.1.1. Differential Pair of ISFET/MOSFET

After the first introduction of operational transducer [59], the ISFET/MOSFET pair has commonly been utilized as the input differential circuit of the ISFET interface circuits. Taking advantage of the same fabrication process of ISFET/MOSFET pair, it provides certain immunity on the temperature sensitivity of MOS structure of ISFET, or called *T.C.F* in (2.21). The original concept of the operational transducer has been demonstrated in Fig. 5.1.

Refer to the circuit schematic, the ISFET is assumed to be well matched with the input MOSFET and those matched devices are operating under the identical thermal and electrical conditions. As illustrated in Fig. 5.1, the matched ISFET/MOSFET pair is in source-coupled differential configuration and the output voltages are coupled to the second stage which operates as a differential-to-single-ended converter. The output voltage of the interface circuit is fed back to the input MOSFET gate such that the drain current of the MOSFET would track that of the ISFET. It satisfies the conditions for ISFET thermal compensation. Therefore, the output voltage can be obtained as

$$V_{out} = V_{G\_ISFET}\left(\frac{A}{A+1}\right) \tag{5.2}$$

where V_{G_ISFET} is the equivalent gate voltage of the ISFET and A represents the overall DC gain of all stages, which include the gain of the source-coupled differential ISFET/MOSFET pair. If the gain factor A is sufficiently large, the output voltage, V_{out} is virtually equal to the equivalent gate voltage of the ISFET device, which is linearly pH dependent. The thermally induced variations on ISFET/MOSFET drain current are rejected by the differential input configuration as a common-mode signal. In other words, the temperature

sensitivity of the MOS part of the ISFET can be cancelled by the MOSFET in the same technology in principle. However, in practical fabrication, the input-referred offset voltage V_{OS}, caused by the device mismatch of the input differential pair and the current mirror pairs, appears as a dc error term and can drift with temperature. Although the temperature characteristic of the MOS part of the ISFET tends to track that of the MOSFET device in the differential pair, the circuit is not able to immune against the temperature effect on the electrochemical components such as the temperature coefficient of reference electrode *(T.C.R)* and electrode/insulator interfacial potential *(T.C.I)*. This will cause serious problems in environmental application. For example, if the temperature coefficient of the chemical part is around 0.69 mV/°C in pH4 buffer solution [18], the variation of the output is translated to an error of ΔpH = 0.276 when the temperature of the solution increases 20°C. Since the *T.C.I.* is also function of the pH value of the solution, the error will be even larger as the pH value of the test solution increases [20], [23].

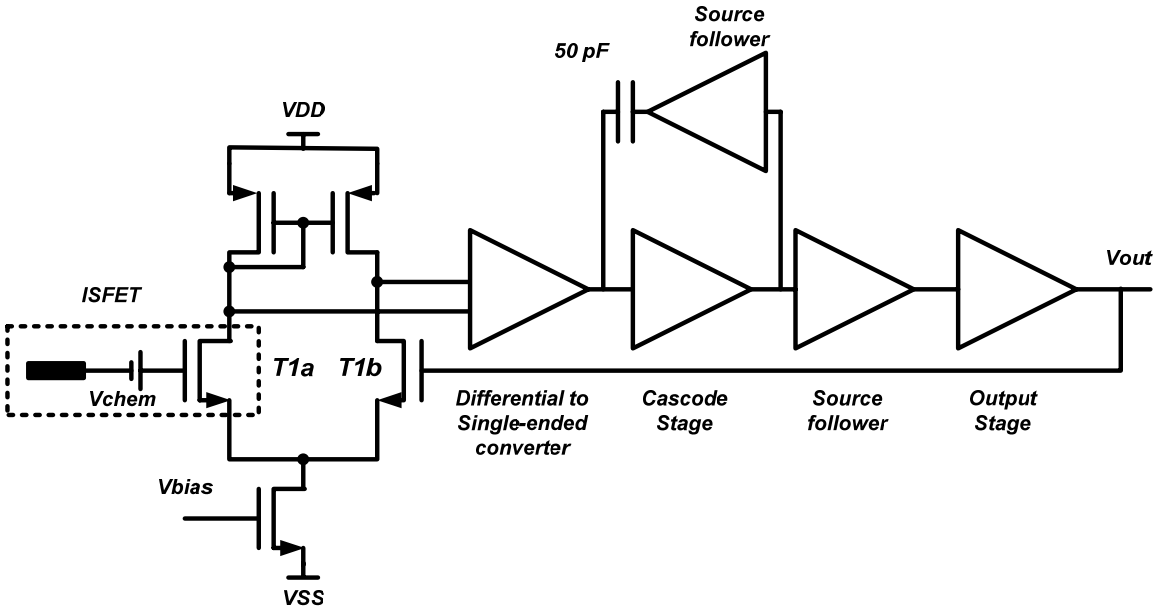

Fig. 5.1 Transistor Schematic of the ISFET/MOSFET differential pair [59]

5.1.2. Differential Pair of ISFET/MOSFET Incorporating a PN Junction Diode Method

The temperature effect of the electrochemical component can be relaxed by using an ISFET/MOSFET source-coupled differential pair configuration in along with a p-n junction diode method [76] shown in Fig. 5.2. It has been reported to achieve well temperature compensation around the pH6 of the buffer solution.

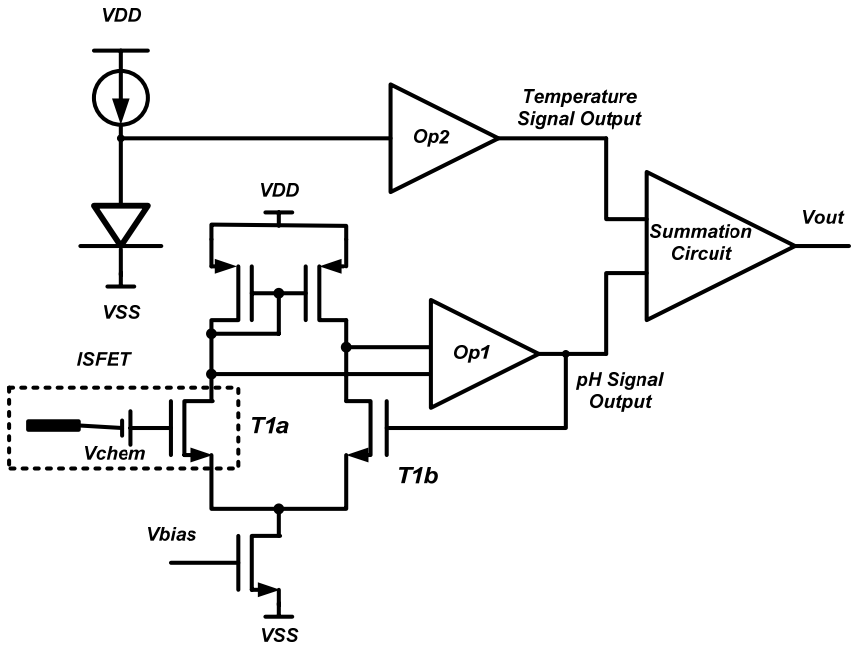

Fig 5.2 Schematic of the ISFET temperature compensation [76]

The basic idea of this technique is to utilize the negative temperature coefficient of the p-n diode to compensate the positive temperature coefficient of the ISFET chemical component by feeding both the output of the pH signal from the ISFET operational amplifier and the temperature signal detected by the p-n junction diode into a summation circuit as shown in Fig. 5.2. *T1a* and *T1b* fabricated at the same technology configure the ISFET/MOSFET source-

coupled input differential pair. The op-amp *Op1* in this circuit is to keep the drain-source voltage as well as the drain-source current of *T1a* equal to those of the *T1b* transistor. These two transistors are operating in linear region. Consider the operation as follows: any change in the pH value of solution will accordingly modulate the threshold voltage of the ISFET, *T1a*. In order to keep the biasing current of *T1a* constant, the drain-source resistance has to be modulated in accordance with the variation of pH value of solution. The *Op1* provides negative feedback to adjust the gate potential of *T1b* in order to modulate the triode resistance such that identical biasing current of *T1b* would be identical with that of *T1a*. Ultimately, the output of the *Op1* becomes proportional to the detected pH value. Besides the ISFET sensor, the other sensor is a p-n planar diffused silicon diode for on-chip temperature measurement and compensation. The diode is operated in forward bias region by a constant biasing current. However, the disadvantage of this circuit will be on following aspects: 1) when it is forward biased, the voltage-current relationship, V_D-I_D, is logarithmic and can be related as

$$V_D = kT/q \ln(I_D / I_S) \tag{5.3}$$

where I_S is known as the scale current and is proportional to the area of the diode junction and inversely proportional to the doping concentration, which is not only strongly temperature dependent but also process dependent. As a result, the temperature coefficient of the V_D is nonlinear as well as process dependent. 2) This method can only compensate the temperature dependence of the ISFET in the vicinity of particular pH value. This is because the pH dependent *T.C.I.* can only be well compensated by the pH independent of

temperature coefficient of V_D in a broad range of pH values. Therefore, this method may not be able to satisfy the requirement for water quality monitoring that ISFET will be immersed in a thermal variation environment with wider pH range.

5.1.3. Differential Sensing with Dual ISFET Operational Amplifiers

Other research study has utilized the Ta_2O_5/SiO_2 and $SiO_XN_y/Si_3N_4/SiO_2$ as two kinds of the pH sensitive layers of the ISFET sensors for two ISFET differential op-amps, as shown in Fig. 5.3.

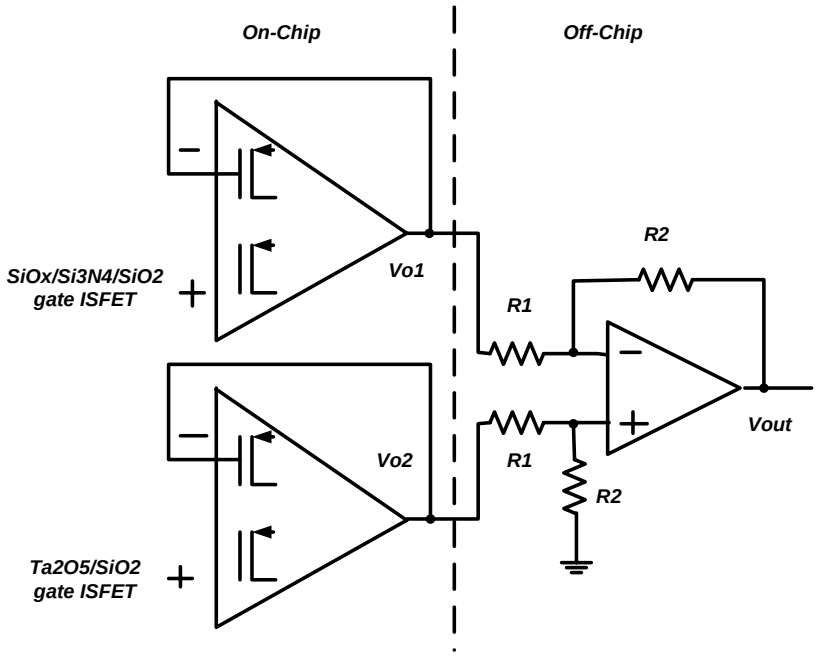

Fig. 5.3 Block diagram of the differential sensing with dual ISFET operational amplifiers [60]

The basic principle is that the output of the ISFET-operational amplifier with a Ta_2O_5/SiO_2 gate (with pH sensitivity of about 58-59 mV/pH) ISFET is differentially amplified against the output of the other on-chip ISFET-operational amplifier with a $SiO_XN_y/Si_3N_4/SiO_2$ gate ISFET (with pH sensitivity

of about 18-20 mV/pH). The offset voltage as well as the temperature dependence of the ISFET electrochemical component of each unity-gain configured ISFET operational amplifier is fed into a differential amplifier, where two offset components were cancelled out through the common-mode rejection. However, this cancellation relies on the precondition that these two ISFET sensors having different sensitivity materials should be electrical identical and matched. However, this is not easy to realize due to the fact that different kinds of the insulator as well as the different thickness of the insulators leads to different values of gate capacitance C_{OX}. According to the Hal and Eijkel's theory [41] on the pH sensitivity of the ISFET expressed by equation (2.18) in Chapter II, the different pH sensitivities of different materials are reflected by the pH sensitivity parameter α. Therefore, the electrochemical components with respective sensing materials have different temperature coefficients which would generate a differential signal at different temperatures. Based on (2.18), the *T.C.I.* of the two types of ISFET device in Fig. 5.3 can be expressed as:

$$\frac{\partial \psi_{eo1}}{\partial T} = -2.303 \frac{k * pH}{q} \alpha 1 \tag{5.4.a}$$

$$\frac{\partial \psi_{eo2}}{\partial T} = -2.303 \frac{k * pH}{q} \alpha 2 \tag{5.4.b}$$

With (5.4.a ─ 5.4.b), It can be obtained that

$$\frac{\partial \psi_{eo1}}{\partial T} - \frac{\partial \psi_{eo2}}{\partial T} = -2.303 \frac{k * pH}{q} (\alpha 1 - \alpha 2) \tag{5.4.c}$$

Obviously, the T.C. of the insulator-electrolyte potential of different sensors cannot be fully cancelled each other due to the different pH sensitivity parameters, $\alpha 1$ and $\alpha 2$. The situation would be worse in case of high pH values,

which can be read from (5.4c) that the value of $\frac{\partial \psi_{eo1} - \partial \psi_{eo2}}{\partial T}$ is proportional to the pH value of the solution, which means the higher pH value, the more temperature sensitivity of the differential insulator-electrolyte potential.

5.1.4. A Differential Configuration with Dual ISFET Devices

Instead of different types of ISFET operational amplifiers, other research works employed two types of ISFET sensors (one with Si_3N_4 ion sensitive layer, the other with SiO_2 ion sensitive layer) with different pH sensitivity in differential configuration [62], [69] as depicted in Fig. 5.4. It consists of two non-saturation ISFET-SF circuits, which have been discussed in Chapter IV, and a voltage-to-current converter that converts the differential output voltage signals into single-ended output current signal. Temperature dependency can be reduced to a certain level through common-mode rejection.

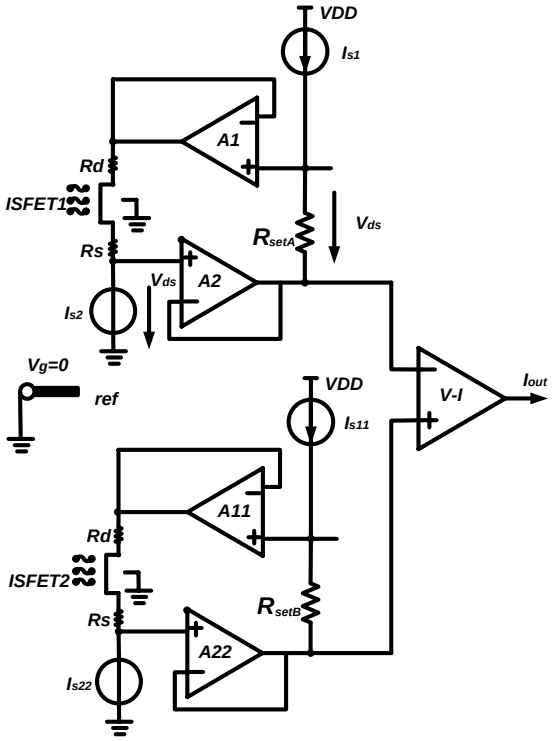

Fig. 5.4 Differential configuration with dual ISFET devices [62]

However, this methodology suffers from several limitations. Firstly, these two ISFET devices in the integrated environment are suffered from the body effect that has the possibility of accuracy limitation, which has already been analyzed in Chapter IV. Secondly, the temperature compensation range is limited due to the non-identical body effects arising from these two ISFETs with different sensitivities. As previously mentioned, the different sensitivities of these two ISFETs will lead to the different *T.C.I.* values. Thirdly, the reliability issue limits the measurement range. It is mainly because the H^+ ion will easily penetrate through the SiO_2 sensitive layer and reach the n-channel under the sensitive insulator layer. Therefore, this ISFET device will be easily damaged in acidic environment. It is only suitable for biomedical application where the pH range is about 6.5 to 7.5.

5.1.5. Summary of Temperature Compensation Techniques

All temperature compensation methods are compared and summarized in Table 5.1. It can be observed that, of those methods aforementioned, the temperature characteristic of the ISFET is stabilized at a particular pH value or in a narrow pH range. The temperature compensation of the ISFET becomes more difficult in solutions of a broader range of pH values because the temperature coefficient (*T.C.*) of electrochemical component is a function of pH value. More importantly, the ISFET temperature characteristic tends to exhibit nonlinear behavior. The straight-line-based temperature compensation techniques as reviewed above limit the scope when dealing with actual nonlinear temperature characteristic of the ISFET device at different pH values. Therefore, it is

particularly challenging for ISFET sensors to operate in an environment in context of measurement environment with a wider pH range together with fluctuation of temperature. This leads to the research and development of new temperature compensation in the following section 5.3 in order to remove the limitations from the prior-art methods.

Table 5.1 Summary of published techniques for ISFET temperature compensation

Design Technique	ISFET/MOSET Differential Pair [59]	ISFET-MOSFET differential pair with p^+-n diode sensor [76]	Differential sensing of dual ISFET Op-amps [60]	Differential configuration with dual ISFET devices [62]
Temperature compensation approach	Differential	Differential plus Diode temperature sensor	Differential	Differential
pH Range	pH: 6.5-7.5	vicinity of particular pH value	pH: 6.5-7.5	pH: 6.5-7.5
Number of ISFET sensors with different sensing material	1	1	2	2

5.2 A Review of Time-Variant Compensation Techniques

As revealed in (5.1), the accuracy of ISFET would also be strongly impeded by the time-variant parameters, such as the drift and slow pH response. Little research has been conducted in this area but it is now emerging as an important topic for ISFET sensor circuit. However, few research works have been seen on the ISFET drift and slow pH response compensation techniques [80]-[83]. In one reported study [81], it made use of the relatively small instantaneous drift

rate in the ISFETs to compensate the drift signal superimposed on the sensor output. This method is based on the fact that the time constant characterizing drift is in the order of several hours. This implies that over an individual sampling time of several seconds, the variation in the ISFET output signal contributed by drift can be negligible when compared to that contributed by a change of the pH input signal. As the drift and temporal variations in the pH arise from the independent physicochemical process, the differential of the ISFET output voltage, *dM*, can be written as [81]:

$$dM = \frac{\partial M}{\partial pH} \times dpH + \frac{\partial M}{\partial t} \times dt \tag{5.5}$$

Dividing (5.5) by Δt, and let Δt → 0, it yields

$$\frac{dM}{dt} = \frac{\partial M}{\partial pH} \times \frac{dpH}{dt} + \frac{\partial M}{\partial t} \tag{5.6}$$

$\frac{\partial M}{\partial t} \to 0$ as Δt → 0 for the inherently slow nature of drift. Therefore, over a sufficiently small time interval, (5.6) implies that the instantaneous time rate of change of the ISFET output voltage is dominated by the temporal variation of pH. As a result, a correct device response can be obtained by integrating the differential change in the measured ISFET output voltage. However, one of the main limitations of this method is that of the thermo-stable measurement set-up being required to avoid the influence of ambient temperature variation due to strongly temperature dependence of the ISFET device. Meanwhile, the ISFET drift rate has an exponential increasing tendency with increasing the pH value as well as with increasing temperature value [94]. Furthermore, comparing (5.6) with (5.1), it can be observed that another nonideal effect, slow pH response, in time domain had not been taken into account in the work [81].

In another research work [82], it employed negative feedback in the electronic path to overcome the long-term drifts. This method is based on the fact that if the drain-to-source current (I_{DS}) of ISFET is kept constant, an increase in drain-to-source voltage (V_{DS}) produces a decrease in gate-to-source voltage (V_{GS}) with constant pH value. Thus, the variation of V_{GS} of ISFET caused by drift in time domain can be counteracted by regulating the V_{DS}, which is controlled by the electronic conditioning circuit. However, this method will only be effective when the temperature is kept constant. Since the pH sensitivity of ISFET device ($\partial V / \partial pH$) is strongly temperature dependent, the integral of the differential change in the measured output voltage of the ISFET is not only a function of pH but also a function of temperature.

Further recent work has employed a corrected double sampling (CDS) technique for ISFET drift reduction [84]. The CDS technique samples the continuous signal during two clock phases and the difference between these two samples is resolved through computation of MATLAB. However, it also requires a thermal stable environment to avoid the thermal drift of ISFET device. The change caused by the drift and temperature effect simultaneously would jeopardize the accuracy of the final results.

Based on this observation, there is a need of new drift compensation technique combined with the new method to overcome the above stated limitations. This will be discussed in the following section 5.4.

5.3 Proposed Temperature Compensation Technique

5.3.1 ISFET Athermal Biasing Points in Reference pH7 Buffer Solution

This proposed temperature compensation technique stems from the physical theory of mutual compensation of the temperature variation of the mobility and threshold voltage to achieve the zero temperature coefficients (*Z.T.C.*) biasing point in MOSFET. However, the main difficulty arises from the fact that the *T.C.* of the ISFET threshold voltage is a function of the pH value. To deal with this problem, the electrochemical theory of ISFET is combined with the physical theory of MOS transistor to establish the theoretical basis for the research of dynamic biasing current temperature compensation technique. Mutual compensation of the temperature effects of the mobility and threshold voltage in field-effect transistors are exploited in the literature [90] [95]-[98]. Detailed investigation for the *Z.T.C* point in the MOS transconductance characteristics has been reported by [97]. Despite the difference between the MOSFET and ISFET comes from their threshold voltages, the mutual compensation analytical approach on the MOSFET aspect can be extended to the ISFET counterpart. Due to the variation of the *T.C.* of the ISFET threshold voltage in different pH buffer solutions, it is natural to choose the pH7 buffer solution as the reference parameter with respect to other buffer solutions. The measured and analytical results of the reference parameters form the initial guess values for solving the nonlinear equations in the temperature compensation process in next phase. Therefore, the analysis of mutual compensation on the ISFET in *pH7* buffer solution is firstly carried out. Similar

to the analysis on the MOSFET in [97], it is possible to incorporate temperature effect on mobility (2.23) and threshold voltage (2.24) and neglecting the dc voltage drop of source diffusion resistor in an ISFET. When a constant current source $I_B = I_{DS}$ is applied to an ISFET-LSD interface circuit in Fig. 4.6, the gate-to-source voltage of the ISFET (4.13) in pH7 buffer solution, for a given temperature T_1 can be approximated as

$$V_{GS(pH7)}(T)\Big|_{T=T_1} \approx V_{th(pH7)}(T_0) + K_{VT(pH7)} \times (T_1 - T_0) + \sqrt{\frac{2I_{DS}}{\frac{\beta_0}{1+\theta\left[V_{GS(pH7)}(T_1) - V_{th(pH7)}(T_1)\right]}\left(\frac{T_1}{T_0}\right)^m}} \tag{5.7}$$

Here, $V_{th(pH7)}(T_0)$ is the threshold voltage of the ISFET in pH7 buffer solution at room temperature and $K_{VT(pH7)} = \partial V_{th(pH7)} / \partial T$ is the *T.C.* of the ISFET threshold voltage in *pH7* buffer solution. θ is the mobility degradation parameter and $\beta_0 = \mu_0(T_0) C_{OX}(W/L)$. In a saturation-based ISFET, the variation of the temperature-dependent mobility term $\theta\left[V_{GS(pH7)}(T_1) - V_{th(pH7)}(T_1)\right]$, from temperature T_1 to another temperature T_2 can be significantly small due to minute value θ, $\left(V_{GS(pH7)}(T_1) - V_{th(pH7)}(T_1)\right)$ and the square root effect in the gate overdrive term. For this reason, the room temperature-based constant $\left(V_{GS(pH7)}(T_0) - V_{th(pH7)}(T_0)\right)$ as a replacement of $\left(V_{GS(pH7)}(T_1) - V_{th(pH7)}(T_1)\right)$ will be useful to simplify the calculation without losing the accuracy. Therefore, (5.7) can be further approximated as

$$V_{GS(pH7)}(T)\Big|_{T=T_1} \approx V_{th(pH7)}(T_0) + K_{VT(pH7)} \times (T_1 - T_0) + \sqrt{\frac{2I_{DS}}{\frac{\beta_0}{1+\theta\left[V_{GS(pH7)}(T_0) - V_{th(pH7)}(T_0)\right]}\left(\frac{T_1}{T_0}\right)^m}}$$

(5.8)

Then, the *T.C.* of $V_{GS(pH7)}(T)$ can be obtained as

$$\left.\frac{\partial V_{GS(pH7)}(T)}{\partial T}\right|_{T=T_1} = K_{VT(pH7)} + \sqrt{\frac{2I_{DS}}{\beta_0 \left[1+\theta\left[V_{GS(pH7)}(T_0)-V_{th(pH7)}(T_0)\right]\right]}}\left(\frac{T_1}{T_0}\right)^{(-m/2)-1}\left(\frac{-m}{2}\right)\frac{1}{T_0} \tag{5.9}$$

Like the compensation analysis of the MOSFET [97], for any given temperature T_1, one can find a biasing current that is able to satisfy $\left.\partial V_{GS(pH7)}/\partial T\right|_{T=T_1}=0$. This is regarded as *Z.T.C.* point or athermal operating point. This optimum biasing current can be obtained by solving the equation as follows:

$$\left.\frac{\partial V_{GS(pH7)}(T)}{\partial T}\right|_{T=T_q} = 0 \tag{5.10}$$

Thus, the corresponding optimum biasing current for the ISFET to sense in pH7 buffer solution can be derived as:

$$I_{DS(pH7)} = \frac{2K_{VT(pH7)}^2 T_0^2}{m^2} \times \frac{\beta_0}{1+\theta\left[V_{GS(pH7)}(T_0)-V_{th(pH7)}(T_0)\right]}\left(\frac{T_1}{T_0}\right)^{m+2} \tag{5.11}$$

Therefore, the (5.7)-(5.11) form the basis for the nonlinear temperature compensation in next section.

5.3.2 Dynamic Biasing Current Temperature Compensation

Instead of the constant biasing current, the ISFET can be biased dynamically via a systematic calculation of the specific parameters in a smart sensor operation environment. There is a possibility to achieve *Z.T.C.* at different *pH* values in a defined temperature range. In order to accomplish the task, it begins

with the derivation of the temperature-dependent threshold voltage of the ISFET in a unified form and the optimum biasing current for the athermal point at any *pH* in a temperature range. Steps are summarized at the end.

With reference to (2.18), the value of ψ_{eo} at solution of *pH7* and other *pH* values can be expressed as follows:

$$\psi_{eo(pH7)} = -2.303\frac{kT}{q}\alpha \cdot pH7 + C \tag{5.12}$$

$$\psi_{eo(pH)} = -2.303\frac{kT}{q}\alpha \cdot pH + C$$

$$= -2.303\frac{kT}{q}\alpha \cdot (pH - pH7) + \psi_{eo(pH7)} \tag{5.13}$$

When incorporating the *pH7* as a reference value and the respective temperature-dependent term for the threshold voltage related chemical part (5.13) and MOS part (2.24), the unified temperature-dependent threshold voltage of the ISFET in any pH value can be written as:

$$V_{th(ISFET)}|_{T=T_1} = V_{th(pH7)}(T_0) + K_{VT(T_1-T_0)} + 2.303\frac{kT_1}{q}\alpha \cdot (pH - pH7) \tag{5.14}$$

at a temperature T_1. Furthermore, in (5.13)

$$\Delta pH = pH - pH7 \tag{5.15}$$

Similar to (5.7), the temperature-dependent gate-to-source voltage of the ISFET in any pH value can be approximated as

$$V_{GS(pH)}(T)|_{T=T_1} \approx V_{th(ISFET)}(T_1) + \sqrt{\frac{2I_{DS}}{\frac{\beta_0}{1+\theta\left[V_{GS(pH)(T_0)} - V_{th(ISFET)}(T_0)\right]}\left(\frac{T_1}{T_0}\right)^m}} \tag{5.16}$$

at a temperature T_1.

Using the same method of analysis on the pH7 buffer solution and assuming a biasing current of I_{DS}, the *T.C.* of gate-to-source voltage of ISFET in any given pH buffer solution can be derived as follows:

$$\frac{\partial V_{GS(pH)}(T)}{\partial T}\Big|_{T=T_1} = K_{VT(pH7)} + 2.303\frac{k}{q}\alpha\cdot\Delta pH + \sqrt{\frac{2I_{DS}}{\frac{\beta_0}{1+\theta\left[V_{GS(pH)}(T_0)-V_{th(ISFET)}(T_0)\right]}}}\left(\frac{T_1}{T_0}\right)^{(-m/2)-1}\left(\frac{-m}{2}\right)\frac{1}{T_0} \tag{5.17}$$

Similarly, for any given pH buffer solution, the optimum biasing current that forces the ISFET to operate at the athermal point can be obtained from:

$$\frac{\partial V_{GS(pH)}(T)}{\partial T}\Big|_{T=T_1} = 0 \tag{5.18}$$

By solving (5.18), we have

$$I_{DS(pH)} = \left(K_{VT(pH7)} + 2.303\frac{k}{q}\alpha\cdot\Delta pH\right)^2 T_0^2\frac{2}{m^2}\left(\frac{T_1}{T_0}\right)^{m+2}\times\frac{\beta_0}{1+\theta\left[V_{GS(pH)}(T_0)-V_{th(ISFET)}(T_0)\right]} \tag{5.19}$$

Therefore, the optimum biasing current required for the ISFET to work around the athermal point in different pH buffer solutions is a function of ΔpH and pH through (5.19). However, the difficulty of implementing this methodology in practical pH measurement is that the value of ΔpH cannot be obtained directly. It is because the pH value of the measured solution can be unknown. To overcome this obstacle, a numerical iteration technique is proposed. This stems from the fact that V_{out}=V_{GS} is linearly proportional to the pH value in absence of body effect at fixed temperature while the temperature-dependent sensitivity of ISFET device displays nonlinear relationship with the drain current I_{DS}. As the pH is a function of V_{out} and I_{DS} is a function of temperature-dependent sensitivity, the initial guess values at room temperature can be approximated to

obtain $I_{DS(pH7)}$ (5.11) from extracted process parameters and measured reference parameters. Consequently, the *pH* value can be obtained from the ISFET reference sensitivity. It is then solved nonlinearly for finding the optimum biasing current to achieve the *Z.T.C.* of ISFET at different pH values using an iterative method in numerical analysis. The procedures to implement the iteration algorithm are summarized as follows.

Step 1) Measure the V_{out}—pH transfer characteristic of the ISFET at different biasing currents for targeted test solutions pH_{min}, *pH7* and pH_{max} at room temperature as reference data. Since the *pH7* lies between pH_{min} and pH_{max}, for a natural choice, the $I_{DS(pH7)}$ (5.11) is treated as an initial biasing current for ISFET operating around the athermal point in the *pH7* buffer solution. Using the slope concept, the pH_C can be estimated through the reference sensitivity data using the following equations:

$$pH_C = pH_4 + \frac{V_{out} - V_{out(pH4)}}{\left(V_{out(pH7)} - V_{out(pH4)}\right)} \Big/ \left(pH7 - pH4\right) \tag{5.20}$$

or

$$pH_C = pH_7 + \frac{V_{out} - V_{out(pH7)}}{\left(V_{out(pH9)} - V_{out(pH7)}\right)} \Big/ \left(pH9 - pH7\right) \tag{5.21}$$

Note that pH_C is the pH value being converted from the measurement of the output voltage of the transducer. If the V_{out} is smaller than the $V_{out(pH7)}$, (5.20) will be used, otherwise, (5.21) will be selected.

Step 2) Then, the pH_C is substituted into (5.15). Since $\Delta pH = pH - pH7 = pH_C - pH7$, the calculated ΔpH is substituted into (5.19) again to iterate another new biasing current.

Step 3) The ISFET is then applied with the new biasing current to obtain another new voltage output of interface circuit, which is used to find another new pH_C.

The proposed iteration-based temperature compensation method will be demonstrated in the electrochemical measurement in next chapter.

5.4 Proposed Time-Variant Compensation Technique

As described in chapter II, both the ISFET drift and slow pH response are time-variant parameters. Although arising from independent physicochemical processes, they both cause instability in the dc operating point of ISFET as a time-dependent ISFET threshold voltage, which can be quantitatively represented as $\Delta V_{th(ISFET\_Drift)}(t)$ and $\Delta V_{th(ISFET\_Slow)}(t)$, respectively. For these two effects on time-dependent ISFET threshold voltage overlap in time domain, they can be functionally merged together and represented by one lumped parameter, $\Delta V_{th\_time}(t)$:

$$\Delta V_{th\_time}(t) = \Delta V_{th(ISFET\_Drift)}(t) + \Delta V_{th(ISFET\_Slow)}(t) \tag{5.22}$$

The first term in (5.22), which has been postulated to be associated with the slow and temporal change of the overall gate insulator capacitance [26], will always occur in the positive direction. The second term would depend on the positive or negative pH step produced [82]. Therefore, the overall time-variant component, $\Delta V_{th\_time}(t)$, could be in positive or negative direction, as demonstrated in Fig. 5.5 and Fig. 5.6. As will be described in next chapter, the experiment pertaining to the long-term pH monitoring was carried out when the pH value of the solutions was changed in a step sequence of pH7-pH7—

pH5.65—pH4—pH5.65—pH7—pH9 at interval of one hour. So in initial pH7 solution without applying pH step, the lumped parameter in (5.22), $\Delta V_{th\_time}(t)$ is contributed only by $\Delta V_{th(ISFET\_Drift)}(t)$ thus showing positive slop in Fig 5.5. However, in Fig.5.6, a negative slop of ISFET output voltage can be observed, which is due to the applied negative pH steps from pH5.65 to pH4.

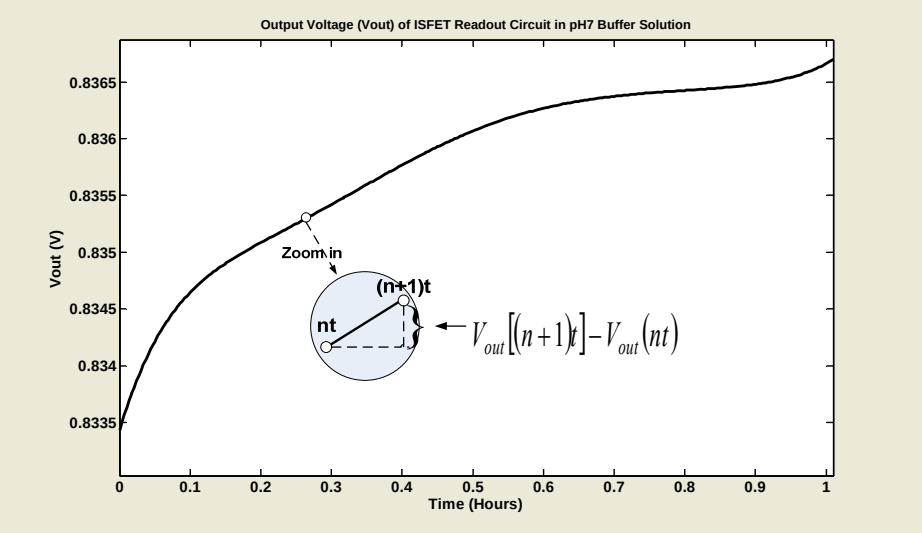

Fig. 5.5 Output voltage of ISFET in pH7 solution without pH step applied

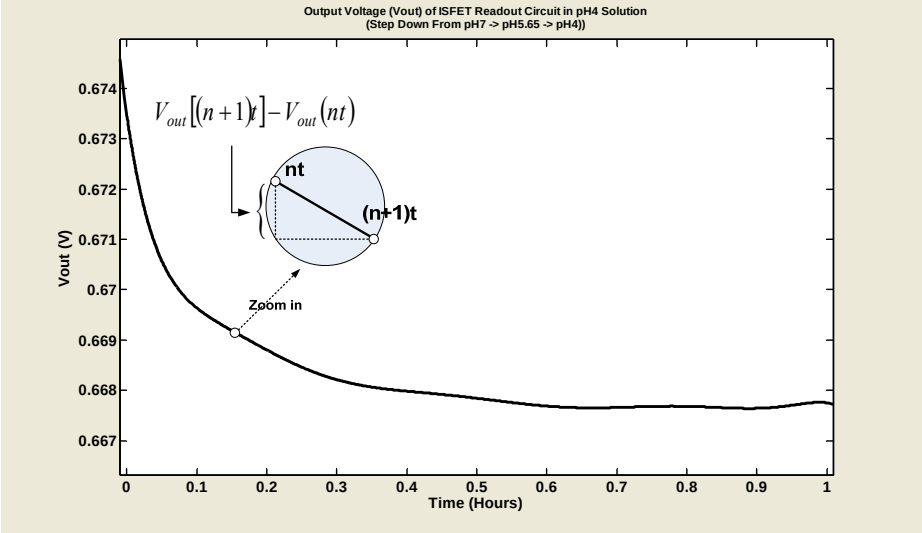

Fig. 5.6 Output voltage of ISFET in a case of pH solution steps from pH5.65 to pH4

The basic concept of the proposed ISFET time-variant compensation technique is to keep the relationship of the input signal (pH value)-output signal (voltage) of the ISFET at a certain level of accuracy by correcting the calibration data stored in the memory by the parameter, $\Delta V_{th\_time}(t)$ in (5.22) on the basis of the predictive result. In case of long-term pH monitoring, the output voltage of the readout circuit that is the gate-source voltage of the ISFET, will deviate by an amount of $\Delta V_{th\_time}(t)$ caused by the deviation of the ISFET threshold voltage through the ISFET drift and slow *pH* response. Therefore, the output voltage of the readout circuit cannot be converted to pH value precisely based on the two equations (5.20) and (5.21), when referenced to the original calibration data, $V_{Calib(pH4)}$, $V_{Calib(pH4)}$, and $V_{Calib(pH4)}$. One way to correct this error is to re-calibrate the ISFET in standard pH buffer solution to update the relationship between the input pH signal and the output voltage value. However, frequently calibrating ISFET sensor is not only costly but also unpractical for long term monitoring purposes. In this proposed ISFET time-variant compensation technique, the calibrated data is automatically updated in real time using the microcontroller hardware and software resource in the process of data acquisition and signal processing in the digital domain. Therefore, the formula (5.20) and (5.21) was modified to:

$$pH_C(t) = pH4 + \frac{V_{out}(t) - \left(V_{Calib(pH4)} + \Delta V_{th\_time}(t)\right)}{\left[\left(V_{Calib(pH7)} + \Delta V_{th\_time}(t)\right) - \left(V_{Calib(pH4)} + \Delta V_{th\_time}(t)\right)\right] / (pH7 - pH4)} \tag{5.23}$$

and

$$pH_C(t) = pH7 + \frac{V_{out}(t) - \left(V_{Calib(pH7)} + \Delta V_{th\_time}(t)\right)}{\left[\left(V_{Calib(pH9)} + \Delta V_{th\_time}(t)\right) - \left(V_{Calib(pH7)} + \Delta V_{th\_time}(t)\right)\right]/(pH9 - pH7)} \tag{5.24}$$

where $V_{out}(t)$ is the measured output voltage of the ISFET readout circuit in time domain. It can be observed that the deviation of $V_{out}(t)$ in time domain by amount of $\Delta V_{th\_time}(t)$ can be compensated by the updated calibration data, which indicates that the output voltage is able to be converted to pH value, $pH_C(t)$ precisely.

The key point of achieving this goal is to precisely detect the value of time-variant component, $\Delta V_{th\_time}(t)$. According to the models [24]-[26], [35] for time-variant nonidealities, the time constants characterizing the drift and slow pH response are in the order of several hours and several minutes, respectively, while the intrinsic pH response time for an ISFET is in the order of milliseconds [26]. Therefore, it is easily to distinguish the time-variation component, $\Delta V_{th\_time}(t)$ from the solution pH-variation component, $(\partial V / \partial pH) \times \Delta pH$ by periodically sampling the output voltage of the readout circuit over a time interval of a few seconds and comparing two successive samples, which is demonstrated as time point of nt and (n+1)t in Fig. 5.5 and Fig. 5.6 in pH7 and pH4 solutions, respectively. For instance, considering the employed embedded 12-bit ADC with ±1 LSB differential (DNL) and ±1 LSB integral nonlinearity (INL) [101], the worst nonlinearity could lead to ±2 LSB in estimation, which is equivalent to ±1 mV with the ADC reference voltage of 1.8V. Therefore, the maximum fluctuation on the

converter results due to the DNL and INL could be 2mVpp (peak-peak). Further considering other potential noise coupling from the digital blocks of the microcontroller, the threshold detection voltage is chosen to be 2.7mV under careful design of the PCB (Printed Circuit Board), which is equivalent to a pH of 0.05 unit. If the differential voltage between every two successive samples is less than the detection threshold of 2.7mV, it is treated as a time-variant component and will be accumulated with the old time-invariant component stored in the memory in time domain. Although the overall time variant component is strongly nonlinear as shown in Fig. 5.5 and Fig. 5.6, the segment of two successive sampling point, nt and (n+1)t with interval of only 2 seconds can be viewed as linear.

Therefore, the time variant component defined in equation (5.22) is approximately evaluated by this accumulated value, $\Delta V_{th\_time}^{*}(t)$, which can be expressed as follows:

$$\Delta V_{th\_time}(t) \approx \Delta V_{th\_time}^{*}(t) = \sum_{n=1}^{\infty} V_{out}[(n+1)t] - V_{out}(nt) \tag{5.25}$$

Alternately, if a differential voltage between two successive samples is more than the detection threshold of 2.7mV, it can be viewed as a change in the pH value of solution, which will trigger the ISFET dynamic current temperature compensation. In this case, the pH measurement system has to restart the temperature compensation procedure in order to bias the ISFET in athermal point for any new pH value. As analyzed in earlier section of the proposed ISFET temperature compensation technique, the ISFET has different athermal biasing points at different pH solutions. Therefore, the integral summary can

precisely reflect the actual time-variation components, $\Delta V_{th\_time}(t)$, and is thus employed to correct the initial calibration data when converting the output voltage of ISFET to corresponding pH value based on the equations (5.23) and (5.24).

As a final remark, the proposed time-variant compensation technique can operate in the temperature fluctuation environment when incorporating nonlinear temperature compensation for wide pH range sensing. This overcomes the conventional long-term drift compensation techniques that rely on constraint of constant temperature.

5.5 Summary

The intrinsic nonideal characteristics of the ISFET sensor, such as the drift mechanism, slow pH response and nonlinear temperature dependence have significantly destroyed the accuracy of the ISFET sensor in application for long term pH monitoring. With support of the intrinsic simple structure of the ISFET-LSD readout circuit presented in chapter IV, a novel ISFET temperature compensation technique which gives a low cost solution at expense of increasing computation complexity is proposed. The derivation of a unified expression for temperature-dependent ISFET threshold voltage in association with the mutual compensation analysis on mobility and threshold voltage establish the theoretical basis equations for temperature compensation purpose. Through the iteration method for solving nonlinear equations, there exists an optimum biasing current for athermal point of the ISFET at different pH values in a temperature range. This is contrasting to the conventional techniques that

use circuit means to provide linear or nonlinear *T.C.* compensation, which is valid for a narrow pH range. A novel ISFET time-variant compensation technique is also proposed to compensate both the ISFET drift and slow pH response. It takes advantage of the microcontroller hardware and software resource to correct the calibration data of the ISFET stored in the memory during the real time measurement. Further incorporating the proposed ISFET dynamic current temperature compensation technique, it overcomes the key drawback of the conventional ISFET drift compensation techniques that rely on the thermo-stable measurement environment to produce quality results. The effectiveness of the proposed compensation methods will be demonstrated by experimental results in following chapter.

CHAPTER VI

Proposed Intelligent ISFET Sensory System

On the basis of the accuracy, programmability, repeatability and easy-to-use feature, a microcontroller-based instrumentation system will provide the desired accuracy and flexibility. It is regarded as the most promising methodology for the design of an ISFET sensory measurement system. Based on the proposed work of ISFET interface circuit in Fig 4.6, this chapter presents a new intelligent ISFET sensory system dedicated to a precision pH sensory function as well as a long-term monitoring capability without being jeopardized by temperature and drift fluctuations in the water-quality monitoring environment. The smart system design includes (i) the dedicated system architecture which comprises the proposed ISFET-LSD interface IC combined with a novel wide dynamic current biasing circuit being controlled by a low-power microcontroller hardware system and (ii) the dedicated instrumentation-based software running the process defined by the proposed temperature and drift compensation techniques presented in Chapter V, for realization of an ultimate smart compensation algorithm.

6.1 System Architecture and Operation

6.1.1. Systematic Overview

Dedicated hardware on basis of flexible programming feature of microcontroller serves as an automation platform for signal translation by the ISFET interface integrated chip (IC), numerical computation, data storage,

implementation of the smart compensation algorithms and communicating with peripherals for the smart sensor signal processing. The system block diagram is depicted in Fig. 6.1, which consists of an improved ISFET interface IC incorporating a recently published ISFET-LSD readout circuit presented in Chapter IV with a new programmable wide dynamic biasing current circuit, a 12-bit Digital-to-Analog Converter IC (TLV5616) [103], a 16-bit high-performance low-power microcontroller (MSP430F149) [101] with built-in 12-bit Analog-to-Digital modular and RS232 facilities for data transmitting, power management unit (PMU) providing power supply to the whole system as well as the precise reference voltages to DAC and ADC, a LCD display module and the keypads module providing the communication channel between the microcontroller and user. The keypads, which actually consist of a number of switches, are often used as a primary input device for the embedded microcontroller. It is noted that the ISFET interface IC has been fabricated using TSMC 0.25 μm CMOS process technology. The whole system is powered at a single 3.3V supply, which is provided by a low dropout regulator (LDO) in the PMU. The biasing current of the ISFET can be fully programmed by microcontroller through the 12-bit DAC, TLV5616, and the output of the ISFET readout circuit is sampled and converted into digital domain for further signal processing. The final measurement results as well as other useful information can be displayed in the LCD or transmit to PC (personal computer) via RS232 port.

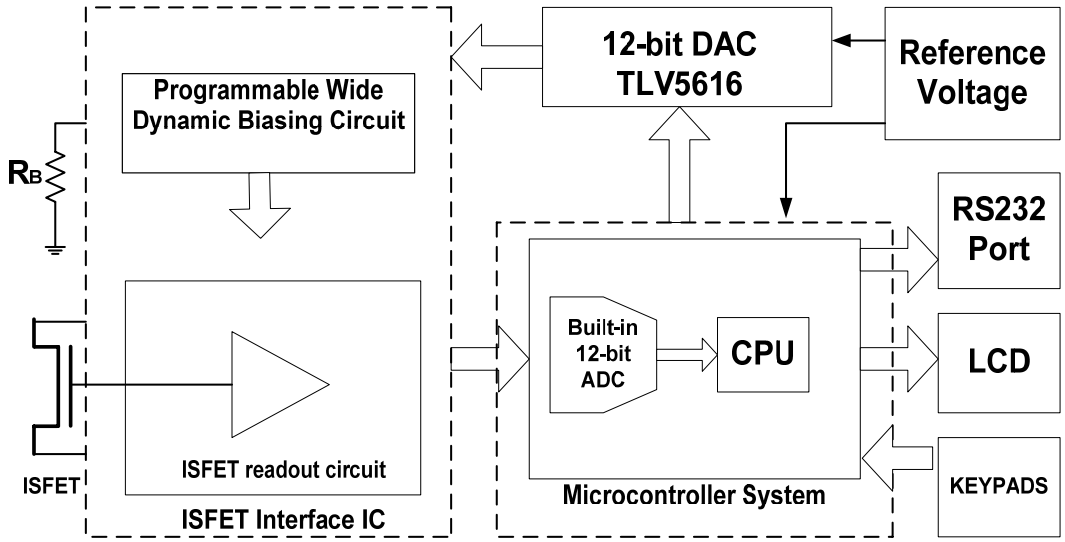

Fig. 6.1 Block diagram of the microcontroller-based pH measurement system

6.1.2. ISFET Readout Circuit with Wide Dynamic Biasing Current Circuit

The ISFET sensor usually operates with an analog readout circuit to translate the pH physical variable to voltage domain for sensor signal processing. It is desirable for the circuit to exhibit good sensitivity, good linearity, insignificant bulk modulation, low circuit temperature dependence and ease of compensation. The ISFET sensory system design strategies follow the desirable goals and extend the ISFET-LSD interface circuit presented in Chapter IV, to the replacement of the conventional current source with a new programmable wide dynamic biasing current circuit as shown in Fig. 6.2. Such an arrangement supports the tasks of long-term monitoring with different temperatures to meet the high precision objective.

As presented in Chapter IV, the ISFET readout circuit aims at detecting the change of the ISFET threshold voltage that reflects the variation of the pH value in the solution. The ISFET working in saturation region is biased by a

constant current I_{B2}. The output of the interface circuit has already derived and presented in Chapter IV, which is repeated here as:

$$V_{out} = V_{gs} = V_{th(ISFET)} + \sqrt{\frac{2I_{B2}}{\mu_n C_{OX}(W/L)}} + I_{B2}R_S \tag{6.1}$$

where the symbols have been defined previously. In order to guarantee that the output V_{out} becomes the only function of the threshold voltage of ISFET, $V_{th(ISFET)}$, which is linearly proportional to the *pH* value of the solution, another design consideration of the ISFET interface circuit involves designing a robust biasing circuit that provides a necessary ISFET biasing current I_{B2}, which should be robust and independent of the *pH*, process and temperature variation. Meanwhile, in order to support the dynamic current temperature compensation algorithm as described in Chapter V in a precision manner, the ISFET drain-source biasing current (I_{B2}) should be precisely programmed by the microcontroller via software. Hence, the circuit technique for improving the precision of the current mirror under dynamic biasing condition is required.

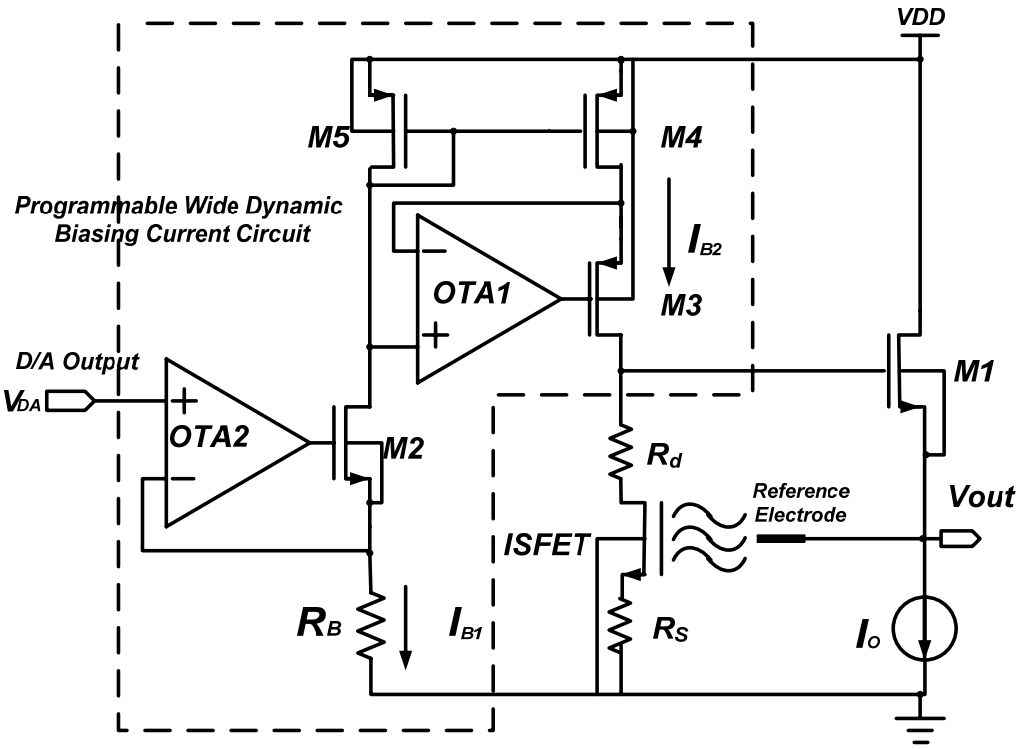

Fig. 6.2 Schematic of ISFET interface IC

(Rd and Rs are ISFET intrinsic drain and source diffusion resistor)

As demonstrated in Fig. 6.2 the biasing portion of the ISFET interface IC, the biasing current I_{B1} is generated by a Voltage-to-Current (VI) converter comprising an operational transconductance amplifier, *OTA2*, a regulated transistor *M2* and an external reference resistor R_B. The *OTA2* is configured in a negative feedback loop to control the voltage from the gate of *M2* to ground. This negative feedback loop adjusts the gate of *M2* until the voltage difference between the two amplifier inputs is zero if the amplifier gain is infinite in ideal case. Therefore, the *OTA2* in association with *M2* clamps the voltage across R_B by the output voltage of the digital-to-analog converter (DAC), V_{DA}, which is programmed by the microcontroller and the biasing current is defined as follows:

$$I_{B1} = \frac{V_{DA}}{R_B} \tag{6.2}$$

The biasing current, I_{B1}, generated by the VI converter is copied to the ISFET device by current mirror. In practice, the amplifier (*OTA2*) gain is finite which means that the voltage across the R_B is not exactly equal to V_{DA}. There are unavoidable static offsets generated by the dc offset of *OTA2* (typically a few mV). So apart from the accuracy of the DAC, the accuracy of the VI converter is limited by the input-referred offset voltage of *OTA2* and the tolerance of external reference resistor R_B (typical of 1%). It is well known that the offset voltage of an op-amp is composed of two components: the systematic offset and the random offset. The random offset primarily results from the mismatches of those devices that are supposedly to be identical in pairs. The schematic of *OTA2* is shown in Fig. 6.3. It is a conventional operational transconductance amplifier (OTA) [102] utilizing the cascode output structure to improve its open-loop gain.

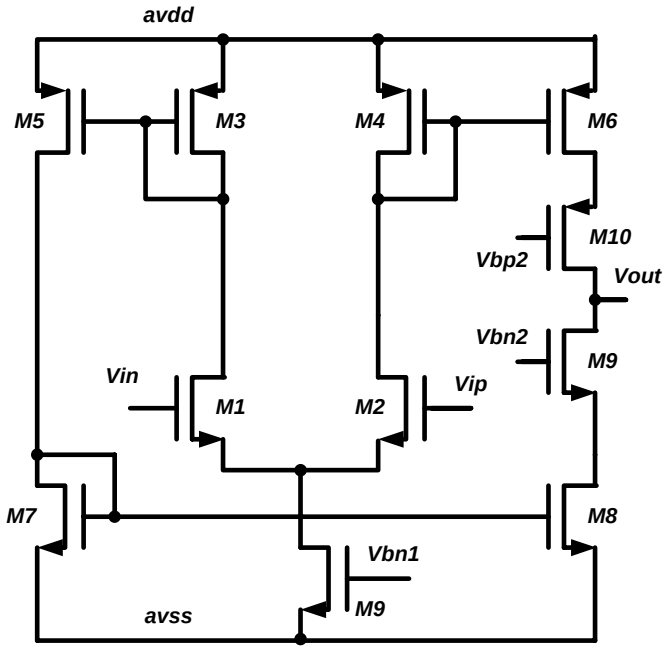

Fig. 6.3 Schematic of Operational Transconductance Amplifier (OTA2) in Fig. 6.2

On the other hand, although there are unavoidable static offsets generated by the dc offset of *OTA2* (a few mV in typical value) and the tolerance of external reference resistor R_B (typical of 1%) to avoid the effect of process and temperature variation on the precision of integrated resistor, these random errors are regarded as the static systematic errors, which will not be harmful to the overall system accuracy because they can be nulled during the system calibration and the measurement procedures. Another dynamic error source coming from the DAC chip can also affect the precision. High accurate DAC chip is therefore needed in the design. The digital-to-analog chip employed in this project is TLV5616 from Texas Instruments, which is a 12-bit voltage output with a flexible 4-wire serial interface. The 4-wire serial interface allows glueless interface to universal synchronous/asynchronous receive/transmit (USART) serial-communication peripheral of MSP430 microcontroller through

serial-peripheral–interface (SPI) protocol. The low differential nonlinearity (DNL), ±0.5LSB in typical case and integral nonlinearity (INL), ±2LSB in typical case, guarantee the precision of the system requirement. This turns out that the dynamic error arising from a wide programmable biasing current becomes one of the most critical design issues. Therefore, in the following section, the prior-published CMOS current mirrors will be reviewed prior to presenting the design consideration of the proposed CMOS current mirror structure.

Generally, there are two types of error sources that limit the accuracy of current mirrors: systematic errors and random errors. Systematic errors are mainly caused by the different voltage across the drain and source terminals of the input and output transistors of current mirror. Meanwhile, the random errors are fundamentally caused by the difference in the electrical parameters between input and output transistors of current mirror, due to the random variations of the process parameter. Refer to the simple CMOS current mirror, it has a merit of wide operation headroom but it displays low resolution due to the potential poor output impedance (dependent upon the choice of channel length) and contributes significant systematic error arising from the different V_{DS} values across the input and output transistor of current mirror. One traditional way to increase the output impedance of the current mirror is to employ the cascode structure, as shown in Fig. 6.4(a). However, the conventional cascode current mirror exhibits a minimum input voltage of $2V_{GS}$, which hinders its application in the proposed ISFET interface circuit with power supply as low as 3.3V. Despite of the high-swing cascode current mirror in Fig. 6.4(b) could further

reduce the input voltage to one V_{GS} by eliminating one diode-connected transistor in the cascode input transistor structure but the constant gate biasing voltage, V_b, applied to the output cascode transistor could only support high precision for a small range of operating current, which can be explained as following. When an input current increases, the gate-source voltage, V_{GS}, of transistor *M2* also increases and so do the V_{GS} and the output current of the output mirror transistor *M3*. As a result, the effective gate-to-source voltage of the cascode transistor *M4* increases as well, thus reducing the drain voltage of *M3* since the cascode biasing voltage, V_b is constant. Towards a limit, it would force the output mirror transistor *M3* into the triode region. Consequently, the accuracy of current mirror is lost. Another method to enhance the output impedance is achieved through the regulated-cascode circuit [104] as shown in Fig. 6.4(c). However, the V_{DS} across the output transistor *M3* is clamped by a constant bias voltage *Vd* and will deviate significantly from the V_{DS} across the input transistor under dynamic biasing operation, introducing dynamic systematic error in a wide input current range. To overcome this problem, the active-input regulated-cascode circuit [105] in Fig. 6.4(d) is able to balance the V_{DS} of both the input and output transistors of the current mirror so as to minimize the systematic offset. However, the active-input regulated-cascode scheme needs two amplifiers that incur extra complexity, power and silicon area. Extra effort has to be paid to guarantee the stability of two high gain loops.

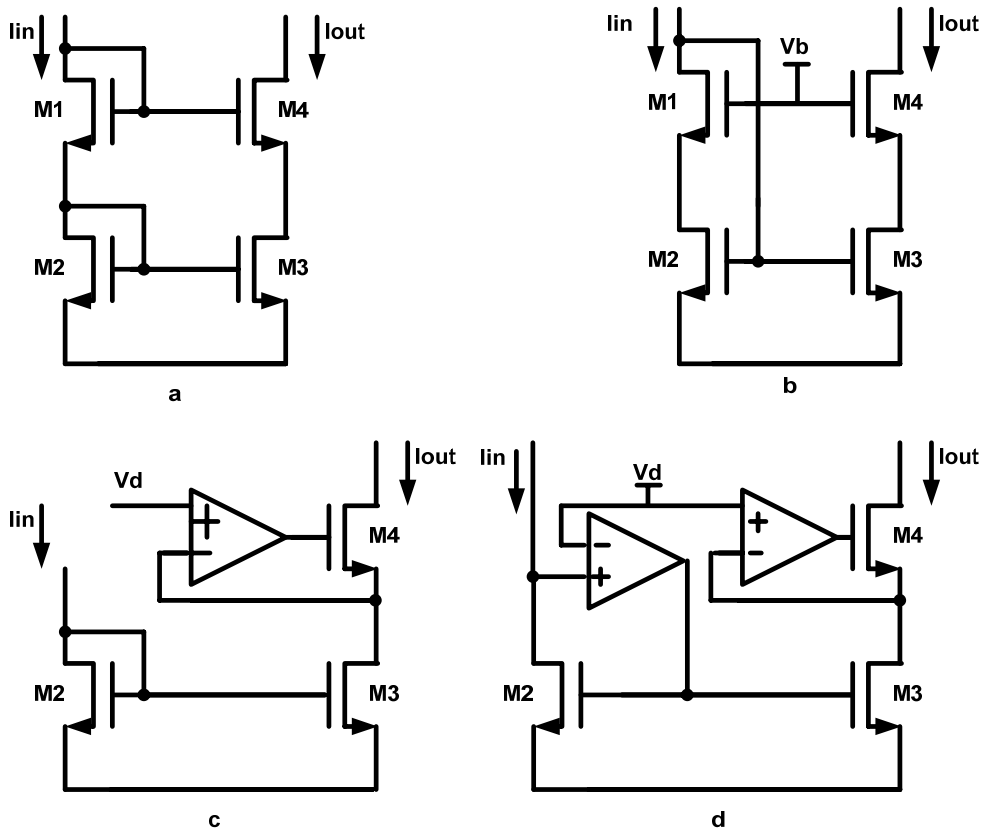

Fig. 6.4 Enhanced current mirror topologies. (a) Basic cascode (b) High-swing cascode (c) Regulated cascade (d) Active-input regulated cascode

In order to meet the requirements of precision as well as to simplify the circuit design, a new V_{DS}-tracked regulated-cascode current mirror topology, consisting of an simple operational transconductance amplifier (*OTA1*) [102], a cascode transistor *M3* and a current mirror transistor pair *M3*-*M4*, is proposed in the robust biasing circuit (dotted box) as shown in Fig. 6.2. The schematic of operational transconductance amplifier (*OTA1*) is demonstrated in Fig. 6.5. The biasing current generated by the VI converter is copied to the ISFET device by this V_{DS}-tracked regulated-cascode current mirror. The input transistor *M5* is diode-configured, having $V_{GS5}=V_{DS5}$ to provide self-biasing voltage for the transistor *M4* to work in saturation region. The *OTA1* is configured in a

negative feedback loop to control the gate voltage of *M3*. This negative feedback loop adjusts the gate-source voltage of transistor *M3* until the voltage difference between the two inputs of *OTA1* is zero, assuming that the *OTA1* gain is infinite. Therefore, the drain-source voltage of transistor *M4* is able to track that of the transistor *M5*, which would significantly reduce the systematic error of the current mirror in wide dynamic input current range. Although there are unavoidable static offsets generated by the dc offset of *OTA1* (few mV in typical value), it will not be harmful to the overall system accuracy because it can be nulled in system calibration. Besides, both the input and output transistors of the current mirror, *M5* and *M4*, are working in saturation region, a typical few mV voltage difference caused by the offset of *OTA1* to the drain-source voltage has negligible effect on the accuracy of the current mirror. Therefore, a simple OTA circuit is adequate to accomplish the task, which would relax the design complexity of *OTA1*. Furthermore, the negative feedback loop configured by *OTA1* would benefit from this simple structure of *OTA1*.

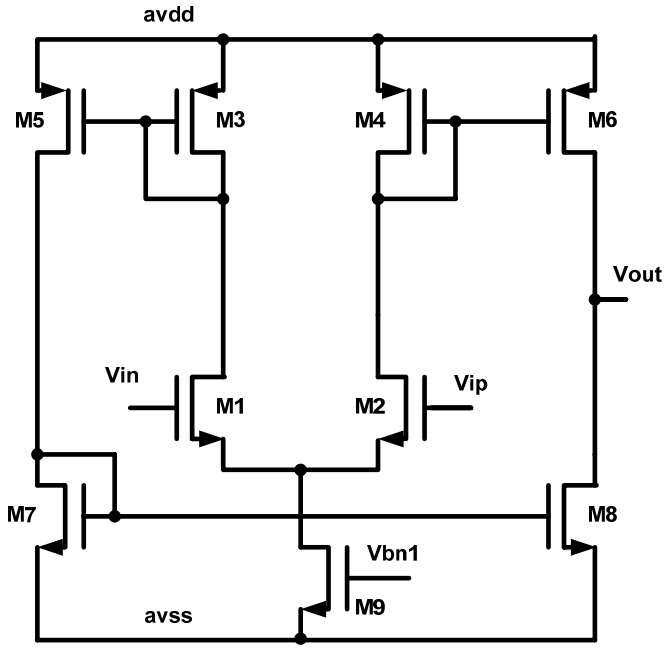

Fig. 6.5 The schematic of operational transconductance amplifier (OTA1 in Fig.6.2)

6.1.3. Microcontroller System with Peripheral Units

The microcontroller in association with its peripherals plays an important role in the intelligent ISFET sensory system. The microcontroller is not only responsible for sampling the analog signal from the output of the ISFET interface circuit and converting to digital domain for further digital signal processing but also implementing the proposed ISFET drift and temperature compensation algorithms proposed in Chapter IV. Therefore, it is also a critical task to choose a suitable microcontroller to satisfy the requirement of current project.

The Texas Instruments MSP430 series [101] is an ultralow power 16-bit RISC (Reduced Instruction Set Computer) microcontroller family consisting of several devices featuring different sets of modules targeted to various

applications. Among the MSP430 series, the device employed in current project is MSP430F149 and its main features are summarized as follows [101]:

- Low Supply-Voltage Range, 1.8V…3.6V
- Ultralow-Power Consumption: Standby mode 1.3μA; RAM Retention off Mode: 0.1 μA
- Low Operating Current: 7 μA at 32kHz, 2.2V; 250 μA at 1MHz, 2.2V
- Five Power-Saving Modes
- Wake-Up from Standby Mode
- 16-Bit RISC Architecture, 125-ns Instruction Cycle Time
- 12-Bit A/D Converter with Internal Reference, Sample-and-Hold and Autoscan Feature
- 16-Bit Timer with Seven Capture/Compare-With-Shadow Registers, Timer_B
- 16-Bit Timer with Three Capture/Compare Registers, Timer_A
- On-Chip Comparator
- Two Universal Serial Synchronous/Asynchronous Communications Interface (USART)
- Serial On-board Programming, No External Programming Voltage Needed; Programmable Code Protection by Security Fuse

The processing unit is based on a consistent and orthogonal CPU (Central Processing Unit) and instruction set. This design structure results in a RISC-like architecture, highly transparent to the application development and notable for its ease of programming. All operations other than program-flow instructions

are consequently performed as register operations in conjunction with seven addressing modes for source and four modes for destination operand. The CPU consists of a 16-bit arithmetic logic unit (ALU), 16 registers, and instruction control logic, which provides reduced instruction execution time and enables the MSP430 to achieve maximum code efficiency as it reduces the register-to-register operation execution time to one cycle of processor frequency. The CPU controls over the program counter, the status register, and the stack pointer (with the reduced instruction set) allows the development of applications with sophisticated addressing modes and software algorithms. The MSP430 devices are configured as von-Neumann architecture, which has code memory, data memory, and peripherals in one address space. As a result, the same instructions are used for code, data, or peripheral accesses. Besides, code may be executed from RAM. Among the MSP430 series, the device employed in current project is MSP430F149, which has 60KB flash memory and 2KB RAM. Instructions fetched from the program memory are always 16-bit accesses, whereas data memory can be accessed using word (16-bit) or byte (8-bit) instructions. Any accessing uses the 16-bit memory data bus (MDB) and as many of the least-significant address lines of the memory address bus (MAB) as required to access the memory locations. Blocks of memory are automatically selected through module-enable signals. This technique reduces the overall current consumption. The program memory is integrated as programmable or mask-programmed memory. In addition to program code, data may also be placed in the ROM section of the memory map and may be accessed using word or byte instructions. This is a useful feature for data tables because the

data tables do not have to be copied to RAM for usage. This unique feature also gives the MSP430 an advantage over other microcontrollers. The data tables are very useful in this project, because calibration of ISFET sensor in standard buffer solutions of different pH values is required prior to the temperature compensation. Thus, the calibration data can be stored in the ROM instead of the extra external memory component. Additionally, since the RAM and ROM are connected to the CPU via the same busses, program code can be loaded into and executed from RAM. This is another unique feature of the MSP430 devices, and provides valuable easy-to-use debugging capability.

Another attractive feature of the MSP430 devices is their low system cost and ultralow-power consumption, which is thank to its basic clock module. The basic clock module of the MSP430 devices allows the best balance of performance and low power consumption with using three internal clock signals. It is very flexible for designer to configure the device working in low-frequency clock source from a watch crystals (32kHz), high-frequency clock source from a standard crystals or Digitally Controlled Oscillator (DCO) clock source, which is an RC-type oscillator with frequency being able to be tuned by software and stabilized by the digital control despite its RC-type characteristics. The MSP430 consumes less than 400μA in active mode when operating at 1 MHz in a typical 3-V system. The DCO provides wake-up operation from the <2 μA standby mode to the fully synchronized operation mode in less than 6 μs. These exceptionally low current requirements, combined with the fast wake-up time, enable building a system with minimum current consumption and maximum battery life.

Another attractive feature of MSP430 devices is its hardware multiplier which is a 16x16 bits peripheral module. As it is not integrated in the CPU, it requires no special instructions and operates independent of the CPU. To use the hardware multiplier, the operands are loaded into registers and the results are available in the next instruction, which means the real-time operation does not require additional clock cycles. In the proposed ISFET measurement system, certain amount of numerical computation as indicated in Chapter V is required for smart compensation algorithm implementation, which would benefit from this hardware multiplier resource.

The embedded 12-bit analog-to-digital converter (ADC) is a high-speed with maximum conversion rate of 200-ksps, extremely versatile analog-to-digital converter implemented on MSP430F149 device. This 12-bit converter with ±1 LSB differential nonlinearity (DNL) and ±1 LSB integral nonlinearity (INL) could introduce the worst nonlinearity of ±2 LSB in estimation, which is equivalent to ±1 mV with ADC reference voltage of 1.8V. This is able to satisfy the target of 0.05 pH accuracy of the pH measurement system.

There are two universal synchronous/asynchronous receive/transmit (USART) serial communication peripherals implemented in the MSP430F149 microcontroller, supporting two serial modes with one hardware configuration. The first mode is the universal asynchronous receive/transmit (UART) communication protocol and the second mode is the serial peripheral interface (SPI) protocol. These modes shift a serial bit stream in and out of the MSP430 at a programmed rate or at a rate defined by an external clock. In current project, one USART was configured as SPI protocol to provide communication

between the microcontroller and external DAC chip, TLV5616. Meanwhile, the other USART was configured as UART protocol to provide communication between the microcontroller and the personal computer (PC).

6.2 Smart Compensation Software Algorithm

Based on the plentiful hardware resource of MSP430 microcontroller, dedicated software has been developed for the intelligent ISFET pH measurement system depicted in Fig. 6.1. The software controls the whole process of pH measurement, including calibration of the ISFET sensor in standard pH buffer solutions, sampling the output voltage of the ISFET readout circuit, nonlinear ISFET temperature compensation at different pH values, ISFET drift and slow pH response compensation, transmitting measurement results into LCD display module and via RS232 port to PC (personal computer). In MSP430 microcontroller design environment, which is the IAR Workbench, both the C and assembler language are supported and can be used together within the MSP430 application. The combination of C and assembler benefits the designer by providing the power of a high-level language as well as the speed, efficiency, and low-level control of assembler. In the following sections, the overall description of the software programming is presented and followed by the description of each block in details.

The overall flow chart of the application specific software programming for the pH measurement system is shown in Fig. 6.6. As described in the flow chart, the system software design enables the users to choose the option of calibrating the ISFET sensor in the standard *pH4*, *pH7* and *pH9* buffer solutions at room

temperature followed by updating the calibration data stored in the memory or skip the calibration procedure but utilizing the previous calibration data read from the memory. This user selectable function provides the flexibility of measurement to the proposed pH measurement system. The function modes are displayed in the LCD as "User Operation Mode Menu" in which the operation mode is entered via the keypads. When the calibration procedure completed, the program returns to the "User Operation Mode Menu" where the user can choose to re-calibrate the ISFET sensor or start measurement procedure. During the measurement procedure, regarding to the temperature and drift compensation, there are four ISFET pH measurement modes: (i) pH measurement with only temperature compensation; (ii) pH measurement with both temperature and drift compensation; (iii) pH measurement with only drift compensation and (iv) pH measurement without temperature or drift compensation. These measurement modes are displayed at the "ISFET Measurement Operation Menu" and can be entered through the keypads device. For measurement mode (ii) involving both temperature and drift compensation, the temperature compensation is carried out prior to drift compensation, during which the ISFET sensor is biased by the optimum biasing current that forces the ISFET to operate at the athermal point. The optimum biasing current for the ISFET is calculated according to the dynamic temperature compensation algorithm proposed in Chapter V. After temperature compensation, the system starts the long-term drift compensation procedure. The timer in the microcontroller is set to be 2 seconds, meaning that the output of the ISFET readout circuit will be sampled by the built-in ADC in every 2 seconds and the difference of every two

successive sampled output voltages will be compared with a detection threshold. The criteria for choosing an optimum detection threshold is based on the fundamental error sources arising from the practical experimental environment, given static parameters such as resolution, differential nonlinearity (DNL) and integral nonlinearity (INL) in the embedded ADC of the microcontroller, static errors of the DAC chip, and the noise plus other potential fluctuations in the output voltage of the ISFET. If the differential value of the two successive sampled output voltage calculated by the controller's computation resource is more than the defined threshold, it can be regarded as change of solution pH value, and hence the ISFET dynamic current temperature compensation will be carried out again, because the optimum biasing current for athermal point would vary in buffer solutions of different pH according to the methodology of dynamic biasing current temperature compensation. On the contrary, if the differential voltage is less than the threshold, it is treated as a random fluctuation caused by the ISFET drift or slow pH response. Then, such differential value is now utilized to be accumulated with the old $\Delta V_{th\_time}(t)$ data stored in the memory. In this way, the calibration data was updated for next compensation. At this juncture, the pH value can be converted from the output voltage of the ISFET through employing the drift-compensated equations that realize time-variant compensation algorithm presented in (5.19) and (5.20) in Chapter V.

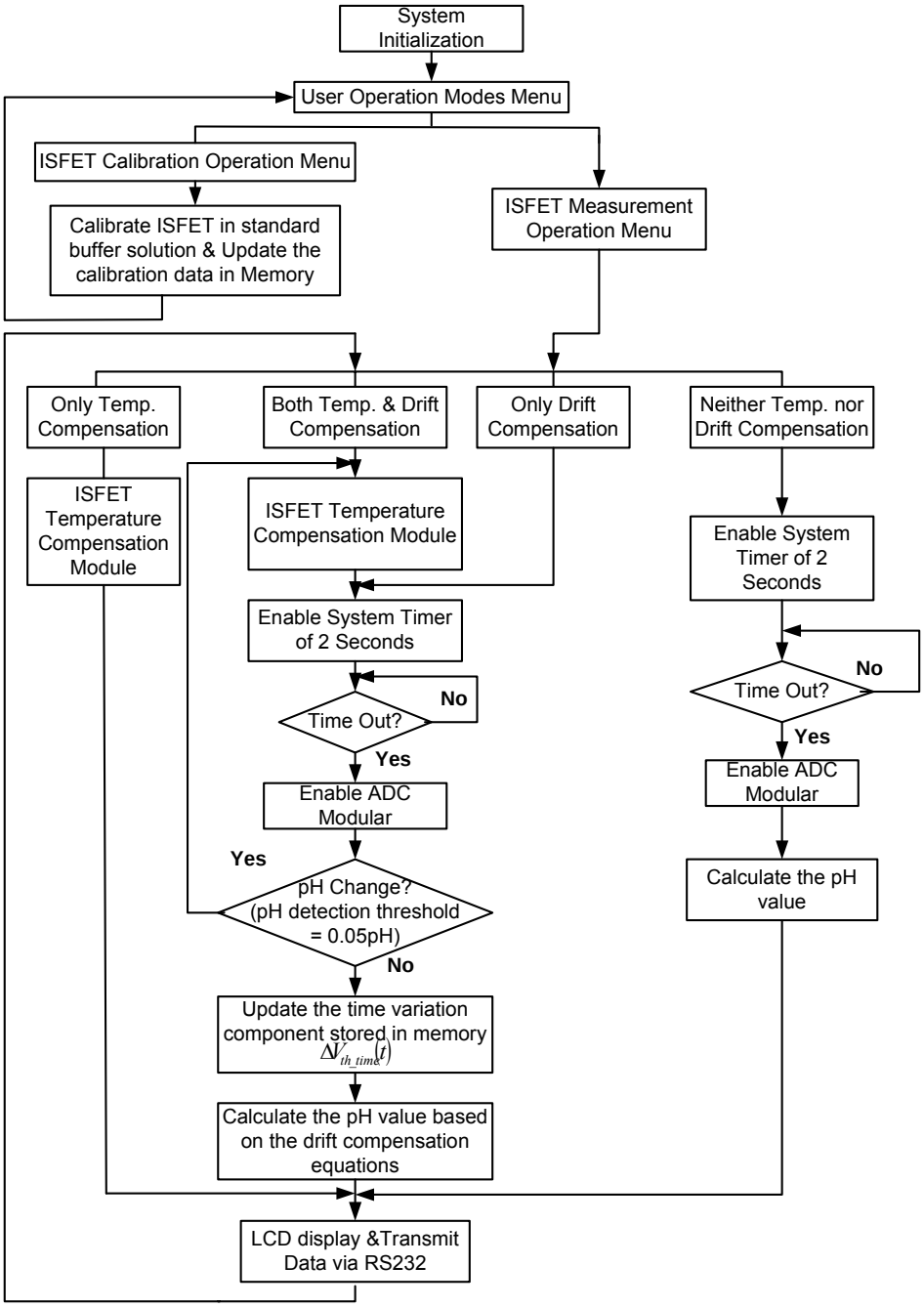

Fig. 6.6 Flow chart of overall software programming

Refer to the step of ISFET calibration, the detail calibration procedure is demonstrated in flow chart in Fig 6.7. According to the requirement of temperature compensation technology of the ISFET sensor on the calibration procedure described in Chapter V, the ISFET sensor is to be individually

calibrated in *pH4*, *pH7* and *pH9* standard pH buffer solutions at room temperature. As demonstrated in the flow chart in Fig. 6.7 that the software program enables the user to choose the option of calibration of the ISFET sensor in the standard *pH4*, *pH7* and *pH9* buffer solutions, which can be selected from "ISFET Calibration Operation Menu" displayed in the LCD. In each standard buffer solution, the biasing current of the ISFET sensor will be stepped from the initial guessing value to the maximum target value in a step of 2μA and the output voltage of the ISFET interface circuit corresponding to each biasing point is stored in a table created in the flash memory of microcontroller. This is supported by the facility of the hardware resource of data table in the MSP430 microcontroller, where data can be placed in the ROM section of the memory map and can be read/write using word or byte instructions. Although the ISFET biasing current needs to step from the initial guessing value to the maximum target value and the output of the ISFET sensor should be sampled and stored in the memory, the overall calibration duration in one particular pH buffer solution can be completed within two seconds. This would greatly help to minimize the drift effect during calibration.

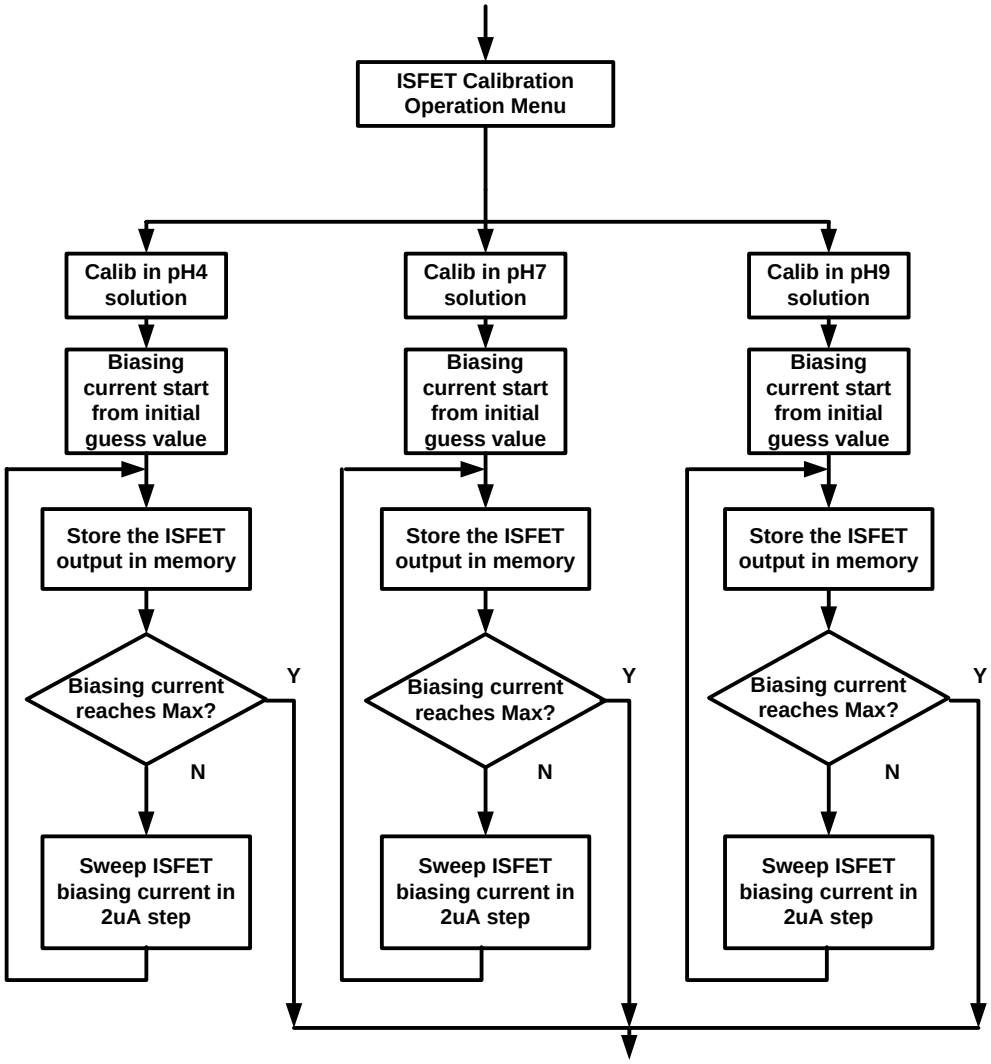

Fig. 6.7 Flow chart of ISFET calibration subprogram

6.3 Summary

A microcontroller-based ISFET sensory system featuring a smart compensation algorithm has been realized in both hardware and software to alleviate the problems associated with the composite temperature-dependence and time-variant effect in a basic ISFET sensing element. A new programmable current mirror that supports a wide range of biasing current with reduced dynamic error in the ISFET interface IC has been presented. The Texas Instruments MSP430 series microcontroller employed in this project in association with its

peripherals plays an important role in the intelligent ISFET sensory system. Incorporating the proposed nonlinear temperature compensation technique and the time-invariant compensation technique, this proposed ISFET sensory system enhances the stability performance of a standard ISFET sensor in the context of time drift and temperature drift for the long-term water quality monitoring environment in a low-cost solution. Dedicated software supported in both C and assemble language has been developed for the intelligent ISFET pH measurement system to control the whole process of pH measurement based on the hardware resource of MSP430 microcontroller.

CHAPTER VII

Results and Discussions

This chapter aims to verify the performance of proposed intelligent ISFET sensory system and to compare with the prior-art works as the ultimate goal. This involves a series of presentation on the results. They are summarized as follows:

(i) Experimental Characterization of the ISFET Device

It involves the measurement of the I-V curve (I_{DS}-V_{GS}) of the ISFET device in different standard pH buffer solutions and the extraction of the parameters of the ISFET based on the I_{DS}-V_{GS} data measured at any particular pH buffer solution (for instance *pH7*) at room temperature (≈23°C) by employing the Matlab software package.

(ii) Comparison of Interface Circuits

The two proposed ISFET readout circuits, ISFET-VI and ISFET-LSD, as well as the prior-art reported works are compared in simulations on the basis of the identical ISFET Behavior-SPICE sensing device model presented in Chapter II and the identical TSMC 0.25 μm CMOS process technology for realizing the sensing circuits.

(iii) Experimental Verification of the Proposed Interface Circuits

It involves the ISFET experimental setup and measurement results of the interface circuits: ISFET-VI and ISFET-LSD. The electrical performance of the proposed readout circuits is verified through the electro-chemical measurements

in realistic electrochemical environment, in which four kinds of standard buffer solutions with the pH value of 4, 7, 9 and 10 are applied for the measurement.

(iv) Experimental Verification of the Dynamic Current Temperature Compensation

The accuracy of the proposed current mirror in the fabricated IC is evaluated in experiment. The proposed dynamic current temperature compensation technique being applied to the ISFET-LSD that incorporates the proposed current mirror in design is validated by the experimental results at pH values ranging from 4 to 9 in a temperature range of 22°C (room temperature) to 50°C based on the measurement setup.

(v) The Experimental Verification of Different Drift/Temperature/Drift-Temperature Compensation Methods for Proposed Intelligent ISFET Sensory System

A series of experiments of the proposed ISFET intelligent sensory system is conducted using either standalone drift/temperature compensation parameter or multiple parameters on the drift and temperature in a simultaneous approach. The measured results are compared with the reported works, demonstrating the technical merits or potentials of the proposed ISFET sensory system using smart compensation strategy.

7.1 Characterization of the ISFET Device

Fig. 7.1 shows the measurement setup by employing the *micro-probing station* and *HP4155 Semiconductor Parameter Analyzer*. To guarantee that the ISFET is working in the linear region, that is, $V_{DS} < V_{GS} - V_{th}$, it is necessary to carry

out the measurements using a small value of V_{DS}. Here, the voltage on the channel is set to be V_{DS}=50mV and in this condition, all the measurements are in the linear region except for those in which V_{GS}-V_{th} < 50mV.

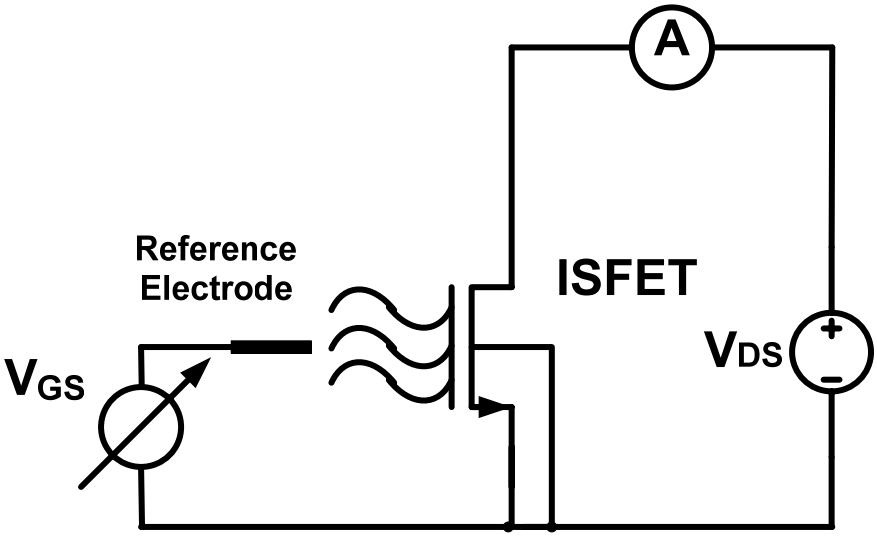

Fig. 7.1 Measurement setup for ISFET transfer characteristics with constant V_{DS}=50mV

The V_{GS} which is actually the voltage applied to the reference electrode of ISFET, was swept from -1V to 3V with a step of 0.05V. Meanwhile, the *HP4155 Semiconductor Parameter Analyzer* can also show the threshold voltage of the ISFET by utilizing the commonly known method of linear-extrapolation, which extrapolates the gate voltage axis from the point of the maximum slope of the current-voltage characteristics ($\partial I_{DS} / \partial V_{GS}$) [88]. The ISFET extracted threshold voltage parameters in *pH4*, *pH7*, *pH9* buffer solutions at room temperature (≈23°C), 30°C, 40°C and 50°C are summarized in Table 7.1.

Table 7.1 Threshold voltage of ISFET under different pH and temperature conditions

V_{th0_ISFET}	Room Temperature (23°C)	30°C	40°C	50°C
pH=4	-243.775 mV	-261.253 mV	-287.87 mV	-315.175 mV
pH=7	-87.6536 mV	-98.127 mV	-119.341 mV	-136.96 mV
pH=9	21.8782 mV	13.6380 mV	-3.761mV	-15.8918 mV
pH sensitivity (mV/pH)				
pH4 – pH7	52.04	54.375	56.176	59.405
pH7 – pH9	54.77	55.88	57.79	60.53
Average	53.405	55.1275	56.983	59.9675
α	0.908	0.915	0.916	0.934

With reference to (3.4), the other two unknown parameters, β_0 and θ, are pH-independent, so the extraction could be carried out based on the I_{DS}-V_{GS} data measured at any particular pH buffer solution (for instance *pH7*) at room temperature (≈23°C). The Matlab software package containing a Newton-Gauss method based automatic procedure was employed to perform these two parameters extraction. Due to the fact that equation (3.4) describing I_{DS}-V_{GS} characteristics would only be valid when the transistor operates in a strong inversion region, the measurement data of I_{DS}-V_{GS} with V_{GS} that was less than the threshold voltage were neglected. The Newton-Gauss method would automatically calculate the optimal values of the two unknown parameters such that the simulated I_{DS}-V_{GS} transfer characteristics obtained through the extraction of the optimal parameters could fit well with the measurement of I_{DS}-V_{GS} transfer characteristics, as presented in Fig. 7.2. The extracted optimal values of the model parameters are shown in Table 7.2.

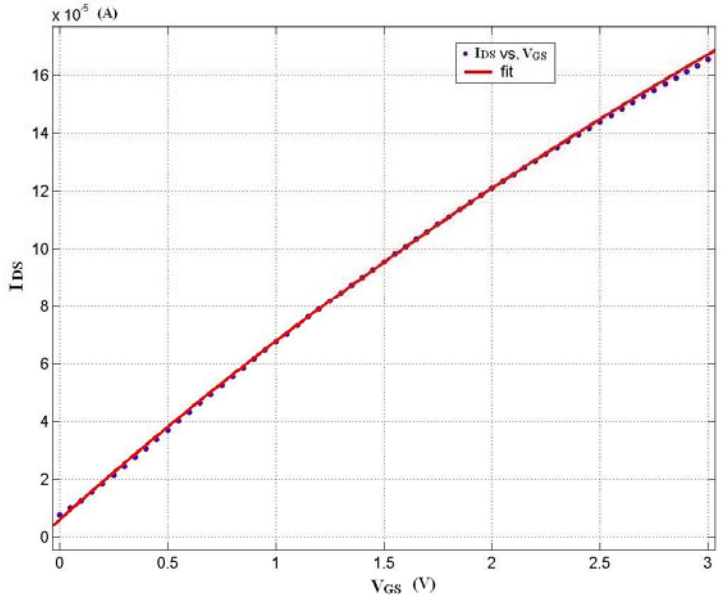

Fig. 7.2 Fitting curve of I_{DS}-V_{GS} transfer characteristics with measurement data for parameters extraction

Table 7.2 Value of extracted parameters

Parameter	Value	Unit
$V_{th0\ ISFET}$ (pH7)	-87.6536	mV
β_0	0.001357	A/V^2
θ	0.0821	V^{-1}

Simultaneously, the pH-sensitivity parameter α in (2.27) can be extracted with the measured ISFET threshold voltages in different pH value solutions as shown in Table 7.1

.

7.2 Simulation Results of ISFET Readout Circuits

In order to evaluate the performance of the two proposed novel interface circuits and provide a fair comparison with the prior-art research works of the ISFET interface circuits reviewed in Chapter IV, those circuits being simulated adopt the proposed ISFET Behavior-SPICE model on the basis of the extracted

ISFET parameters shown in Table 7.1 and Table 7.2 in chapter III. All the interface circuits' transistors except the ISFET device are based on the TSMC 0.25μm CMOS process technology. In the ISFET Behavior-SPICE model, the pH sensitivity of the electrolyte-insulator interface potential which is also the pH sensitivity of the ISFET sensor is about 53.405mV/pH at room temperature (23^{o}C). Therefore, all the output pH sensitivity of ISFET interface circuits would be compared with this reference value as a benchmark. Due to the difficulty of extracting the drain and source diffusion resistance of the commercial ISFET device employed in this project, with an approximate value of 100 Ω [62] has been assumed to these two parasitic resistors. All the operational amplifiers in the circuits employed the identical traditional OTA [102] as illustrated in Fig. 6.5 for fair comparison of the individual interface circuit. Based on the biasing condition of the ISFET device, as discussed in Chapter IV, the ISFET interface circuits are classified into two categories: (i) triode-based ISFET interface circuits in Fig. 4.1, Fig. 4.2, Fig. 4.3 and Fig. 4.5 and (ii) saturation-based ISFET interface circuits in Fig. 4.4 and Fig. 4.6.

7.2.1 Comparison of ISFET Circuits in Linear Region

For those triode-based ISFET interface circuits, in order to guarantee the ISFET device operating in triode region, the drain-source voltage of the ISFET device is set to be 0.3V and the drain-source current is set to be 100 μA. To be noted that, all the simulations are running at the reference temperature of 25°C to avoid the temperature effect on the ISFET device. The simulation results of the triode-based ISFET interface circuits are compared in Fig. 7.3. It also reveals

that the electrolyte/insulator interface potential represents the pH sensitivity of the ISFET device itself. For ease of comparison, all the output voltages are normalized to start from an origin.

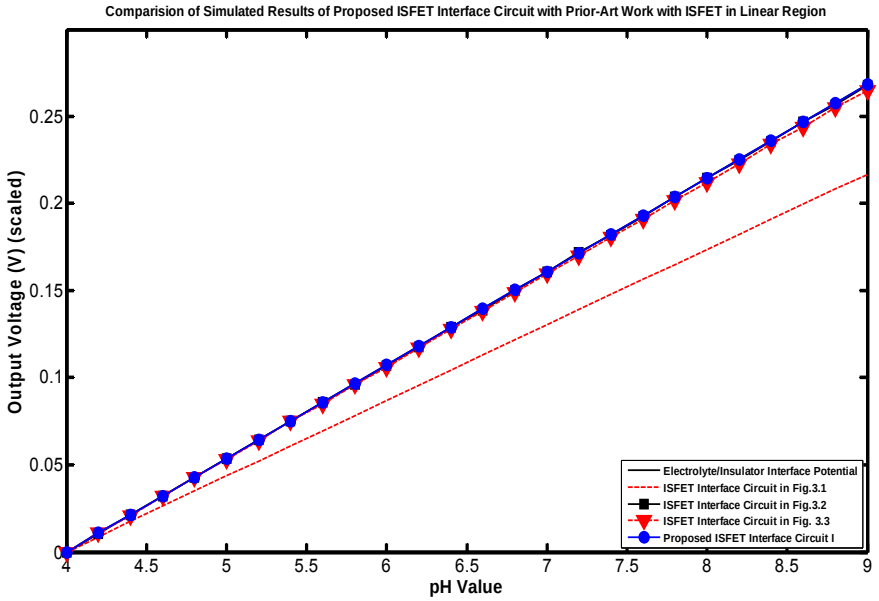

Fig.7.3. Comparison of simulation results of proposed ISFET circuit with prior-art works in linear region
pH sensitivity of Electrolyte/Insulator potential ≈ 53.405mV/pH
pH sensitivity of prior-art circuit (ISFET-SF) in Fig.4.1 ≈ 43.87mV/pH
pH sensitivity of prior-art circuit (ISFET-CVCI) in Fig.4.2 ≈ 53.32mV/pH
pH sensitivity of prior-art circuit (ISFET-OTA) in Fig.4.3 ≈ 52.1mV/pH
pH sensitivity of proposed circuit I (ISFET-VI) in Fig.4.5 ≈ 53.4mV/pH

It can be observed from the simulation results in Fig. 7.3 that the output voltage of prior-art work of ISFET interface circuit (ISFET-SF) in Fig. 4.1, configuring the ISFET device as non-saturation based source follower, demonstrates the lowest pH sensitivity, about 43.87mV/pH. This is due to the body effect of ISFET device as analyzed in Chapter VI. This issue can be solved in discrete ISFET interface electronics because the ISFET sensor and interface are not shared in the same die. However, in the application of integrated micro-system where the ISFET sensor has to be fabricated in the same die, the body effect of

ISFET will degrade the sensitivity of interface circuit whenever an N-type ISFET device is employed for purpose of low drift and high mobility [76]. Regarding the ISFET interface circuit (ISFET-CVCI) with constant V_S and I_{DS} structure, its output pH sensitivity is around 53.32mV/pH, which is not far away from the pH sensitivity of the ISFET sensor. It has shown that the influence of the body effect on the output pH sensitivity is weak even in single chip implementation because the source voltage is constant. Thus, the source-body potential can be kept constant. By observing the result of the output of the ISFET operational transconductance amplifier (ISFET-OTA), a pH sensitivity of 52.1mV/pH can be obtained. This value is lower than the pH sensitivity of the ISFET sensor but it is not far away. The explanation can be referred to Fig. 4.3, the transistor *T1a* is an integrated n-type ISFET device, being modeled with the proposed ISFET Behavior-SPICE model in Chapter III whereas the other reference transistor, *T1b*, of the input differential pair is modeled by REFET having a similar model to ISFET model except that the pH sensitivity parameter $\alpha = 0$. The other transistors are based on the TSMC 0.25μm CMOS process. In the given pH range, the drain-source voltage of ISFET is kept constant, but its source voltage varies by the common-mode effect of pH signal, leading to the variation of the drain-source current of ISFET through bulk modulation effect. In biomedical application where the pH range is narrow, (around 6.5-7.5), the variation of the source potential can be tolerated. However, in environmental applications, the pH range is much larger (around 4-9 or 2-10), so the variation of the source potential would reduce the pH sensitivity of the output voltage. Finally, it can be observed from the simulation

results in Fig. 7.3 that the proposed non-saturation based ISFET interface circuit (ISFET-VI) in Fig. 4.5 displays the pH sensitivity equal to the benchmark of 53.4mV/pH. This is regarded as one of the technical merits of the proposed ISFET interface circuit, which should thank to its intrinsic simple structure that eliminates the body-effect of the ISFET device. The body bias voltage V_{BS} caused by the source diffusion resistor is about a few mV, (if the ISFET is biased in 100μA, and the source drain resistance is 100Ω, V_{BS} is about -10mV) so its influence to the pH sensitivity of the output voltage is insignificant and can be neglected, as confirmed by the simulation results in Fig. 7.3.

7.1.2 Comparison of ISFET Circuits in Saturation Region

The simulation results of the saturation-based ISFET interface circuits are compared in Fig. 7.4. Similarly, the electrolyte/insulator interface potential serves as a reference for a benchmark, which represents the pH sensitivity of the ISFET device itself in Fig. 7.4. For ease of comparison, all the output voltages are normalized to start from an origin point. Regarding the technique of complementary ISFET/MOSFET pair (CIMP) reviewed in Chapter IV, the ISFET operates in saturation region in both direct gate-feedback (CIMP-DGF) and indirect gate-feedback (CIMP-IGF) configurations. The simulation results of these two configurations are illustrated in Fig. 7.4. It can be observed from the simulation result that the pH sensitivity of output voltage of the CIMP-DGF circuit is 53.4mV/pH which is almost the same as the pH sensitivity of electrolyte/insulator potential. This is resulted from the elimination of body-

effect of ISFET device in the CIMP-DGF circuit structure as analyzed in Chapter IV. On the contrary, the pH sensitivity of CIMP-IGF circuit exhibits high variation with respect to the size of P-MOS when referenced to the circuit depicted in Fig. 4.4. It is noted that the pH sensitivity of the output voltage is 40.1 mV/pH in configuration A having P-MOS size of 160um/2um. This value is much smaller when compared to the value of 52.6mV/pH in configuration B having P-MOS size of 160um/3um. This is consistency with the implication from (4.12) that the pH sensitivity being a function of the division factor $\sqrt{\alpha}$ and is confirmed by these simulation results.

It can be observed from the simulation results in Fig. 7.4 that the pH sensitivity of the output voltage of the proposed saturated ISFET based interface circuit (ISFET-LSD) in Fig. 4.5 is 53.2mV/pH, which is slightly less than pH sensitivity of electrolyte/insulator potential, 53.405mV/pH. This can be explained by the minute effect of the channel-length modulation of the ISFET that comes from the change of the V_{DS} of ISFET in different pH solutions when the drain potential of the ISFET follows the gate potential of ISFET. However, the ISFET normally has long channel length that is able to minimize the effect of channel-length modulation. For final remarks, by comparing the two values, they are almost very close to each other. In worst scenario, a cascode MOS device can be added on top of the ISFET to further reduce channel length effect but the experiment result reveals that there is no need for such an improvement because the difference is too small.

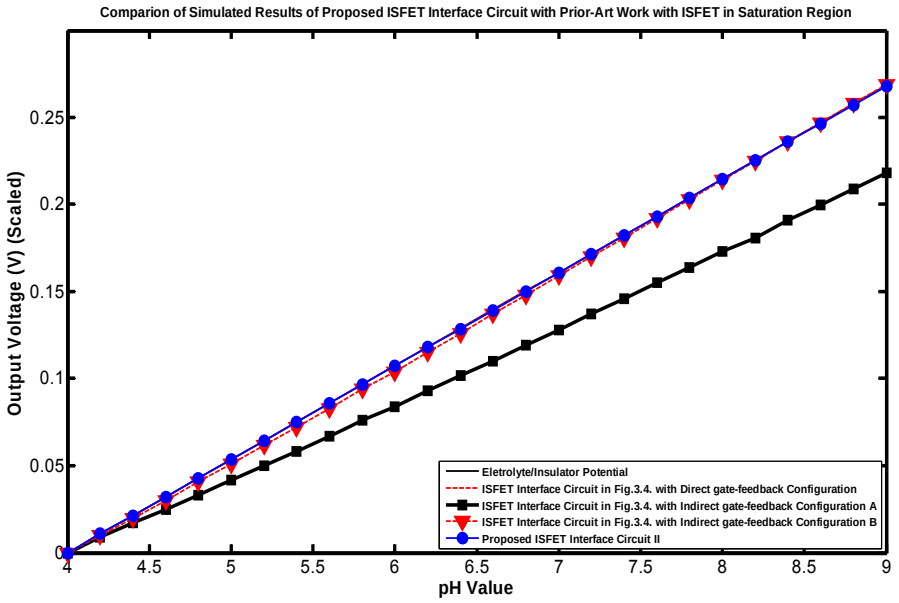

Fig.7.4. Comparison of simulation results of proposed ISFET circuit with prior-art works in saturation region
pH sensitivity of Electrolyte/Insulator potential ≈ 53.405mV/pH
pH sensitivity of prior-art circuit in Fig.4.4 with direct gate-feedback configuration ≈ 53.4mV/pH
pH sensitivity of prior-art circuit in Fig.4.4 with indirect gate-feedback configuration A (with P-MOS size= 160um/2um) ≈ 40.1mV/pH
pH sensitivity of prior-art circuit in Fig.4.4 with indirect gate-feedback configuration B (with P-MOS size= 160um/3um) ≈ 52.6mV/pH
pH sensitivity of proposed ISFET interface circuit II in Fig.4.6 ≈ 53.2mV/pH

7.3 Measured Results of Proposed ISFET Interface Circuits

In order to verify the electrical performance of the proposed ISFET-VI in Fig. 4.5 and ISFET-LSD in Fig. 4.6, the electro-chemical measurements have been performed. The main purpose of this characterization is to test the functionality of the proposed readout circuits, evaluating their output linearity as well as sensitivity in a realistic electrochemical environment, in which four kinds of standard buffer solutions with pH value of 4, 7, 9 and 10, are applied for pH measurement. To test the ISFET interface circuits, the Si_3N_4-gate pH-sensitive ISFET sensor, which is commercially available by D+T Microelectrónica, A.I.E (CNM), Spain, is employed.

7.3.1 The Measurement Result of the ISFET-VI

The interface circuit was built on a prototyping board using discrete electronic components. The ISFET sensor was biased in non-saturation region with V_{ds} of 0.3V. The transistors *M1* and *M2* in Fig. 4.5 were realized by CD4007 which comprised four NMOS transistors as well as four PMOS transistors. The constant biasing current I_B and I_O, being set at 100μA and 20μA respectively, were provided by LM134, a 3–terminal adjustable current sources that was programmable from 1μA to 10mA. The op-amp *Op1* was realized by using TLV2252, a low input offset and rail-to-rail operation amplifier. The whole circuit was powered at a single 3.3V supply. The output of the circuit was monitored by an HP 3486A multi-meter. The output signal was measured when the ISFET sensor was inserted into different standard buffer solutions with pH value of 4, 7, 9 and 10. The ISFET sensor was cleaned by the Deionized (DI) water every time before it was inserted into a new buffer solution with different pH values. The temperature had been controlled at room temperature to avoid extra temperature effect on the ISFET sensor. The measurement result for the relationship between *Vout* and pH value is plotted in Fig. 7.5. The slope denotes the pH sensitivity of output signal of readout circuit, which is about 53.3mV/pH and is very close to that obtained from the ISFET sensor characterization shown in Table 7.1. This has validated that the proposed readout circuit is able to accurately detect the variation of the ISFET threshold voltage.

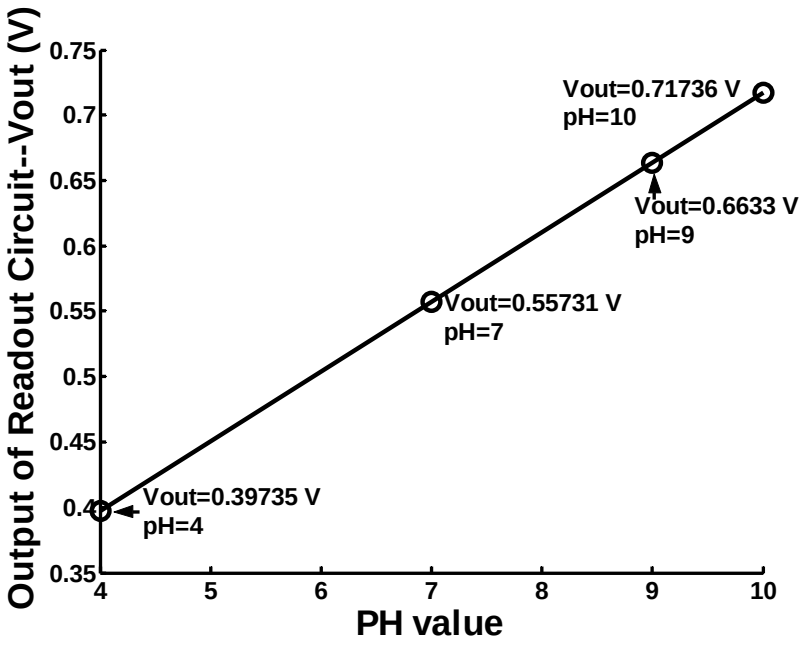

Fig. 7.5 Measurement result of output signal of readout circuit (Vout) with ISFET in non-saturation configuration as function of the solution pH value at 20°C. The *Vout* at pH value of 4, 7, 9 and 10 are 0.39735V, 0.55731V, 0.6633V and 0.71736V, respectively.

7.3.2 Measurement Result of the ISFET-LSD

The electrical performance of the proposed saturation-based ISFET interface circuit given in Fig. 4.6 had also been verified by the electro-chemical measurements. Similar to the measurement of non-saturation based ISFET interface circuit, the saturation based ISFET interface circuit was also built on a prototype board using discrete electronic components. The MOS transistor *M1* was realized by a CD4007 transistor array IC chip and the constant currents, I_B and I_O, were established through two LM134ICs, each with a 3-terminal adjustable current source. The whole circuit was powered at a single 3.3V supply, having adequate headroom for the ISFET device to operate in saturation region under discrete implementation. The output of the circuit, V_{out} and the biasing current I_B, were monitored by two HP 3486 multi-meters. The electro-

chemical measurements of the proposed readout circuit were conducted in three kinds of standard buffer solutions having pH value of 4, 7 and 9. The ISFET and source follower was biased at respective constant biasing current, with I_B=100μA and I_O=30μA under room temperature. The output signal was measured when inserting the ISFET sensor into different standard buffer solutions. The ISFET sensor had been cleaned by Deionized (DI) water every time before it was inserted into a new buffer solution. The measurement result is plotted in Fig. 7.6. The slope denotes the pH sensitivity of the readout circuit, showing about 53.8mV/pH. Hence, the experimental result has validated that the proposed interface circuit is able to detect the variation of the ISFET threshold voltage.

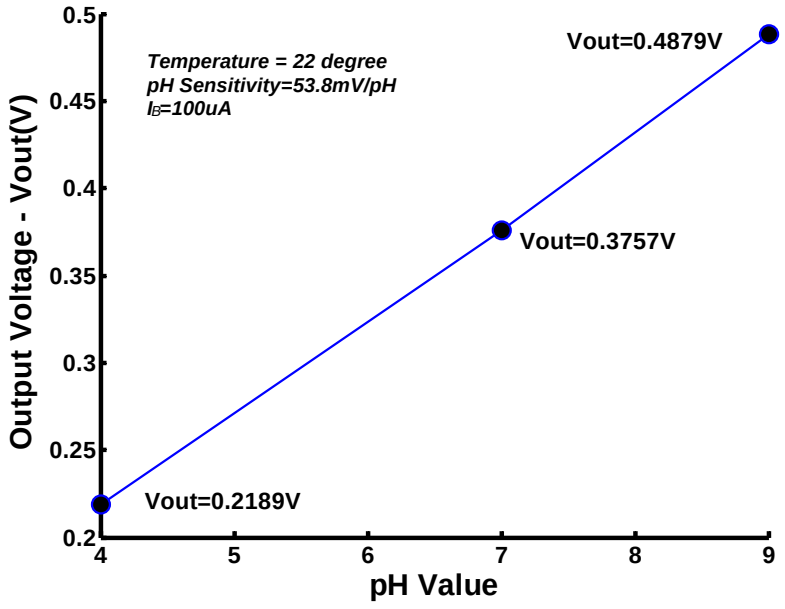

Fig. 7.6 Measurement result of output signal of readout circuit (Vout) with ISFET in saturation configuration as function of the solution pH value at 22°C. The Vout at pH value of 4, 7 and 9 are 0.2189V, 0.3757V and 0.4879V, respectively.

7.3.3 Discussion of Non-Ideal Effects

Unlike part of previous works, there is no matching requirement in the design of these two proposed interface circuits, such as the clamping transistor and the source follower. The major advantage of these two circuits is that it will respond accurately for the simultaneous threshold voltage fluctuation caused by the variation of pH value. Another important advantage is that both circuits eliminate the body effect of the ISFET. In these proposed circuits, the body bias voltage V_{SB} will only be generated when current flows through the source diffusion resistor, R_S. The impact of this slight source-body biasing on the ISFET performance can be analyzed as follows:

The voltage across R_S will introduce a DC offset in the output voltage of the ISFET readout circuit, which has been derived in (4.13) and (4.14) in Chapter IV. For ease of explanation, the equation (4.14) is repeated as

$$V_{out} = V_{gs} = V_{th(ISFET)} + \sqrt{\frac{2I_B}{\mu_n C_{OX}(W/L)}} + I_B R_S \tag{7.1}$$

The threshold voltage of ISFET, taking into account the body-effect, can be expressed as

$$V_{th(ISFET)} = V_{th0(ISFET)} + \gamma\left(\sqrt{2\phi_f + V_{SB}} - \sqrt{2\phi_f}\right) \tag{7.2}$$

with $V_{SB}=I_B R_S$ (7.3)

Therefore, (7.1) can be fully expressed as

$$V_{out} = V_{th0(ISFET)} + \sqrt{\frac{2I_B}{\mu_n C_{OX}(W/L)}} + \gamma\left(\sqrt{2\phi_f + I_B R_S} - \sqrt{2\phi_f}\right) + I_B R_S \tag{7.4}$$

The last three terms can be viewed as dc components, which will keep constant and independent of pH value with constant biasing current for the ISFET. Therefore, the pH sensitivity of the output voltage of readout circuit will not be jeopardized by the body effect introduced by R_S. For example, if the output voltages of ISFET sensor, which is biased at constant I_B, are measured in pH4 and pH7 buffer solutions. The dc components of the output voltage expressed in (7.4) are identical in both pH4 and pH7 solutions. Therefore, the pH sensitivity can be derived as:

$$\frac{V_{out(pH7)} - V_{out(pH4)}}{7-4} = \frac{V_{th0(pH7)} - V_{th0(pH4)}}{7-4} \tag{7.5}$$

Here, $V_{out(pH7)}$ and $V_{out(pH4)}$ are the output voltages of the readout circuit when the ISFET in pH7 and pH4 buffer solutions, respectively. Therefore, it can be observed that the pH sensitivity of output voltage will not be affected by the body effect introduced by the voltage drop across the *Rs* for the last two terms in (7.4). This is because they are treated as the common mode components in both $V_{out(pH4)}$ and $V_{out(pH7)}$, thus cancelling each other in (7.5) .

On the other hand, the temperature dependence of the body-effect coefficient γ, Fermi potential ϕ_f and source resistance R_S will introduce additional temperature effects on the output voltage of ISFET readout circuit. Fortunately, due to the small value of the voltage across R_S, the output voltage variation, caused by the temperature dependence of above-mentioned parameters, γ, ϕ_f and R_S, can be small. In order to validate this statement, a measurement was

carried out. The measurement setup as well as the measurement result is presented as follows:

The measurement was conducted in *pH7* buffer solution at temperature of 23ºC and 40ºC with constant drain-source biasing current of 100μA. For commercial ISFET sensor, the value of parameters R_S is unavailable. According to reference [62], a typical value of 100Ω for R_S is assumed here. In order to demonstrate the effect of the 100Ω source resistance, an additional external resistor, R_{Ext} = 100Ω, is connected to the source of ISFET in the interface circuit to introduce an additional body-effect. The measurement result with and without involving this external resistor is shown in Table 7.3.

Table 7.3 Measurement result of ISFET with and without involving external resistor

External resistor R_{Ext}= 100 Ω and I_{DS}= 100μA		
	Vout (without R_{Ext})	*Vout* (with R_{Ext})
23 ºC	0.3815 V	0.4012 V
40 ºC	0.3724 V	0.3924 V
T.C.	5.35294×10^{-4} V/ºC	5.17647×10^{-4} V/ºC

The contribution of the temperature dependence of the body-effect related term in (7.2), $\gamma\left(\sqrt{2\phi_f + V_{SB}} - \sqrt{2\phi_f}\right)$ can be calculated based on the measurement data in Table 7.3. That is

$$(5.35294\times10^{-4}-5.17647\times10^{-4}) / 5.35294\times10^{-4} \approx 3.3\% \qquad (7.6)$$

Hence, the temperature dependence of the body-effect related term in (7.2) is about 3.3% of the total temperature sensitivity of the output voltage. Based on the *T.C.* of 5.17647×10^{-4} V/ºC, the pH sensitivity of about 53mV/pH from the previously published paper [73] and the measurement temperature range from

temperature 23°C to 40°C, the maximum thermal drift with respect to the reference temperature is given in the form of pH unit as

$$5.17647\times 10^{-4} \times (40 - 23) / (53\times 10^{-3}) = 0.166 \text{ pH} \quad (7.7)$$

Hence, the estimated temperature-dependent accuracy error contributed by the slight body-effect of ISFET for the small voltage drop across the R_S is translated to about 0.166 × 3.3% = 0.005 pH. This value is lower than the resolution of 0.01 pH in the 12-bit ADC employed in current measurement system. Hence, the thermal drift introduced by the R_S would not significantly affect the accuracy as well as resolution to the measurement system.

7.3.4 Comparison with Other Published Circuits

Due to neglectable body effect, an excellent linear response has both been obtained on the two proposed ISFET interface circuits. Only a few other reported works have claimed such an advantage. Table 7.4 compares the proposed non-saturation based ISFET-VI with previously published circuits. Among the works, ISFET-VI shows the most simplicity whilst maintaining pH sensitivity and insensitivity to the body effect.

Table 7.4 Comparison of proposed non-saturation based ISFET readout circuit with previously published works

Parameter	ISFET-SF [61]	ISFET-CVCI [65]	ISFET-OTA [64]	Proposed ISFET-VI Fig. 4.5
Output pH sensitivity	43.87mV/pH (simulated)	53.32mV/pH (simulated)	52.1mV/pH (simulated)	(simulated) 53.4mV/pH (measured) 53.3mV/pH
Sensitivity to body effect	Yes	Yes (slightly)	Yes	No
No. of major op-amps	3	2	1	1
DC offset sensitivity to non-ideal components	Offsets in 3 op-amps + 2 current sources	Offsets in 2 op-amps + 2 current sources	Offsets in ISFET/RFET pair + two current mirrors	Offset in 1 op-amp + 1 current source

Table 7.5 further compares the performance of the category of the saturation-based ISFET readout circuits. Although Morgenshtein's CIMP-DGF circuit [69] is a simple design, it has the stability issue due to the existence of an extra high impedance node in the feedback loop, which will be particularly pronounced for the low power implementation. On the contrary, the proposed ISFET-LSD readout circuit can be further simplified from the case that the only one amplifier in the ISFET-VI readout circuit can be eliminated from the core circuit when the ISFET is biased towards the saturation region, leading to the circuit structure having utmost simplicity when compared to the published works. Besides, the source follower, like that of ISFET-VI, offers a wide bandwidth operation and the circuit stability can be easily guaranteed even at the low power implementation.

Table 7.5 Comparison of proposed saturation based ISFET readout circuit with previously published works

Parameter	CIMP-DGF [68]	CIMP-IGF [68]	Proposed ISFET-LSD Fig. 4.6
Output pH sensitivity	53.4mV/pH (simulated)	40.1 mV/pH (W/L of P-MOS = 160µm/ 2µm) (simulated)	(simulated) 53.2mV/pH (measured) 53.8mV/pH
Sensitivity to body effect	Yes	Yes (slightly)	No
No. of major op-amps	1	1	0
DC offset sensitivity to non-ideal components	Offset in 1 op-amp + 1 current source	Offset in 1 op-amp	1 current source

7.4 Measured Results of the Proposed ISFET Dynamic Current Temperature Compensation Technique

The experiment of the proposed ISFET dynamic current temperature compensation technique involves numerous preparation tasks such as the sensor device characterization, parameter extraction, equipment setup, fabrication of integrated chip (IC) of the ISFET interface circuit, test circuit prototype of microcontroller based pH measurement system. The functionality and effectiveness of the proposed novel temperature compensation method for the ISFET sensor as well as its transducer are confirmed by the electro-chemical measurements at different pH values against different temperatures. Prior to this, the functionality of the proposed V_{DS}-tracked regulated-cascode current mirror as well as the accuracy of the fabricated ISFET interface circuit chip are verified by the measurements.

7.4.1 Measured Results of the V_{DS}-Tracked Regulated-Cascode Current Mirror

The ISFET interface circuit has been fabricated in TSMC CMOS 0.25μm process technology, with the micrograph shown in Fig. 7.7. Prior to verifying the functionality of the entire pH measurement system, the proposed V_{DS}-tracked regulated-cascode current mirror on the basis of Fig. 6.2 was tested. The experimental dc characteristic of the current mirror were measured by sweeping its input current I_{B1} for two decades, ranging from 10μA to 1mA. The error of the current mirror within the measured current range is illustrated in Fig. 7.8. It is noted that the error of the current mirror is defined as the difference between the input and output current value of the current mirror. Based on the ISFET dynamic current temperature compensation technique in this design, the ISFET operating current range is approximately between 100 μA and 400 μA. The measured results in Fig. 7.8 have shown that the error of the current mirror is less than 0.5 μA in the operating current range. The results are reasonably good because the channel length of the current mirror transistor pair in this design is only 2 μm in order to save silicon area. A better matching characteristic can be obtained if the channel length is further increased at the expense of the increased silicon area.

In terms of the ISFET temperature compensation methodology presented in Chapter V, some of the important parameters in (5.19) have been extracted in Chapter III, and the values of those parameters are repeated here: $V_{th(pH4)}$= –244.775 mV, $V_{th(pH7)}$= –87.6536 mV, $V_{th(pH9)}$= –21.8782 mV, $\beta_0 = 0.001357 A/V^2$, $\theta = 0.0821 V^{-1}$ and m= –2.2. With reference to the ISFET gate-source voltage expression in Chapter IV:

$$V_{GS(pH)}(T)\big|_{T=T1} \approx V_{th(pH)}(T_0) + K_{VT(pH7)} \times (T_1 - T_0) + \sqrt{\frac{2I_{DS}}{\frac{\beta_0}{1+\theta\left[V_{GS(pH)}(T_1) - V_{th(pH7)}(T_1)\right]}\left(\frac{T_1}{T_0}\right)^m}}$$

(7.8)

In the presence of biasing current error, ΔI_{DS}, the ISFET gate-source voltage can be shown as

$$V^*_{GS(pH)}(T)\big|_{T=T1} \approx V_{th(pH)}(T_0) + K_{VT(pH7)} \times (T_1 - T_0) + \sqrt{\frac{2(I_{DS} + \Delta I_{DS})}{\frac{\beta_0}{1+\theta\left[V_{GS(pH)}(T_1) - V_{th(pH7)}(T_1)\right]}\left(\frac{T_1}{T_0}\right)^m}}$$

(7.9)

It can be observed from Fig. 7.8 that in the ISFET operating current ranging from 100 µA to 400 µA, the largest current mismatch appears at a biasing current of 400 µA. Hence, the ΔV_{GS} error can be calculated by setting the worst case condition as I_{DS}= 400µA, ΔI_{DS} = 0.5µA and T_1= (50+273) K. Therefore, we have

$$\Delta V_{GS} = V^*_{GS(pH)}(T)\big|_{T=T1} - V_{GS(pH)}(T)\big|_{T=T1} \approx 0.56\text{mV} \qquad (7.10)$$

This value is approximately equal to a pH of 0.01 unit, which has negligible impact on the long-term monitoring applications, suggesting that the dynamic accuracy of the proposed current mirror is satisfactory.

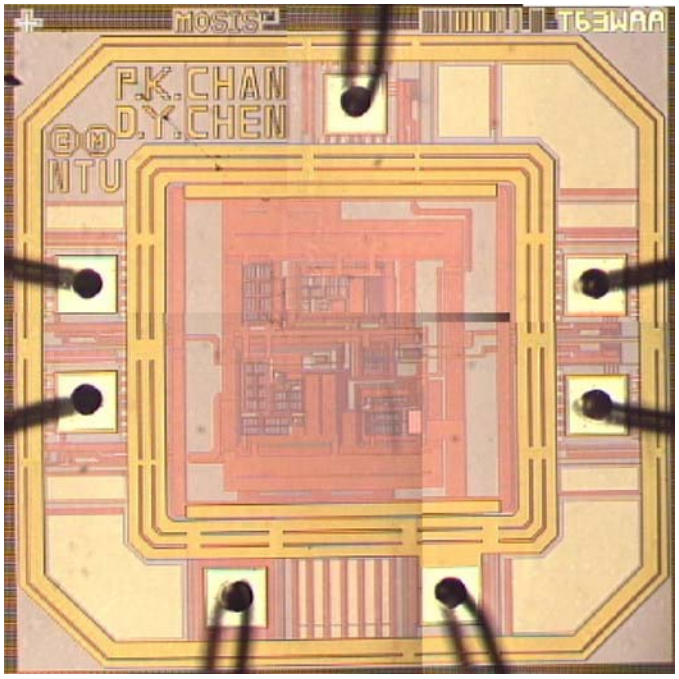

Fig .7.7 Micrograph of the integrated ISFET interface circuit

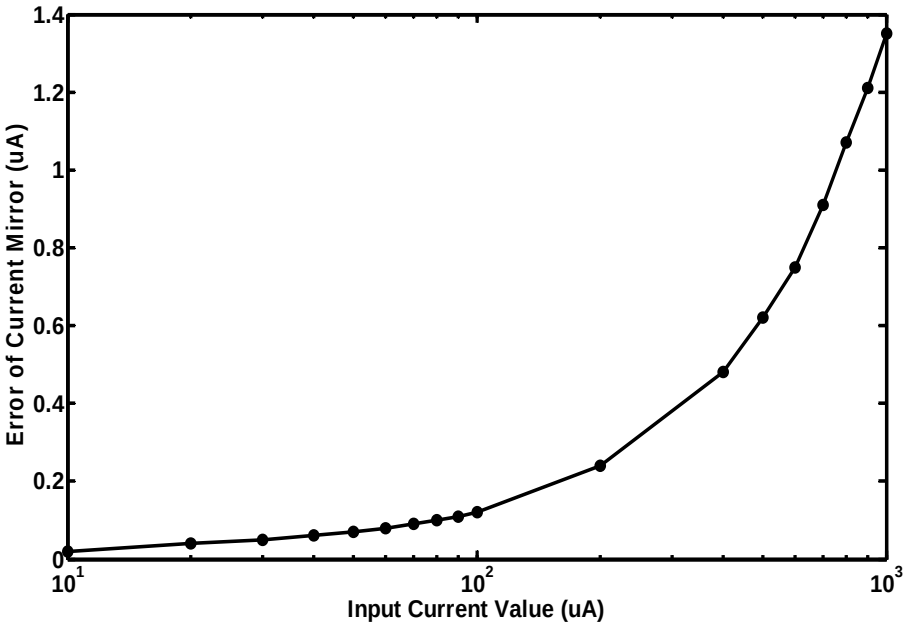

Fig .7.8 Error of the proposed current mirror structure at different input currents

7.4.2 Hardware of Microcontroller Based pH Measurement System and Measurement Setup

The hardware of the proposed microcontroller based pH measurement system presented in Chapter VI was built in a Printed Circuit Board (PCB) with size of 10cm x 12cm, as shown in Fig. 7.9.

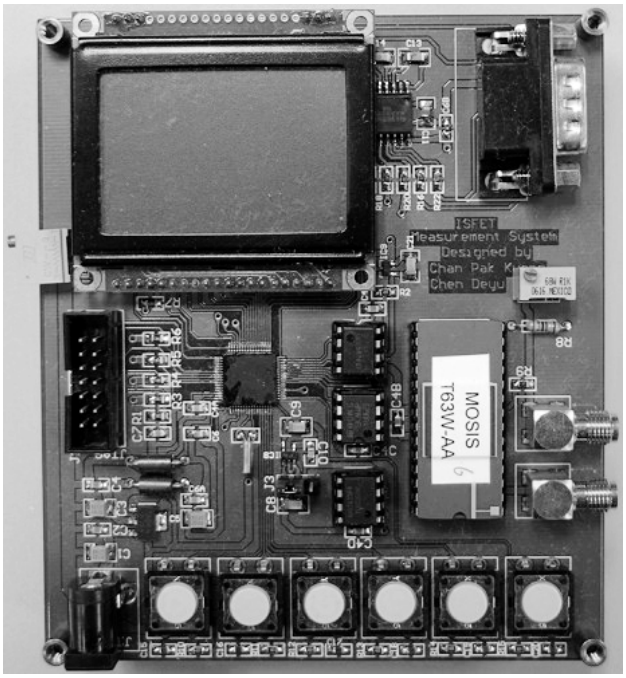

Fig. 7.9 Printed circuit board of microcontroller based pH measurement system

To achieve high-resolution pH measurement system, care and special attention must also be paid to the printed-circuit-board layout and the grounding scheme to eliminate ground loops and any unwanted parasitic components/effects and noise. Industry-standard grounding and layout techniques should be followed to reduce these unwanted effects. For instance, for an ADC being employed in the proposed pH measurement system, the ground loops will be formed when the

return current from the ADC flows through paths that are common with other analog or digital circuitry. If care is not taken, this current can generate small, unwanted offset voltages that can add to or subtract from the reference or input voltages of the ADC. One way to avoid ground loops is to use a star connection scheme for analog ground. This methodology is applied for all the components in the PCB board.

In addition to grounding, ripple and noise spikes on the power supply lines due to the digital switching or switching power supplies can corrupt the conversion result. The ripple can become more dominant by reducing the value of the conversion voltage range, therefore reducing the value of the LSB and the noise margin. Thus, a careful setup becomes even more important to achieve the desired accuracy. Adding carefully placed bypass capacitors returned to the respective ground planes can help in reducing ripple in the supply current and minimizing these effects. In addition, another important point is that of sensitive signal paths, such as the output signal of the ISFET interface circuit from the gate of ISFET sensor, are shielded by ground area to avoid the interference from other signal lines.

The measured pH buffer solution where the ISFET was inserted was kept in a thermal buffer so as to control the temperature of buffer solution during the measurement process. Although the thermal buffer supported the measurement at room temperature or above, the temperature compensation method was still able to be verified. Fig. 7.10 shows the experimental setup for the proposed pH measurement system.

A FLUKE 87 III TRUE RMS hand-held multi-meter was employed to monitor the drain-source biasing current of the ISFET. The meter value was compared with the expected biasing current, which was calculated by the microcontroller in the process of running the ISFET dynamic current temperature compensation algorithm and displayed on the LCD module. At this juncture, the measurement results were also transmitted via RS232 port to a PC and stored as a text file for further result analysis. The pH value of the solution was monitored by the commercial glass electrode pH meter, *CyberScan 1000*, with a resolution of 0.01pH and accuracy of ±0.01pH.

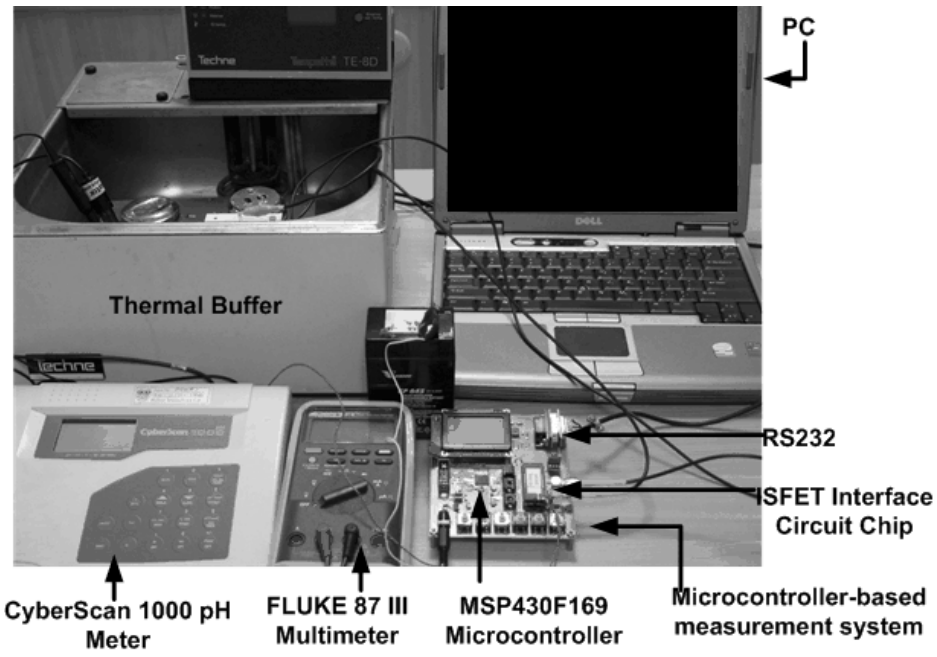

Fig. 7.10 Experiment setup for the microcontroller-based pH measurement system

7.4.3 Measurement Results of the Accuracy and Linearity of the Proposed pH Measurement system at Room Temperature.

The measurement of the proposed pH measurement system is conducted at instant time point (to avoid the drift effect) and static room temperature as the pH value of the solution started from *pH4* to *pH9* by adding the alkaline solution. The solution pH value was monitored by the CyberScan 1000 pH meter. Both the proposed ISFET measurement system and the CyberScan 1000 pH meter were calibrated in the standard *pH4*, *pH7* and *pH9* buffer solutions (three point calibration) prior to the measurements. The measurement data is shown in Table 7.6.

Table 7.6 Measurement results of proposed ISFET measurement system at instant time point and static room temperature

Measurement Steps	Reading of Proposed pH measurement System (pH unit)	Reading of *CyberScan* 1000 pH meter (pH unit)	Difference (pH unit)
1	4.01	4.00	0.01
2	4.09	4.07	0.02
3	4.34	4.34	0
4	4.75	4.74	0.01
5	5.18	5.17	0.01
6	6.01	6.00	0
7	6.25	6.25	0
8	7.15	7.13	0.02
9	7.32	7.31	0.01
10	7.73	7.72	0.01
11	8.20	8.19	0.01
12	8.46	8.45	0.01
13	8.69	8.68	0.01
14	9.06	9.05	0.01

It can be observed from the results that the accuracy of the proposed ISFET measurement system is about 0.01pH in the deviation from the commercial

CyberScan 1000 pH meter, which is close to the target resolution of the data acquisition system being used in the sensory system.

7.4.4 Measurement Results of the Proposed ISFET Dynamic Current Temperature Compensation Technique

The proposed ISFET dynamic current temperature compensation technique has been presented in Chapter V that it relies on the physical theory of the mutual compensation of the temperature variation of the mobility and threshold voltage to achieve the zero temperature coefficient (*Z.T.C*) biasing point of the ISFET. For demonstrating the temperature compensation method, different buffer solutions (*pH4*, *pH7* and *pH9*) were used in the experiment. Referring to the flow chart of the overall software programming in Fig. 6.6, the calibration of the ISFET sensor was conducted in the standard *pH4*, *pH7* and *pH9* buffer solutions at room temperature before starting the dynamic temperature compensation. The detailed procedure of the calibration has been illustrated in Fig 6.7, which will be implemented by the microcontroller within two seconds. The drift effect of the ISFET can be neglected in this two seconds period. Table 7.7 presents an example of the calibration data which is stored in the ROM section of the memory map of microcontroller.

The calculation of the optimum biasing current for ISFET, according to the dynamic temperature compensation algorithm proposed in Chapter V, was done by the microcontroller. The software program of the microcontroller follows the procedures of implementing the steps of iteration algorithm summarized in Chapter V. The measurements were conducted in *pH4*, *pH7* and *pH9* buffer

solutions at 23°C, 30°C, 40°C and 50°C. The measurement results for *pH4*, *pH7* and *pH9*, with and without temperature compensation, are depicted in Figs. 7.11 - 7.13, respectively. The final optimum biasing current for each measurement was also displayed in the LCD, as shown in Fig 7.14 as an example of the optimum biasing current in *pH4* buffer solution at 50°C. The biasing current of the ISFET device was also monitored by the FLUKE multi-meter as shown in Fig 7.14. Other biasing currents that achieved the ISFET temperature compensation in above mentioned pH buffer solution as well as the temperature points are summarized and shown in Table 7.8.

Table 7.7 Measured results of ISFET readout circuit at room temperature (23°C) for reference data

Biasing Current I_B (μA)	Output Voltage of Readout Circuit – (V)		
	$V_{out(PH4)}$ *(at pH4)*	$V_{out(PH7)}$ *(at pH4)*	$V_{out(PH9)}$ *(at pH4)*
I_B=100	0.2189	0.3757	0.4879
I_B=102	0.2244	0.3814	0.4937
:	:	:	:
I_B=192	0.4286	0.5863	0.6989
:	:	:	:
I_B=306	0.6319	0.7901	0.9031
I_B=308	0.6351	0.7933	0.9062
:	:	:	:
I_B=316	0.6477	0.9058	0.9186
:	:	:	:
I_B=360	0.7214	0.8798	0.9935

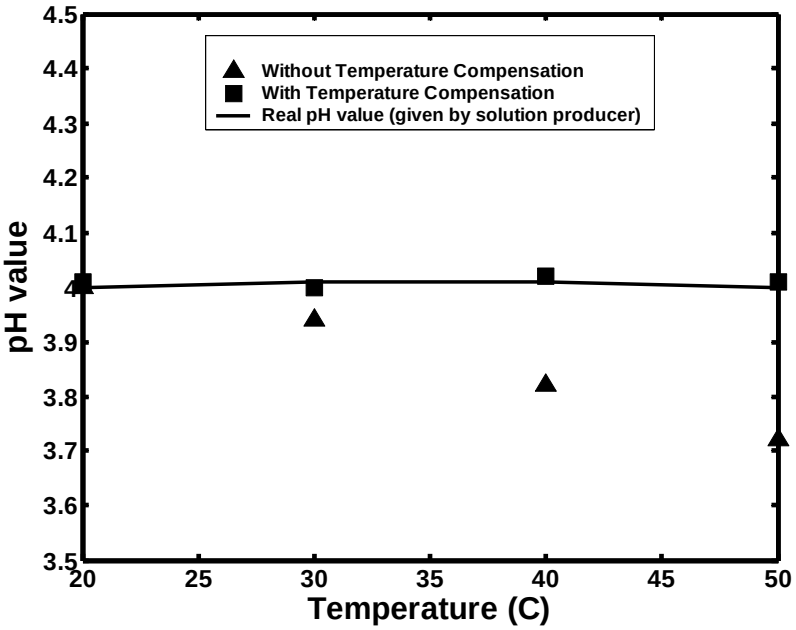

Fig. 7.11 Measured results of temperature compensation in pH4

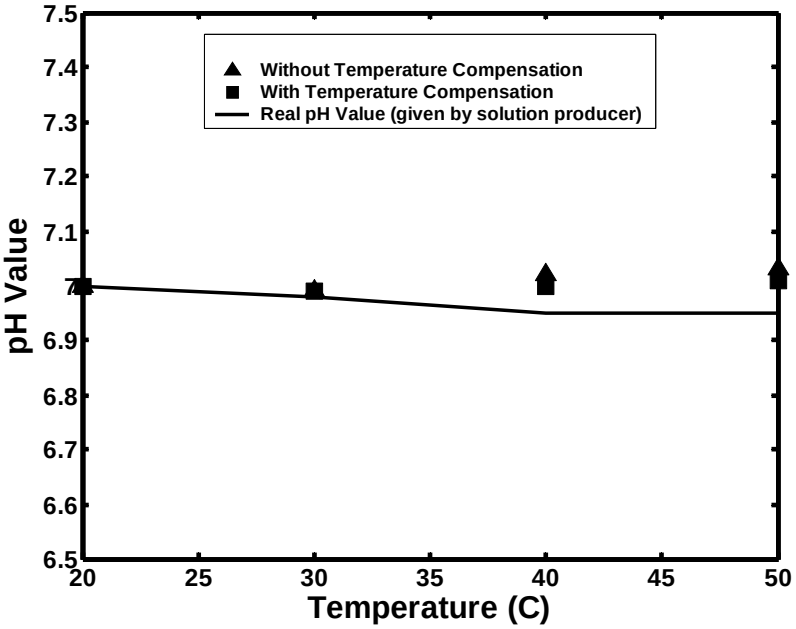

Fig. 7.12 Measured results of temperature compensation in pH7

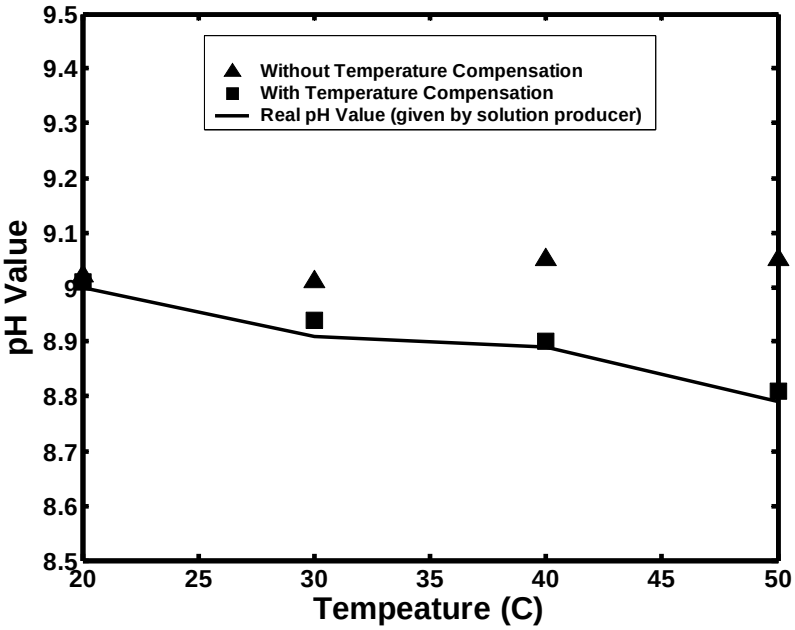

Fig. 7.13 Measured results of temperature compensation in pH9

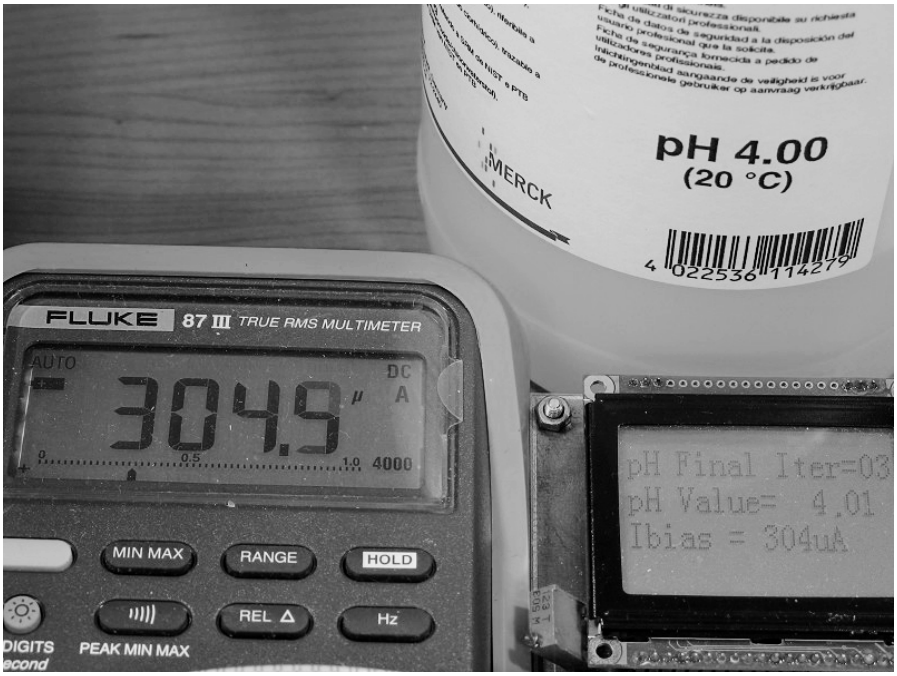

Fig. 7.14 LCD display of measurement result of optimum biasing current and pH value in pH4 buffer solution at 50°C

Table 7.8 The optimum biasing current of ISFET in pH4, pH7 and pH9 buffer solutions at 23°C, 30°C, 40°C, 50°C.

Temperature	pH4	pH7	pH9
23°C	305µA	191 µA	120 µA
30°C	305 µA	192 µA	119 µA
40°C	305 µA	191 µA	120 µA
50°C	304 µA	191 µA	118 µA

It can be observed from the data in Table 7.8 that in particular pH buffer solution, the optimum biasing currents of the ISFET device at different temperatures after iterative calculations are almost the same. It means those optimum biasing points are the athermal points of the ISFET device in different pH buffer solutions. It has proved that the proposed theory of the ISFET dynamic current temperature compensation technique is able to bias the ISFET at athermal points.

Fig. 7.11 shows the negative T.C. (without compensation) in *pH4* is compensated. However, the minute compensation in *pH7* shown in Fig. 7.12 can be explained by the fact that it is used as the reference in the compensation process and the calculated initial current (5.11) already forces the ISFET to work in athermal point in *pH7.* The compensation method also works for compensating positive *T.C.* (without compensation) in *pH9* as demonstrated in Fig. 7.13. Hence, the experimental evidence has confirmed that the proposed ISFET iteration temperature compensation technique is able to perform compensation in the pH measurement range of 4 to 9. It is noted that the full solid line within each figure from Fig. 7.11 to Fig. 7.13 represents the temperature effect of the pH buffer solution, which is provided by the manufacturer and is served as a reference.

A quadratic polynomial is employed to approximate a pH temperature-dependent function as follows:

$$f(T_1) = a_0 + a_1(T_1 - T_0) + a_2(T_1 - T_0)^2 \quad (7.11)$$

where T_0 is the reference temperature (room temperature). $f(T_1)$ is defined as the pH value at a given temperature T_1 in the range of T_0 to 50°C. a_0 is defined as the pH value at T_0. The respective value obtained for a_0 in *pH4*, *pH7* and *pH9* buffer solution is 4, 7 and 9. a_1 and a_2 is the corresponding first-order and second-order temperature coefficient. The extracted values for a_1 and a_2 by employing MATLAB are given in Table 7.9.

As observed, the small difference in first-order and second-order temperature coefficients between the buffer solution and measured pH value with temperature compensation reflect the effectiveness of the temperature compensation scheme. As *pH7* is treated as reference, the temperature coefficients remain very close with or without temperature compensation. The reason has already been mentioned. Unlike prior-art work of ISFET temperature compensation techniques, this proposed technique is nonlinear temperature compensation. This is very suitable for compensation of nonlinear *T.C.* of the ISFET threshold voltage in different pH buffer solutions such that the deviation of the measured pH value from actual pH value will not be enlarged significantly with temperature, thus demonstrating its advantage for supporting wider temperature range. Since the ISFET temperature compensation techniques can compensate the temperature effect on a single ISFET, it supports ease of fabrication, thus leading to a low cost solution for smart sensors. Besides, the fabrication process for the separated functional

devices can be optimized to improve the performance of the ISFET sensor [5]. Finally, there is no temperature sensor such as p-n junction diode [77], to be fabricated and calibrated, which would also reduce the cost of calibration procedure for the temperature sensor. The biasing current of mutual compensation can be further minimized by reducing the W/L aspect ratios of the ISFET device for lowering the total power consumption [73] or optimized in the ISFET process technology. Besides, through the use of microcontroller, it can carry out the ISFET temperature compensation within one second in automation procedure. The drift effect of ISFET device can be neglected in such a short time, which would guarantee the accuracy of temperature compensation.

Table 7.9 Temperature coefficients of buffer solution provided by manufacture and measured pH values

	pH4	pH7	pH9
	a_1 (pH/°C) a_1 [(pH/°C)^2]	a_1 (pH/°C) a_1 [(pH/°C)^2]	a_1 (pH/°C) a_1 [(pH/°C)^2]
Buffer solution	0.0015 -5E-05	-0.003079 4.474E-05	-0.006579 -5.263E-06
Without temp. Compensation	-0.006158 -1.105E-04	-0.0006316 5.789E-05	0.002262 -1.576E-05
With temp. compensation	0.0009736 -1.842E-05	-0.001211 5.263E-05	-0.004248 -6.553E-05

7.5 Measurement Results of the Proposed Sensory System in the Long-Term Monitoring Using Smart Compensation

7.5.1 Measurement Results of Proposed Sensory System in Long-Term Monitoring at Room Temperature

Chapter VII Results and Discussions

To demonstrate the effectiveness of the proposed ISFET time-variant (include ISFET drift and slow pH response) compensation technique at room temperature, an experiment pertaining to the long-term pH monitoring was carried out when the pH value of the solutions was changed in a step sequence of *pH7—pH5.65—pH4—pH5.65—pH7—pH9* at one hour intervals. The pH values with the symbol "X" denote the readings of the *CyberScan 1000* pH meter at defined time points in the pH measurement experiments. The *CyberScan 1000* pH meter measured each pH value twice, once at the beginning of the one hour interval and again at the end to monitor the stability of the solution across each time period being monitoring. Fig. 7.15 illustrates the comparison of the measured results based on an uncompensated scheme and various compensated schemes. It has confirmed that both the ISFET drift and slow pH response can be compensated with long-term monitoring. It is interesting to observe that there exists some minute compensation when the solution's pH value changes from *pH7* to *pH4* but not when it moves from *pH4* onwards. This confirms that the positive slope of V_{GS} of the ISFET caused by the drift mechanism is intrinsically counteracted by the negative slope of V_{GS} caused by the ISFET slow pH response in negative pH step [35], [66]. Meanwhile, it is also noted that the measurement results with standalone ISFET drift compensation are almost identical to dual compensation. This is due to the fact that both the measurement and calibration are conducted under the same room temperature (23°C). Thus, the temperature sensitive parameters, such as $V_{th(ISFET)}$ and μ_n in measurement would not deviate from those in calibration. The measurement results are compared in Table 7.10, which suggests that the

proposed ISFET system, under long-term measurement at room temperature, would produce a maximum of 0.02 pH deviations with respect to the reference pH value measured by the *CyberScan 1000* pH meter. Thus, for pH measurement range of 4 to 9, the drift rate is about 0.003 pH/hour (≈0.167mV/hour).

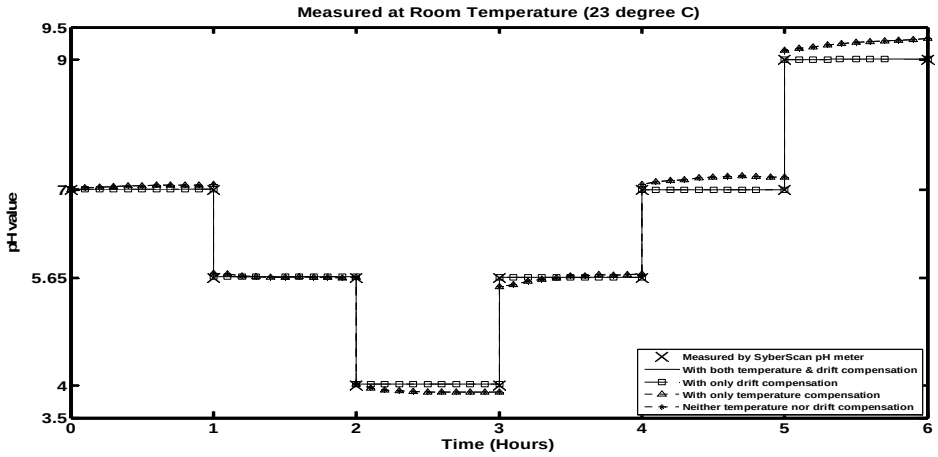

Fig. 7.15 Comparison of measured results with and without dual compensation at room temperature (23°C)

Table 7.10 Comparison of measured values between the proposed pH measurement system with dual compensation and the *CyberScan 1000* pH meter at 23°C

Time Interval (Hours)	Reading of Proposed pH measurement System (pH unit)	Reading of *CyberScan* 1000 pH meter (pH unit)	Difference (pH unit)
1st hour	7.01	7.00	0.01
2nd hour	5.67	5.65	0.02
3rd hour	4.02	4.00	0.02
4th hour	5.65	5.66	0.01
5th hour	6.99	7.00	0.01
6th hour	9.00	9.01	0.01

7.5.2 Measurement Results of the Proposed Sensory System in Long-Term Monitoring at Other Temperatures

In order to further demonstrate the effectiveness of the ISFET drift and the slow pH response compensation technique in the case of other temperatures, the experiment was conducted at 40°C in a thermal buffer depicted in Fig. 7.10. The pH values of the measured buffer solutions at 40°C were *pH6.95, pH5.67, pH4.01 and pH8.85*, which were recorded by the *CyberScan 1000* pH meter with automatic temperature compensation. It is evident from the Fig. 7.16 that the dual compensation scheme is far more superior to the ISFET sensing system without any compensation, and significantly better than that of the standalone drift compensation or that of the standalone temperature compensation. Of the measurement data being jointed at periodic sample time points of two seconds under the smart compensation algorithm, almost straight lines are formed at different pH values across each duration of the monitoring period. The readings of the CyberScan 1000 pH meter have been indicated with the symbol X while the readings of the proposed pH measurement system, illustrated as the corresponding solid line in Fig. 7.16, are *pH7.00, pH5.70, pH4.04, pH5.68 and pH8.90*. It should be noted that the commercial CyberScan 1000 pH meter only measures at any instant time point (to avoid the drift effect), with the purpose of providing an accurate solution pH value as a reference. A comparison of the readings between the proposed pH measurement system having dual compensation and the *CyberScan 1000* pH meter is summarized in Table 7.10. Using the measured data in Fig. 7.16 and Table 7.11, it can be calculated that after dual compensation, the output of the proposed measurement system only

produces an average temperature drift of 0.00049pH/hour/^{o}C over a pH range of 4 to 9 at a temperature range of (40^{o}C - 23^{o}C). This shows that the proposed sensory system achieves respectful precision for the long-term monitoring condition even at different temperatures. This suggests that not only does the sensory system compensate the drift against time, but it also demonstrates good immunity against the temperature-dependent drift which is regarded as the technical merit of this work. Comparing the results at room temperature in Table 7.10 and 40 ^{o}C in Table 7.11, it can be observed that the proposed ISFET system would generate additional error at other temperatures than at the room temperature. Since the ISFET calibration was carried out at the room temperature, the ISFET system can get more accurate result at room temperature. The extra error at other temperatures was introduced during the temperature compensation stage by using the dynamic temperature compensation technique. However, this extra error is acceptable low for water quality monitoring application [106]. This does not jeopardize the monitoring task of the system.

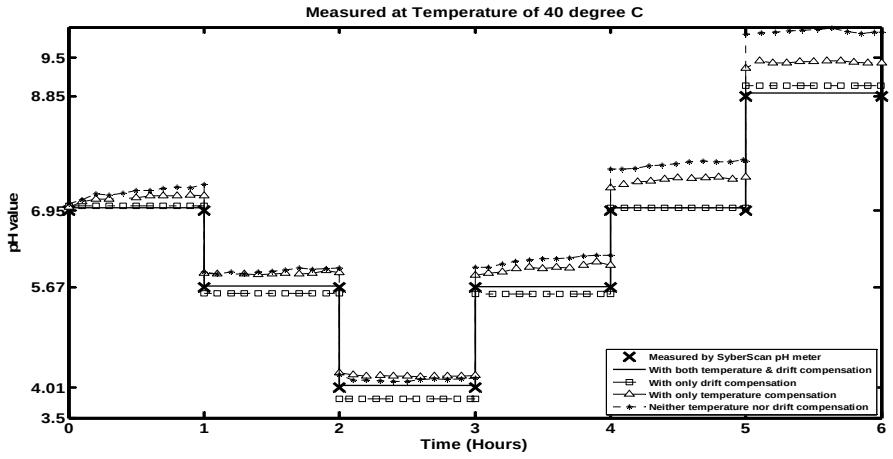

Fig. 7.16 Comparison of measured results with and without dual compensation at a temperature of 40°C

Table 7.11 Comparison of measured values between the proposed pH measurement system with dual compensation and the *CyberScan 1000* pH meter at 40°C

Time Interval (Hours)	Reading of Proposed pH measurement System (pH unit)	Reading of *CyberScan* 1000 pH meter (pH unit)	Difference (pH unit)
0 to 1	7.00	6.95	0.05
1 to 2	5.70	5.67	0.03
2 to 3	4.04	4.01	0.03
3 to 4	5.68	5.67	0.01
4 to 5	7.00	6.95	0.05
5 to 6	8.90	8.85	0.05

7.5.3 Comparison of Drift Performance with Prior-Art Works

The overall drift performances of the prior-art works and the proposed work are compared in terms of the time drift, temperature drift, pH range, incorporation of initial drift rate and incorporation of slow pH response. The results are demonstrated in Table 7.12 together with the performance of a standard uncompensated ISFET device as a reference. The proposed sensory system improves the time drift by at least one order of magnitude with respect to an uncompensated ISFET device and about twice the reduction with respect to the analytical drift reduction technique. Besides, the magnitude of the temperature drift of this work is also one order lower than that of the instrumentation system drift reduction technique. More importantly, the computation of the measured drift data also involves the effect of initial drift and slow response. This suggests that the sensory system can offer robust measurements because it takes a full range of drift data and handles slow response in view of a potential larger step change in pH value, which can happen in water quality monitoring. It has

been validated that the proposed smart compensation technique has the key advantages of low time drift and low temperature drift.

Table 7.12 Comparison of proposed ISFET drift compensation technique with previously reported works

Parameter	Conventional ISFET [29]	Analytical Technique [81]	Instrumentation System [83]	Proposed ISFET Sensory System
Time Drift at room temperature	0.06 pH/hour	0.005 pH/hour	N.A.	0.003 pH/hour
Temperature Drift	0.024 pH/hour/ ^{o}C	N.A.	0.0033 pH/hour/ ^{o}C	0.00049 pH/hour/ ^{o}C
pH range	pH1 - pH7	pH3.5 - pH10.1	pH3.34 - pH7	pH4 - pH9
Temperature	15 ^{o}C ─ 45 ^{o}C	Room Temp.	20 ^{o}C ─ 26 ^{o}C	23^{o}C , 40^{o}C
Consider initial drift	No	No	Yes	Yes
Consider slow pH response	No	No	Yes	Yes

7.5.4 Remarks of Proposed Sensory System

As the ADC has been involved in the data acquisition of the proposed ISFET measurement system, the resolution of the pH measurement system is limited by the resolution of the 12-bit ADC embedded in the microcontroller MSP430F149. In the design, the reference voltage of the commercial ADC is set as 1.8V, translating to the resolution of 0.4391mV, with resolution approximately on the order of 0.01pH (assuming the pH sensitivity of ISFET sensor = 50mV/pH at room temperature). In the current work, the power supply of the proposed ISFET measurement system is 3.3V. However, this does not jeopardize the measurement in water quality monitoring environment. It is

because the most important issue is to ensure the stability performance rather than highly accurate performance. Reasonable resolution and accuracy is adequate for the application. Furthermore, it is possible to extend the system to meet the requirements in other higher precision areas, This can be achieved by choosing a suitable higher resolution ADC together with higher power supply as stated above. Besides, the commercial meters, like example VWR pH meters, do not give the stability performance metric such as drift rate per temperature etc.. On the contrary, such the performance metric is emphasized in this work and is used as a figure of merit (FOM) to assess the temperature drift stability of the sensor. Therefore, one of the key contributions of the work (dual drift and temperature compensation) is that of proposal of a sensory system that permits low drift rate per temperature, which is an important for applications that encounter the changes arising from the drift and temperature together. Despite of 0.01 pH resolution for current data acquisition system design in the sensory system as discussed above, it is adequate for the long-term water-quality monitoring applications.

CHAPTER VIII

Conclusions and Recommendations

8.1 Conclusions

The operation mechanism of the ISFET sensor, the mechanism of the H^+ sensitivity of the ISFET, the nonidealities of the ISFET device such as time-invariant nonlinear temperature dependence on various pH values and time variant fluctuation arising from both drift mechanism and slow pH response have been studied. The prior-art modeling works such as the sophisticated ISFET built-in model and the ISFET macro-SPICE model are investigated with respect to their methodologies, advantages and disadvantages. Followed by the modeling review, the prior-art research efforts on the various ISFET nonidealities compensation techniques in along with representative ISFET readout circuits have been critically reviewed. This forms the foundation work on understanding the fundamental problems of the current-art research works.

A dedicated smart compensation algorithm is proposed to employ both the nonlinear temperature compensation technique and the time-variant compensation technique. It is being realized by both hardware and software to alleviate the problems associated with the composite temperature-dependence and time-variant effect in a basic ISFET sensing element.

The proposed ISFET-based intelligent pH measurement system consists of several research results. They include a new ISFET behavior-SPICE model for ISFET sensor simulation, a new non-saturation based ISFET interface circuit, a new saturation based ISFET interface circuit, a novel ISFET nonlinear

temperature compensation method, a novel ISFET drift and slow pH response compensation method, a microcontroller-based ISFET sensory system that realizes the proposed temperature and drift compensation technique for the precision pH sensing in long-term monitoring under different temperatures.

In the proposed ISFET behavior-SPICE model, it comprises a simplified behavior model that describes the pH sensitivity of the ISFET in chemical portion on the basis of Hal and Eijkel's theory using the highly-flexible mixed-signal Verilog-A language and a simplified SPICE LEVEL 3 model for the MOS device portion of the ISFET. The easy of usage and simplification but without sacrificing the accuracy is an important technical merit of the proposed model.

The proposed two new ISFET interface circuits, non-saturation based ISFET-VI interface circuit and saturation-based ISFET-LSD interface circuit have demonstrated the significant advantage of the insensitivity to the body effect. Therefore, the pH sensitivity of interface circuit well reflects the pH sensitivity of the ISFET sensor. Besides, the simplest structure of ISFET-LSD among all the interface circuit, reducing the circuit components as well as the circuit sensitivity, gives significant benefit for ISFET temperature compensation implementation.

The proposal of a novel technique for the ISFET temperature compensation with detail analysis and the proposal of a novel compensation method for ISFET time-variant nonideal effects are presented. With support of the intrinsic simple structure of ISFET-LSD readout circuit, this proposed dynamic biasing current temperature compensation technique gives a low cost solution at the

expense of increased computation complexity. A series of theoretical basis equations for temperature compensation purpose are established with the derivation of a unified expression for temperature-dependent ISFET threshold voltage in association with mutual compensation analysis on mobility and threshold voltage. Through iteration method for solving nonlinear equations, there exists an optimum biasing current for an athermal point of the ISFET at different pH values in a temperature range. A novel ISFET time-variant compensation technique is also proposed to compensate both the ISFET drift and slow pH response. Its basic idea is to correct the ISFET calibration data stored in the memory during real time measurement by taking advantage of the microcontroller hardware and software resource. Further incorporating the proposed ISFET dynamic current temperature compensation technique, it overcomes the key drawback of the conventional ISFET drift compensation techniques that rely on thermo-stable measurement environment to produce quality results.

In ISFET sensory system hardware implementation perspective, an improved ISFET interface IC has been presented. It incorporates the ISFET-LSD readout circuit with a new programmable current mirror that supports a wide range of biasing current with reduced dynamic error. The Texas Instruments MSP430 series microcontroller employed in this project in association with its peripherals plays an important role in the intelligent ISFET sensory system. Based on the hardware resource of the MSP430 microcontroller, dedicated software supported in both C and assemble language has been developed for the

intelligent ISFET pH measurement system to control the whole process of pH measurement.

To verify the performance of proposed intelligent ISFET sensory system and to compare with the prior-art works as the ultimate goal, a series of the characterization, simulation works and measurement results is conducted. This confirms that the proposed intelligent ISFET sensory system meets its objectives and outperforms the prior-art reported works. This should thank to the valuable combination of novel circuit architectures, novel compensation methodologies and reliable software programming to drive the microcontroller for realization of an intelligent ISFET sensory system.

8.2 Recommendations for Future Research

With involving of the ADC in data acquisition of the proposed ISFET measurement system, the resolution of the 12-bit ADC embedded in the microcontroller MSP430F149 is the main limitation on obtaining higher resolution of the pH measurement. Although the given ADC having a resolution of 0.01pH is adequate the for water quality monitoring application, it is still possible to extend the system to meet other higher precision areas by choosing or designing a high-resolution ADC, for instance, 16-bit ADC together with higher power supply.

With the development of semiconductor fabrication technology, many research efforts have investigated on fabricating ISFET device in standard CMOS process by post processing. Due to the proposed interface circuits has the key advantage of eliminating the body effect of ISFET device, they can be

fabricated on the same die as ISFET device to realize the monolithic implementation of the ISFET microsystem. Furthermore, other modules, such as ADC and microcontroller, can also be integrated in the same die, providing single chip solution of the sensor system, for instance, Sensor System on Chip (SSOC).

Future ISFET interface circuit design as well as the Sensor System on Chip (SSOC) design would be greatly benefited from the ISFET model with less complexity and higher flexibility. Based on the proposed ISFET Behavior-SPICE model, which has already contained the temperature characteristics of the ISFET behaviour, there is a possibility to include the time-variant effect of ISFET such that the time domain simulations can be conducted. This will be useful for the study of the impact of ISFET interface circuits to drift phenomena.

Since the invention of the ISFET sensor in about 30 years ago, the ISFET sensor has been successfully developed for various types of chemical sensors with dedicated ion-selective membrane. Therefore, a similar type of interface circuit architecture on the basis of the proposed circuits in this thesis can be applied for other chemical sensors. Finally, the circuit techniques as well system design methodology presented herewith can be extended to build a multi-parameter sensor system for monitoring of concentrations of different ions in the solution for both environmental and biomedical applications.

REFERENCES

[1] http://www.freedrinkingwater.com/water-education/quality-water-ph.htm

[2] http://www.jp.horiba.com/story_e/ph/ph05_01.htm

[3] P. Bergveld, "Development of an Ion-sensitive Solid-state Device for Neurophysiologic Measurements," *IEEE Trans. Biomed. Eng.*, vol. 17, pp. 70-71, Jan. 1970.

[4] L.Bousse, J. Shott, J.D.Meindl, "A Process for the Combined Fabrication of Ion Sensors and CMOS Circuits," *IEEE Electron Device Letters,* vol. 9, No. 1, pp. 44-46, Jan. 1997

[5] C.Cane, I.Gracia and A.Merlos, "Microtechnologies for pH ISFET Chemical Sensors," *Microelectronic Journal,* vol. 28, No. 4, pp. 389-405, 1997.

[6] C.G.Jakobson, U.Dinnar, M.Feinsod and Y.Nemirovsky, "Ion-Sensitive Field-Effect Transistors in Standard CMOS Fabricated by Post Processing," *IEEE Sensors Journal,* vol. 2, No. 4, pp. 279-287, Aug. 2002

[7] L.Sudakov-Boreysha, A.Morgenshtein, U.Dinnar, Nemirovsky, Y, "ISFET CMOS Compatible Design and Encapsulation Challenges," *Proc. of the 2004 11th IEEE International Conf. on Electronics, Circuits and Systems.* Vol. 13-15, pp.535-538, Dec. 2004

[8] W.Oelbner, JZosel, U.Guth, "Encapsulation of ISFET sensor chips," *Sensors and Actuators B*, vol. 105, pp. 104-117, 2005

[9] Rotithor, H.G, Trutt, F.C, "Microprocessor Based pH Monitoring and Transmitting System", *6th IEEE Instrumentation and Measurement Technology Conference,* vol. 25-27, pp. 141-145, Apr 1989

References

[10] A.Cambiaso, S. Chiarugi, M. Grattarola, "An H^+-FET-based System for On-line Detection of Micro-organism in Waters" *Sensors and Actuators B*, vol. 24-25, pp. 218-221, 1996

[11] Denise Michele Wilson, Sean Hoyt, Jiri Janata, Karl Booksh, and Louis Obando, "Chemical Sensors for Portable, Handheld Field Instruments", *IEEE Sensors Journal,* vol. 1, No. 4, pp. 256-273, Dec 2001

[12] A.Poghossian, A.Baade, H.Emons, M.J.Schöning "Application of ISFET for pH Measurement in Rain Droplets," *Sensors and Actuators B*, vol. 76, pp. 634-638, 2001

[13] Chung-Huang Yang, Wen-Yaw Chung, "A Low-Power Telemetric System Design for ISFET-Based Sensor Array Application", *ECCTD'03-European Conference on Circuit Theory and Design*, September 1-4, 2003, Poland

[14] P. Bergveld, "Thirty years of ISFETOLOGY What Happened In The Past 30 Years And What May Happen In The Next 30 Years," *Sensors and Actuators B*, vol. 88, pp. 1-20, 2000.

[15] P.R. Barabash, R.S.C Cobbold and W.B.Wlodarski, "Analysis of the Threshold Voltage and its Temperature Dependence in Electrolyte-Insulator-Semiconductor Field-Effect Transistor (EISFET's)," *IEEE Trans. Electron Devices*, vol. 34, no.6, pp. 1271-1282, 1987

[16] H.-H. van den Vlekkert, L. Bousse, N. de Rooij, "The Temperature Dependence of the Surface Potential at The Al_2O_3/Electrolyte Interface", J. Colloid Interface Sci. vol. 122 (2), pp. 336-345, 1988.

References

[17] H. Gelsfer, *pH Measurements: Fundamentals, Methods, Applications, Instrumentation,* VCH, Weinheim, 1991.

[18] S. Martinoia, L. Lorenzelli, G. Massobrio, Paolo Conci and Alberto Lui, "Temperature Effects on the ISFET Behaviour: Simulations and Measurements," *Sensors and Actuators B*, vol. 50, pp. 60-68, 1998

[19] H.K. Liao, E.S. Yang, J.C. Chou, "Temperature and Optical Characteristics of Tin Oxide Membrane Gate ISFET," *IEEE Trans on Electron Device*, vol. 46, no. 12, pp. 2278-2281, Dec. 1999

[20] J.C. Chou, Y.F. Wang and J.S. Lin, "Temperature effect of a-Si:H pH-ISFET", *Sensor and Actuators B*, vol.62, pp.92-96, 2000

[21] Jung-Chuan Chou, Ying Shin Li, Jung Lung Chiang, "Simulation of Ta_2O_5-gate ISFET Temperature Characteristics", *Sensor and Actuators B*, vol. 71, pp. 73-76, 2000

[22] Murray, "Determination of meat pH – temperature", *Meat Science*, vol. 58, pp. 145-150, 2001

[23] J.C. Chou, C.Y. Weng and H.M Tsai, "Study on The Temperature Effect of Al_2O_3 Gate pH-ISFET," *Sensors and Actuators B*, vol. 81, pp. 152-157, 2002

[24] Shahriar Jamasb, Scott D. Collins, and Rosemary L. Smith, "A Physically-based Model for Drift in Al_2O_3-gate pH ISFET's," *International Conf. on Solid State Sensors and Actuators, 1997. TRANSDUCERS'97 Chicago,* vol. 5, pp. 2337-2340, 1997

References

[25] Shahriar Jamasb, Scott D. Collins and Rosemary L. Smith, "A Physical Model for Drift in pH ISFETs", *Sensor and Actuator B,* vol. 49, pp. 146-155, 1998

[26] Shahriar Jamasb, Scott D. Collins and Rosemary L. Smith, "A Physical Model for Threshold Voltage Instability in Si_3N_4-Gate H^+-Sensitive FET's (pH ISFET's)," *IEEE Transactions on Electron Devices,* vol. 45, No. 6, pp. 1239-1245, JUNE 1998.

[27] Jung-Chuan Chou, Ching-Nan Hsiao, "Drift Behavior of ISFETs with a-Si: H-SiO_2 Gate Insulator," *Materials Chemistry and Physics,* vol. 63, pp. 270-273, 2000

[28] C.G. Jakobson, M. Feinsod, Y.Nemirovsky, "Low Frequency Noise and Drift in Ion Sensitive Field Effect Transistors," *Sensor and Actuator B,* vol. 68, pp. 134-139, 2000

[29] Jung Chuan Chou, Hsjian Ming Tsai, Ching Nan Shiao, Jin Sung Lin, "Study and Simulation of the Drift Behaviour of Hydrogenated Amorphous Silicon Gate pH-ISFET," *Sensors and Actuators B*, vol. 62, pp. 97-101, 2000

[30] L.J. Bousse, D. Hafeman, N. Tran, "Time dependence of the chemical response of silicon nitride surfaces," *Sensors and Actuators B*, Vol. 1, pp. 361-367, 1990

[31] Jung-Chuan, Chou, Ching-Nan Hsiao, "Drift Behavior of ISFETs with a-Si:H-SiO_2 Gate insulator," *Materials Chemistry and Physics,* vol. 63, pp. 270-273, 2000

References

[32] Yoshitaka Ito, "Long-term Drift Mechanism of Ta_2O_5 Gate pH-ISFETs" *Sensors and Actuators, B*, vol. 64, pp. 152-155, 2000

[33] Dun Yu, Ya-Dong Wei, Gui-Hua Wang, "Time-dependent response characteristics of pH-sensitive FET," *Sensors and Actuators B*. Vol. 3, pp. 279-285, 1991

[34] Luc Bousse and Shahriar Mostarshed, "Comparison of the Hysteresis of Ta_2O_5 and Si_3N_4 pH-sensing Insulators," *Sensors and Actuators B*, vol.17 pp. 157-164, 1994

[35] P. Woias, L. Meixner and P. Fröstl, "Slow pH response effects of silicon nitride ISFET sensors," *Sensors and Actuators, B*, vol. 48, pp. 501-504, 1998

[36] Jung Chuan Chou, Yii Fang Wang, "Preparation and Study on the Drift and Hysteresis Properties of The Tin Oxide Gate ISFET by The Sol-gel Method" *Sensors and Actuators, B*, vol. 86, pp. 58-62, 2002

[37] D. E. Yates, S. Levine, and T. W. Healy, "Site-binding Model of The Electrical Double Layer At The Oxide/Water Interface ", *J.Chem. Soc. Faraday I,* vol. 70, pp.1807-1818, 1974.

[38] Luc Bousse, Nico F.de Rooij, P. Bergveld, "Operation of Chemically Sensitive Field-Effect Sensors as a Function of thee Insulator-Electrolyte Interface", *IEEE Trans. On Electron Devices,* vol. ED-30, No. 10, pp. 1263-1270 Oct. 1983

References

[39] Clifford D. Fung, Peter W. Cheung, Wen H. Ko, "A Generalized Theory of an Electrolyte-Insulator-Semiconductor Field-Effect Transistor", *IEEE Trans. On Electron Devices,* vol. ED-33, No. 1, pp.8-18 Jan. 1986

[40] David L. Harme, Luc Bousse, "Ion-Sensing Device with Silicon Nitride and Borosilicate Glass Insulators", *IEEE Trans. On Electron Devices,* vol. ED-34, No.8, pp. 1700-1707 Aug. 1987

[41] R. E. G. Van Hal, J. C. T. Eijkel, P. Bergveld, " A Novel Description of ISFET Sensitivity with the Buffer Capacity and Double-layer Capacitance as Key Parameters", *Sensors and Actuators B* vol. 24-25 pp. 201-205, 1995

[42] R. E. G. Van Hal, J. C. T. Eijkel, P. Bergveld, " A General Model to Describe The Electrostatic Potential at Electrolyte/Oxide Interfaces", Adv. Coll. Interf. Sci. vol. 69, pp. 31-62, 1996

[43] Meng-Nian, Niu, Xin-Fang Ding, Qin-Yi Tong, "Effect of Two Type of Surface Sites on The Characteristics of Si_3N_4-gate pH-ISFETs", *Sensors and Actuators B* vol. 37 pp. 13-17, 1996

[44] Meng-Nian, Niu, Xin-Fang Ding, Qin-Yi Tong, "Effect of Two Type of Surface Sites on The Characteristics of Si_3N_4-gate pH-ISFETs", *ICSE'96 Proc.,* pp. 189-193 Nov. 1996, Penang, Malaysia

[45] L.W. Nagel, SPICE2: A Computer Program to Simulate Semiconductor Circuits, Electronics Research Laboratory, Rep. nr. ERL-M520, University of California, Berkeley, USA, 1975

References

[46] L.K.Meixner, S. Koch, "Simulation of ISFET Operation Based on the Site-Binding Model", *Sensors and Actuators B*, vol. 6 pp. 315-318, 1992

[47] Massimo Grattarola, Giuseppe Massobrio, Sergio Martinoia, "Modeling H^+-sensitive FET's with SPICE", *IEEE Trans. On Electron Devices,* vol. 39, No.4, pp. 813-819, Apr. 1992

[48] Sergio Martinoia, Giuseppe Massobrio, Massimo Grattarola, "An ISFET Model for CAD Applications", *Sensors and Actuators B*, vol.8, pp. 261-265, 1992

[49] Massimo Grattarola, Giuseppe Massobrio, Sergio Martinoia, "Use of SPICE for modeling silicon-based chemical sensors", *Sensors and Materials* vol. 6 No. 2 pp. 101-123, 1994

[50] Sergio Martinoia, Massimo Grattarola, Giuseppe Massobrio, "Modeling Nonideal Behaviors in Sensitive FETs with SPICE", *Sensors and Actuators B* vol. 7 pp. 561-564, 1992

[51] Giuseppe Massobrio, Sergio Martinoia, "Modeling the ISFET behavior under temperature variations using BIOSPICE", *Electronics Letters* vol. 32 No. 10, pp. 936-938, 1996

[52] Wladyslaw Torbicz, Zofia Sypniewska, "An extended model of the electrolyte/hydrogen ion-sensitive field-effect transistor system", *Sensors and Actuators B* vol. 7 pp. 567-571, 1992

References

[53] S. Martinoia, L. Lorenzelli, G. Massobrio, B. Margesin, "A CAD System For Developing Chemical Sensor-based Microsystems With An ISFET-CMOS Compatible Technology", *Sensor and Materials*, vol. 5, pp. 32-49, 1999

[54] Sergio Martinoia, Giuseppe Massobrio, "A behavior macro-model of the ISFET in SPICE", *Sensors and Actuators B* vol. 62 pp. 182-189, 2000

[55] R. Kühnhold, H. Ryssel "Modeling The pH Response of Silicon Nitride ISFET Devices", *Sensors and Actuators B* vol. 68 pp. 307-312, 2000

[56] Sergio Martinoia, Giuseppe Massobrio, Leandro Lorenzelli, "Modeling ISFET Microsensor and ISFET Microsystems: A Review", *Sensors and Actuators B* vol. 105 pp. 14-27, 2005

[57] P. Bergveld, "The Operation of an ISFET as an Electronic Device", *Sensors and Actuators B* vol. 1 pp. 17-29, 1981

[58] P. Bergveld, "Design Consideration for ISFET Multiplexer and Amplifier", *Sensors and Actuators B* vol. 5 pp. 13-20, 1984

[59] A. Sibbald, "A Chemical-Sensitive Integrated-Circuit: The Operational Transducer," *Sensors and Actuators*, vol. 7, pp. 23-38, 1985

[60] H.S. Wong and M. H. White, "A CMOS-Integrated 'ISFET-Operational Amplifier Chemical Sensor Employing Differential Sensing" *IEEE Tans. on Electron Devices*, vol. 36, No. 3, pp. 479-487, Mar. 1989

[61] L. Ravezzi and P. Conci, "ISFET Sensor Coupled with CMOS Read-out Circuit Micro-system", *IEE Electronics Letters*, vol. 34, No. 23, November 1998

[62] B. Palán, F.V. Santos, J.M. Karam, B. Courtois and M. Husák, "New ISFET Sensor Interface Circuit for Biomedical Applications," *Sensors and Actuators B*, vol. 57, pp. 63-68, 1999

[63] L. Ravezzi, D. Stoppa, M. Corrá, G. Soncini, G.-F. Dalla Betta and L. Lorenzelli, "A CMOS ASIC for Differential Read-out of ISFET Sensors," *International Conference on Ele4tronics, Circuits and Systems*, vol. 3, no. 2-5, Sept. 2001

[64] Erik Lauwers, Jan Suls, Walter Gumbrecht, "A CMOS Multi-parameter Biochemical Micro-sensor With Temperature Control and Signal Interfacing", *IEEE Journal Of Solid-State Circuits*, vol. 36, no. 12, Dec. 2001

[65] K. Tukkineami, "Study of CHMFET Interface Electronics", MIXDES Conference, Wroclaw, pp. 20-22, 2002

[66] S. Casans, A.E. Navarro, D. Rmirez, E. Castro and A. Baldi, N. Abramova, "Novel Voltage-controlled Conditioning Circuit Applied to the ISFETs Temporary Drift and Thermal Dependency," *Sensors and Actuators B*, vol. 91, pp. 11-16, 2003

[67] Ghallab. Y.H, Badawy, Badawy. W, "A Novel pH Sensor Current Mode Read-Out Circuit Using Operational Floating Current Conveyor", *Proc. International Conf. on MEMS, NANO and Smart Systems,* vol. 25-27, pp. 262-265, Aug, 2004

[68] A. Morgenshtein, L. Sudakov-Boreysha and U. Dinnar, "CMOS Readout Circuitry for ISFET Micro-systems", *Sensors and Actuators B*, vol. 97, pp. 122-131, 2004

References

[69] V. P. Chodavarapu, A. H. Titus, and A. N. Cartwright, "CMOS ISFET Microsystem for Biomedical", *IEEE Conference on Sensors*, pp. 109- 112, Irvine, USA, Nov. 2005

[70] Shepherd, L.M, Toumazou. C, "A Biochemical Translinear Principle with Weak Inversion ISFETs", *IEEE Tran. Circuits and Systems I: Fundamental Theory and Application,* vol. 52, Issue 12, pp. 2614-2619, Dec. 2005

[71] Wen-Yaw Chung, Pijanowska. D.O, and Torbicz.W, "A New Body-Effect Elimination Technique for ISFET Measurement," *IEEE Conference on Sensors*, pp. 1046- 1049, Irvine, USA, Nov. 2005

[72] D.Y. Chen, P.K. Chan and M.S. Tse, "A CMOS ISFET Interface Circuit for Water Quality Monitoring", *IEEE Conference on Sensors*, pp. 1217- 1220, Irvine, USA, Nov. 2005

[73] P. K. Chan and D. Y. Chen, "A CMOS ISFET Interface Circuit with Dynamic Current Temperature Compensation Technique," *IEEE Tran. Circuits and Systems I: Fundamental Theory and Application,* vol. 54, Issue 1, pp. 119-129, 2007

[74] C.Y. Aw and Peter W. Cheung, "A pH-ISFET Sensor With On-Chip Temperature Sensing", *International Conference on IEEE Engineering in Medicine & Biology Society*, pp. 772-773, 1988

[75] Y. Lung Chin, J. C. Chou, T. P. Sun, "A Novel SnO2/Al Discrete Gate ISFET pH Sensor with CMOS Standard Process", *Sensors and Actuators B*, vol. 75 pp. 36-42, 2001

References

[76] Y. Lung Chin, J.C. Chou, T.P. Sun, W.Y. Chung and S.K. Hsiung, "A Novel pH Sensitive ISFET with on Chip Temperature Sensing using CMOS Standard Process," *Sensors and Actuators B*, vol. 76, pp. 582-593, 2001

[77] A. Morgenshtein, L. Sudakov-Boreysha, U. Dinnar, Claudio G. Jakobson and Y. Nemirovsky, "Wheatstone-Bridge Readout Interface for ISFET/REFET Applications", *Sensors and Actuators B*, vol. 98, pp. 18-27, 2004

[78] M. Chudy, W. Wroblewski, Z. Brzoka, "Towards REFET", *Sensors and Actuators B*, vol. 57, pp. 47-50, 1999.

[79] Wen-Yaw Chung, Chung-Huang Yang, Ming-Chia Wang, Dorota G. Pijanowska, Wladyslaw Torbicz, "Temperature Compensation Electronics for ISFET Readout Application," *IEEE International Workshop on Biomedical Circuits & Systems,* pp. S1.6-5 – S1.6-8, Dec. 1-3, 2004

[80] P. Bergveld, "*Implantable Sensors for Closed-loop Prosthetic Systems*," W.H.Ko, Ed. Mount Kisco, NY: Futura, 1985

[81] Shahriar Jamasb, "An Analytical Technique for Counteracting Drift in ion-Selective Field Effect Transistors (ISFETs)," *IEEE Sensors Journal,* Vol. 4, No. 6, Dec. 2004.

[82] S. Casans, Diego Ramirez Munoz, A.E. Navarro, A. Salazar, "ISFET drawbacks minimization using a novel electronic compensation", *Sensors and Actuators B,* vol. 99, Issue 1, pp. 42-49, Apr. 2004

[83] S. Casans, A.E. Navarro, D. Ramirez, J.M. Espi, N. Abramova and A.Baldi, "Instrumentation System to Improve ISFET Behaviour", IEEE Instrumentation and Measurement Technology Conference, Anchorage, AK, USA, pp. 1291-1294, 21-23 May 2002.

References

[84] Premanode, B, Silawan. N and Toumazou. C, "Drift Reduction in Ion-Sensitive FETs Using Correlated Double Sampling", *Electronic Letters*, vol. 43, Issue 16, pp. 857-859, Aug. 2007.

[85] R. S. C Cobbold, *Theory and Application of Field-Effect Transistors.* New York: Wiley, 1970.

[86] A. D. Evans, Ed., *Designing with Field-Effect Transistors.* New York: McGrwa-Hill, 1981

[87] S. M. Sze, *Physics of Semiconductor Device*, 2nd ed. New York: Wiley, 1982

[88] G. Massobrio, P. Antognetti, *Semiconductor Device Modeling with SPICE,* 2nd ed., McGraw-Hill, New York, 1993.

[89] Y. P. Tsividis, *Operation and Modeling of The MOS Transistor.* New York: McGraw-Hill, 1999.

[90] I. M. Filanovsky, "Voltage Reference Using Mutual Compensation of Mobility and Threshold Voltage Temperature Effects", *Proceedings of IEEE International Symposium on Circuits and Systems*, vol. 5, pp. 197-200, May, 2000.

[91] Dan Fitz Patrick, Ira Miller, "Analog Behavioral Modeling With The Verilog-A Language", Kluwer Academic Publishers, 1998

[92] Hung-Kwei Liao, Li-Lun Chi, Jung-Chuan Chou, Wen-Yaw Chung, Tai-Ping Sun, Shen-Kan Hsiung, "Study on pH_{PZC} and surface potential of tin oxide gate ISFET", *Materials Chemistry and Physics* vol. 59 pp. 6-11, 1999

References

[93] A.A. Poghossian, "Determination of the pH_{PZC} of insulators surface from capacitance-voltage characteristics of MIS and EIS structures", *Sensors and Actuators B* vol. 44, pp551-553, 1997

[94] Jung-Lung, Shiun-Sheng Jan, Jung-Chuan Chou, Ying-Chung Chen, "Study on the temperature effect, hysteresis and drift of pH-ISFET devices based on amorphous tungsten oxide," *Sensor and Actuator B*, vol. 76 pp. 624-628, 2001

[95] T. Manku and Y. Wang, "Temperature-independent output voltage generated by threshold voltage of an NMOS transistor", *Electron. Lett*., vol. 31, no. 6, pp. 935-936, 1995.

[96] I. M. Filanovsky, Su Tarn Lim, "Interaction of Threshold Voltage and Mobility Temperature Dependencies Applied to Stabilization of Current and Voltage", *Proceeding of the 43rd IEEE Midwest Symposium on Circuits and Systems,* vol. 3, pp. 1022-1025 Aug. 2000.

[97] I. M. Filanovsky and A. Allam, "Mutual Compensation of Mobility and Threshold Voltage Temperature Effects With Applications In CMOS Circuits," *IEEE Trans. Circuits Syst. I, Fundam. Theory Appl.*, vol. 48, no. 7, pp. 876-884, Jul. 2001

[98] F. M. Klaassen and W. Hes, "On The Temperature Coefficient of The MOSFET Threshold Voltage," *Solid State Electron.*, vol. 29, no. 8, pp. 787-789, 1986.

[99] D. K Schroeder, *Semiconductor Material and Device Characterization*. New York: Wiley, 1990

References

[100] P. Bergveld, "*Implantable Sensors for Closed-loop Prosthetic Systems*," W.H.Ko, Ed. Mount Kisco, NY: Futura, 1985

[101] "MSP430x13x, MSP430x14x Mixed Signal Microcontroller", SLAS272A, Texas Instruments, 2000.

[102] R. J. Baker, H. W. Li, and D. E. Boyce, *CMOS Circuit Design, Layout, and Simulation*. Piscataway, NJ: IEEE Press, 1998

[103] "TLV5616C, TLV5616I 2.7-V To 5.5-V Low Power 12-Bit Digital-To-Analog Converters with Power Down", Texas Instruments, April, 2004

[104] E. Säckinger and W. Guggenbühl, "A High Swing, High Impedance MOS Cascode Circuit," *IEEE J. Solid-State Circuits,* vol. 25, pp.289-298, Feb. 1990

[105] T. Serrano and B. Linares-Barranco, "The Active-Input Regulated-Cascode Current Mirror", *IEEE Trans. on Circuits and Systems-I: Fundamental Theory and Applications,* vol. 41, no. 6, pp. 464-467, June 1994

[106] J. Bartram and R. Balance, "Water Quality Monitoring: A Practical Guide to the Design and Implementation of Freshwater Quality Studies and Monitoring Programmes", United Nations Environment Programme, World Health Organization, Technology and Engineering 1996.

AUTHOR'S PUBLICATIONS

[1] D.Y. Chen, P.K. Chan and M.S. Tse, "A CMOS ISFET Interface Circuit for Water Quality Monitoring", *IEEE Conference on Sensors*, pp. 1217- 1220, Irvine, USA, Nov. 2005

[2] P. K. Chan and D. Y. Chen, "A CMOS ISFET Interface Circuit with Dynamic Current Temperature Compensation Technique," *IEEE Tran. Circuits and Systems I: Fundamental Theory and Application,* vol. 54, Issue 1, pp. 119-129, 2007

[3] D.Y. Chen and P.K. Chan "An Intelligent ISFET Sensory System with Temperature and Drift Compensation for Long-Term Monitoring," *IEEE Sensors Journal,* vol. 8, No. 12, pp. 1948-1959, Dec. 2008

Appendix A

Software Programming Code of ISFET Sensory System

```
/*----------------Head file--------------------*/
#include <MSP430x14x.h>
#include "MSP149_Define.h"
#include "character.h"
/*-----------Function define---------------*/
void Init(void);                              //Systerm initialize
void Sw_FLL(void);                            //DCO frequency adjust 1.0M for
AMCLK and MCLK
void delay(unsigned int);                     //delay sub-routine
void Timer(void);                             //calculate the time
/*--------The following functions are for Matrix-dot LCD display---------*/
void HY12864_Init(void);            //HY12864 Dot-Matrix LCD initiation
void HY12864_CodeWrite(unsigned char, unsigned char, unsigned char);
void HY12864_DataWrite(unsigned char, unsigned char, unsigned char);
void HY12864_Addr_Set(unsigned char, unsigned char);
void HY12864_Startline_Set(unsigned char);
void HY12864_CLR(unsigned char);
void HY12864_FULL(void);
void Title(unsigned char);
void eepromok(void);
void eepromerror(void);
void menu1A(void);
void menu2A(unsigned char);
void menu2B(void);
void menu3A(unsigned char);
void menu4A(unsigned int, unsigned char);
```

Appendix A Software Programming Code of ISFET Sensory System

```
void menu4B(unsigned int, unsigned char);
void menu4C(unsigned int, unsigned char);
void menu4D(void);
void pHfinal(unsigned int);
void pHready(void);
void menu5A(unsigned int, unsigned char);
void menuEEPR(void);
void Time_display(unsigned char, unsigned char);
void menuFixBias(void);
void pHSensResult(void);
void battery_icon(unsigned char);
void set_row(unsigned char);
void set_cross(unsigned char);
void set_triangle(unsigned char);
void LCD_type_8x16(unsigned char, unsigned char const **);

/*----------The following functions are for DAC----------------*/
void DAC_SPI(unsigned int);
unsigned int M93C86_Read(unsigned int);
void M93C86EN_DS(unsigned int);
void M93C86_W(unsigned int, unsigned int);
//*****************************************************************************
void main(void)
{
        /*Initialize the Microcontroller*/
         unsigned int i;
        Init();
        P1IE |= 0x3F;         //Enable the P1.0 interruption
        P1IFG = 0x00;         //Clear the interrupt flag for P1.0
```

Appendix A Software Programming Code of ISFET Sensory System

```
while(1){
        while (status & menu1){
                menu1A();
                //display_flag &= ~renewal;
        }
        while (status & EEPROMClear){
                menuEEPR();
                HY12864_CLR(2);
                HY12864_CLR(3);
                HY12864_CLR(4);
                HY12864_CLR(5);
                HY12864_CLR(6);
                HY12864_CLR(7);
                pHdriftVoltageSum = 0.0;
                for(i=1;i<=100;i++) delay(5000);  //just for delay
                status &= ~EEPROMClear;
                status |= menu1;
        }
        while (status & menu2){
                switch(menu_status & (pH4C+pH7C+pH9C+pHM)){
                        case 0x0000  :   break;
                        //select pH4 calibration
                        case pH4C    :   menu2A(pH4); break;
                        //select pH7 calibration
                        case pH7C    :   menu2A(pH7); break;
                        //select pH9 calibration
                        case pH9C    :   menu2A(pH9); break;
                        //select pH measurement
                        case pHM     :   menu2B();    break;
```

Appendix A Software Programming Code of ISFET Sensory System

```
                        default      :   break;
                    }
                }
/*Process the ISFET calibration wiht biasing current increase from Min to Max */
                while (status & menu3){                 //ISFET Sensor Calibration
                    if (!(display_flag & menu3_ren)){       //display the menu
                        if(menu_status & pH4C) menu3A(4);
                        else if(menu_status & pH7C) menu3A(7);
                        else if(menu_status & pH9C) menu3A(9);
                        display_flag |= menu3_ren;
                        TACTL &= ~MC0;                  //halt the TimerA
                        TAR = 0;                        //clear the TimerA
                        CCR0 = 0x00F6;                  //60ms interruption
                        TACTL |= MC0;                   //start the TIMERA
                    }
                    if(Flag & ADC12cycleend){    //the A/D conversion finished
                        Flag &= ~ADC12cycleend;
                //in case of fails: for instance the DAC output is 0
//the program should return to the menu3 and restart the calibration
                        if(ADC12resultAverage <= 100){
                            display_flag &= ~menu3_ren;
                            continue;
                        }
                        DACdata = 502+5.015923f*(calib_counter+1);
                        DAC_SPI(DACdata-6);     //sent digital data to DAC
                        if(menu_status & pH4C)
                            M93C86_Addr = M93C86_Index_pH4
                        else if (menu_status & pH7C)
                            M93C86_Addr = M93C86_Index_pH7
```

Appendix A Software Programming Code of ISFET Sensory System

```
else if(menu_status & pH9C)
        M93C86_Addr = M93C86_Index_pH9

_NOP();
M93C86_W(M93C86_Addr,ADC12resultAverage);
//display the process in LCD
if (calib_counter == 0)
       HY12864_Addr_Set(7,0);
if(Flag & CalibProcess){
       Flag &= ~CalibProcess;
       if (calib_counter <= 127)
              HY12864_DataWrite(0xFF, 1, 0);
       else if (calib_counter <= 255)
              HY12864_DataWrite(0xFF, 0, 1);
       }
else Flag |= CalibProcess;
       calib_counter ++;
if(calib_counter == 301){
       TACTL &= ~MC0;
       TAR = 0;
       calib_counter = 0;
       status &= ~menu3
       status |= menu1;
       DAC_SPI(502-6);
       pHdriftVoltageSum = 0.0;
       pHdriftVoltageSumSave = 0;
       M93C86_W(0x3FC,0xA5A5);
       P2OUT |= M93C86_CS;
       while(1){
```

Appendix A Software Programming Code of ISFET Sensory System

```
                                if(P2IN & 0x40) break;
                        }
                        _NOP();
                        M93C86_W(0x3FD,pHdriftVoltageSumSave);
                }
        }
}
//ISFET iteration measurement
while (status & menu4){
        //display the menu
        if (!(display_flag & menu4_ren)){
                display_flag |= menu4_ren;
                pHMeasurValueFOld = 0.0;
                //set initial biaing current
                DACdata = 502+5.015923f * 92;
                DAC_SPI(DACdata-5);
                IBiasCurrentF = 192.0;
                IBiasCurrent = (int)IBiasCurrentF;
                //start the TimerA
                TACTL &= ~MC0;              //stop first
                TAR = 0;              //clear the timerA
                CCR0 = 0x800;
                TACTL |= MC0;
                iteration_counter = 1;
                pHfinal(iteration_counter);
                if(!(display_flag & menu4_result)){
                        display_flag |= menu4_result;
                        HY12864_CLR(2);
                        HY12864_CLR(3);
```

```
                HY12864_CLR(4);
                HY12864_CLR(5);
                HY12864_CLR(6);
                HY12864_CLR(7);
        }
}
if (Flag & ADC12cycleend){
        Flag &= ~ ADC12cycleend;

        //in case of error
        if(ADC12resultAverage <= 100){
                display_flag &= ~menu4_ren;
                continue;
        }
        pHMeasurValueI = ADC12resultAverage;
        //get the three corresponding calibration value
M93C86_Addr = M93C86_Index_pH4 + IBiasCurrent - 100;
        pH4CalibValue = M93C86_Read(M93C86_Addr);
        _NOP();
M93C86_Addr = M93C86_Index_pH7 + IBiasCurrent - 100;
        pH7CalibValue = M93C86_Read(M93C86_Addr);
        _NOP();
M93C86_Addr = M93C86_Index_pH9 + IBiasCurrent - 100;
        pH9CalibValue = M93C86_Read(M93C86_Addr);
        _NOP();
        //calculate the pH value
//if the pH<=7 then use the pH sensitivity from pH4-pH7
        if(pHMeasurValueI <= pH7CalibValue){
                pHMeasurValueF = ((float)pHMeasurValueI)-
```

Appendix A Software Programming Code of ISFET Sensory System

```
                ((float)pH4CalibValue)-pHdriftVoltageSum;
pHMeasurValueF = pHMeasurValueF / ((float)(pH7CalibValue)-
                        (float)(pH4CalibValue));
pHMeasurValueF = pHMeasurValueF * 3.0f + 4.0f;
        }
        else {
//if the pH>7 then use the pH sensitivity from pH7-pH9
                pHMeasurValueF = ((float)pHMeasurValueI)-
                   ((float)pH7CalibValue)-pHdriftVoltageSum;
pHMeasurValueF = pHMeasurValueF / ((float)(pH9CalibValue)-
                          (float)(pH7CalibValue));
pHMeasurValueF = pHMeasurValueF * 2.0f + 7.0f;
        }
//compare the measured pH value with previous value
pHdiff = pHMeasurValueF*1000.0f-pHMeasurValueFOld*1000.0f;
        if(pHdiff != 0){
                pHMeasurValueFOld = pHMeasurValueF;
                DeltapH = pHMeasurValueF - 7.0f;
                if(DeltapH <= 0.0)
        Oneplusk = (1.0f - 0.0880224444f * DeltapH)* (1.0f
                        - 0.0880224444f * DeltapH);
                else
        Oneplusk = (1.0f - 0.105626933f * DeltapH)* (1.0f
                        - 0.105626933f * DeltapH);
                IBiasCurrentF = 192.0 * Oneplusk;
                        biasing current
                IBiasCurrent = (int)IBiasCurrentF;
        DACdata = (int)(IBiasCurrentF * 5.015923567f);
                DAC_SPI(DACdata-6);   //DAC output
```

```
                iteration_counter++;
                //display pH Final iter=xx
                pHfinal(iteration_counter);
        }
        //convergence
        else {
                //stop TimerA
                TACTL &= ~MC0;
                TAR = 0;
        pHMeasurValueI = (int)(pHMeasurValueF * 100.0f);
                if (pHMeasurValueI >= pHMeasurValueI_Old)
 pHMeasurValueI_D = pHMeasurValueI - pHMeasurValueI_Old;
                else
 pHMeasurValueI_D = pHMeasurValueI_Old - pHMeasurValueI;
                if(pHMeasurValueI_D == 0){
                        pHMeasurValueI_Old = 0;
                        if(pHMeasurValueI > 730){
                                Flag_Drift |= Alkaline;
                                Flag_Drift &= ~Acid;
                                Time_Minute_drift = 0;
                        }
                        else {
                                Flag_Drift &= ~Alkaline;
                                Flag_Drift |= Acid;
                                Time_Minute_drift = 0;
                        }
                        pHready();
                        menu4C(pHMeasurValueI, 2);
                        menu4A(IBiasCurrent, 4);
```

```
                                HY12864_CLR(6);
                                HY12864_CLR(7);
                                status &= ~menu4;
                                status |= menu5;
                                display_flag |= Driftrenwal;
                                break;
                        }
                        else {
                                pHMeasurValueI_Old = pHMeasurValueI;
                                menu4C(pHMeasurValueI, 2);
                                //display Ibias = xxx uA
                                menu4A(IBiasCurrent, 4);
                                HY12864_CLR(6);
                                HY12864_CLR(7);
                                display_flag &= ~menu4_ren;
                                        delay(50000);
                                delay(50000);
                                delay(50000);
                                delay(50000);
                                continue;
                        }
                }
        }
}
while (status & menu5){
        if(display_flag & Driftrenwal){
                display_flag &= ~Driftrenwal;
                menu_status &= ~PositiveDrift;
                menu_status &= ~NegativeDrift;
                Flag_Drift |= Drift_initiate;
```

```
                Time_Minute_drift = 0;
                TACTL &= ~MC0;
                TAR = 0;
                CCR0 = 0x2000;//set 2s timer
                Flag_Drift |= Drift_2s;
                TACTL |= MC0;
        }
        else if(Flag & ADC12cycleend){
                Flag &= ~ADC12cycleend;
                TACTL &= ~MC0;//halt the TimerA
                TAR = 0;        //Clear the TimerA
                /*Calculate and Display the time*/
                Time_Second += 2;
                Timer();
                /*in case of error, return to the initiate state*/
                if(ADC12resultAverage <= 100){
                        display_flag |= Driftrenwal;
                        continue;
                }
                if(display_flag & VoltageCurrent){
                        display_flag &= ~VoltageCurrent;
                        ADC12resultAverage_2 = (int)(4.407081807f *
                        (float)ADC12resultAverage);
                        menu4B(ADC12resultAverage_2, 4);
                }
                else {
                        display_flag |= VoltageCurrent;
                        menu4A(IBiasCurrent, 4);
                }
```

Appendix A Software Programming Code of ISFET Sensory System

```
                /*if it is the first time*/
                if(Flag_Drift & Drift_initiate) {
                        Flag_Drift &= ~Drift_initiate;
                        ADC12resultAverage_3 = ADC12resultAverage;
                        CCR0 = 0x5000;
                        TACTL |= MC0;
                        continue;
                }
                /* calculate the drift */
                if(ADC12resultAverage >= ADC12resultAverage_3){
                        menu_status &= ~NegativeDrift;
                        menu_status |= PositiveDrift;
        pHdriftI = ADC12resultAverage - ADC12resultAverage_3;
                }
                else { //if negative drift
                        menu_status |= NegativeDrift;
                        menu_status &= ~PositiveDrift;
            pHdriftI = ADC12resultAverage_3 - ADC12resultAverage;
                }
                ADC12resultAverage_3 = ADC12resultAverage;
                if(pHdriftI > 7){
                        Flag |= pHValueChange;
                        CCR0 = 0x5000;//set 5 seconds in timerA
                        TACTL |= MC0; //enable the timeA
                        continue;
                }
                else {   //accumulate the drift data
                        if(Flag_Drift & Alkaline){
                                if(Time_Minute_drift < 2){
```

Appendix A Software Programming Code of ISFET Sensory System

```
                    if(pHdriftVoltageSum >= 0.0f){
        pHdriftVoltageSumI =(int)(pHdriftVoltageSum * 4.407081807f);
                menu5A(pHdriftVoltageSumI,0);
                    }
                    else{
      pHdriftVoltageSumI = (int)(- pHdriftVoltageSum * 4.407081807f);
                menu5A(pHdriftVoltageSumI,1);
                    }
                    CCR0 = 0x5000;
                    TACTL |= MC0;
                    continue;
                }
                    else Flag_Drift &= ~Alkaline;
            }
            else if(Flag_Drift & Acid){
                    if(Time_Minute_drift < 0){
                    if(pHdriftVoltageSum >= 0.0f){
    pHdriftVoltageSumI = (int)(pHdriftVoltageSum * 4.407081807f);
            menu5A(pHdriftVoltageSumI,0);
                    }
                    else{
    pHdriftVoltageSumI = (int)(- pHdriftVoltageSum * 4.407081807f);
            menu5A(pHdriftVoltageSumI,1);
                    }
                    CCR0 = 0x5000;
                    TACTL |= MC0;
                    continue;
                }
                    else Flag_Drift &= ~Acid;
```

Appendix A Software Programming Code of ISFET Sensory System

```
                    }
                    if(menu_status & PositiveDrift){
                    pHdriftVoltageSum += (float)pHdriftI;
                    }
                    else if(menu_status & NegativeDrift){
                    pHdriftVoltageSum -= (float)pHdriftI;
                    }
                    if(pHdriftVoltageSum >= 0.0f){
pHdriftVoltageSumI = (int)(pHdriftVoltageSum * 4.407081807f);
                    menu5A(pHdriftVoltageSumI,0);
                pHdriftVoltageSumSave = (int)pHdriftVoltageSum;
                        M93C86_W(0x3FC,0xA5A5);
                    }
                    else {
 pHdriftVoltageSumI = (int)(-pHdriftVoltageSum * 4.407081807f);
                    menu5A(pHdriftVoltageSumI,1);
                pHdriftVoltageSumSave = (int)(-pHdriftVoltageSum);
                M93C86_W(0x3FC,0x5A5A);  //M93C86_W(Address, Data)
                    }
                    P2OUT |= M93C86_CS;
                    while(1){
                        if(P2IN & 0x40) break;
                    }
                    _NOP();
                    M93C86_W(0x3FD,pHdriftVoltageSumSave);
                    CCR0 = 0x5000;
                    TACTL |= MC0;
                    continue;
                }       //end of else
```

```
        }  //end of ADC12cycleend
        else if(Flag_Drift & Drift_10s){
                Flag_Drift &= ~Drift_10s;
                TACTL &= ~MC0;
                TAR = 0;
                /*Calculate and Display the time*/
                Time_Second += 5;
                Timer();
                if(Flag & pHValueChange){
                        Flag &= ~pHValueChange;
                        status &= ~menu5;
                        status |= menu4;
                        display_flag &= ~menu4_ren;
                        continue;
                }
                else {
                        CCR0 = 0x2000;
                        Flag_Drift |= Drift_2s;
                        TACTL |= MC0;
                        continue;
                }
        }
}
while (status & ADtest){
        if(display_flag & DACrenewal){
                DAC_SPI(ManualVoltage-6);
                display_flag &= ~DACrenewal;
                Time_display(0, Time_Second2);
                HY12864_CLR(2);
```

Appendix A Software Programming Code of ISFET Sensory System

```
                HY12864_CLR(3);
                HY12864_CLR(4);
                HY12864_CLR(5);
                HY12864_CLR(6);
                HY12864_CLR(7);
        }
        if(Flag & ADC12cycleend){
                Flag &= ~ADC12cycleend;
                Time_Second2 += 1;
                if(Time_Second2 == 60){
                        Time_Second2 = 0;
                        Time_Minute ++;
                }
                if(Time_Minute == 60){
                        Time_Minute = 0;
                        Time_Hour ++;
                }
                Time_display(0, Time_Second2);
                if(ADC12resultAverage <= 100){
                        display_flag |= DACrenewal;
                        continue;
                }
                ADC12resultAverage_2 = (int)(4.407081807f *
                       (float)ADC12resultAverage);
                if(display_flag & OutputVoltage)
                        menu4B(ADC12resultAverage_2, 2);
                else{
                        HY12864_CLR(2);
                        HY12864_CLR(3);
```

Appendix A Software Programming Code of ISFET Sensory System

```
                        }
            IBiasCurrent = (int)(((float)ManualVoltage) * 0.199365079f );
                        menu4A(IBiasCurrent, 6);
            pH4CalibValue = M93C86_Read(M93C86_Index_pH4+IBiasCurrent-100);
                        _NOP();
            pH7CalibValue = M93C86_Read(M93C86_Index_pH7+IBiasCurrent-100);
                        _NOP();
            pH9CalibValue = M93C86_Read(M93C86_Index_pH9+IBiasCurrent-100);
                        _NOP();
                    if(ADC12resultAverage<=pH7CalibValue){
                            if(ADC12resultAverage < pH4CalibValue)
                        pHMeasurValueF = 4.0f-((float)(pH4CalibValue-
        ADC12resultAverage)+pHdriftVoltageSum)/(float)(pH7CalibValue-
pH4CalibValue)*3.0f;
                            else
                       pHMeasurValueF = 4.0f+((float)(ADC12resultAverage-
        pH4CalibValue)-pHdriftVoltageSum)/(float)(pH7CalibValue-
pH4CalibValue)*3.0f;
                        }
                        else
                        pHMeasurValueF = 7.0f+((float)(ADC12resultAverage-
         pH7CalibValue)-pHdriftVoltageSum)/(float)(pH9CalibValue-
pH7CalibValue)*2.0f;
                        pHMeasurValueI = (int)(pHMeasurValueF * 100.0f);
                        menu4C(pHMeasurValueI, 4);
                }
            }
                    while (status & Drifttest){
                    if(display_flag & DrifttestRenew){
                        DAC_SPI(502-6);
```

Appendix A Software Programming Code of ISFET Sensory System

```
            display_flag &= ~DrifttestRenew;
            status &= ~Drifttest_2;
            Flag &= ~Drifttest_5sec;
            Time_display(0, Time_Second2);
            HY12864_CLR(2);
            HY12864_CLR(3);
            HY12864_CLR(4);
            HY12864_CLR(5);
            HY12864_CLR(6);
            HY12864_CLR(7);
            TACTL &= ~MC0;
            TAR = 0;
            CCR0 = 0x2000;
            TACTL |= MC0;
        }
        if(Flag & Drifttest_5sec){
            Flag &= ~Drifttest_5sec;
            status &= ~Drifttest_2;
            DAC_SPI(502-6);
            TACTL &= ~MC0;
            TAR = 0;
            CCR0 = 0x2000;
            TACTL |= MC0;
        }
        if(Flag & ADC12cycleend){
            TACTL &= ~MC0;
            CCR0 = 0xA000;
            TAR = 0;
            TACTL |= MC0;
```

Appendix A Software Programming Code of ISFET Sensory System

```
                        Flag &= ~ADC12cycleend;
                        DAC_SPI(0x05);
                        Time_Second2 += 2;
                        if(Time_Second2 == 60){
                                Time_Second2 = 0;
                                Time_Minute ++;
                        }
                        if(Time_Minute == 60){
                                Time_Minute = 0;
                                Time_Hour ++;
                        }
                        Time_display(0, Time_Second2);
                        if(ADC12resultAverage <= 100){
                                display_flag |= DrifttestRenew;
                                continue;
                        }
                        ADC12resultAverage_2 = (int)(4.407081807f *
                    (float)ADC12resultAverage);
                        menu4A(IBiasCurrent, 6);
                pH4CalibValue = M93C86_Read(M93C86_Index_pH4+IBiasCurrent-100);
                        _NOP();
                pH7CalibValue = M93C86_Read(M93C86_Index_pH7+IBiasCurrent-100);
                        _NOP();
                pH9CalibValue = M93C86_Read(M93C86_Index_pH9+IBiasCurrent-100);
                        _NOP();
                        if(ADC12resultAverage<=pH7CalibValue){
                                if(ADC12resultAverage < pH4CalibValue)
                        pHMeasurValueF = 4.0f-((float)(pH4CalibValue-
              ADC12resultAverage)+pHdriftVoltageSum)/(float)(pH7CalibValue-
pH4CalibValue)*3.0f;
```

Appendix A Software Programming Code of ISFET Sensory System

```
                                    else
                        pHMeasurValueF = 4.0f+((float)(ADC12resultAverage-
                    pH4CalibValue)-pHdriftVoltageSum)/(float)(pH7CalibValue-
pH4CalibValue)*3.0f;
                                    }
                                    else
                        pHMeasurValueF = 7.0f+((float)(ADC12resultAverage-
                    pH7CalibValue)-pHdriftVoltageSum)/(float)(pH9CalibValue-
pH7CalibValue)*2.0f;


                                    pHMeasurValueI = (int)(pHMeasurValueF * 100.0f);
                                    menu4C(pHMeasurValueI, 4);
                        }
                }
                while (status & pHSensitive){
                        if(display_flag & pHSensiRenew){
                                    display_flag &= ~pHSensiRenew;
                                    P2OUT &= ~M93C86_CS;
                        pH4CalibValue = M93C86_Read(M93C86_Addr+M93C86_Index_pH4);
                                    _NOP();
                                    _NOP();
                                    P2OUT &= ~M93C86_CS;
                        pH7CalibValue = M93C86_Read(M93C86_Addr+M93C86_Index_pH7);
                                    _NOP();
                                    _NOP();
                                    P2OUT &= ~M93C86_CS;
                        pH9CalibValue = M93C86_Read(M93C86_Addr+M93C86_Index_pH9);
                                    _NOP();
                                    _NOP();
                                    pHSensResult();
```

Appendix A Software Programming Code of ISFET Sensory System

```
                    }
                }


            }
}
```

Appendix B

Information of ISFET Sensor

D+T company sells ISFET devices (mounted on a PCB probe stick, wire bonded and encapsulated) that have been developed in our Chemical Transducers Group of IMB-CNM.

B. 1. The Structure of D+T Si_3N_4-gate ISFET Sensor

The ISFET is fabricated in standard NMOS based technologies on bulk and BESOI substrates in p-type 4-inch silicon wafers. It has the Si3N4/SiO2 based sensitive membranes and is biocompatible and organic membranes for elective detection. It is the automatic packaging and photo-curable encapsulate polymers.

The chip dimensions of the ISFET are 3x3 mm and have gate-length of 10μm and gate-width of 500μm. The typical ISFET die carrying one ISFET and a MOSFET (MOSFET may be wire-bonded on order) is presented on Fig. B.1. There can be variations of sensor layout that do not alter the output parameters of an ISFET.

Appendix B Information of ISFET Sensor

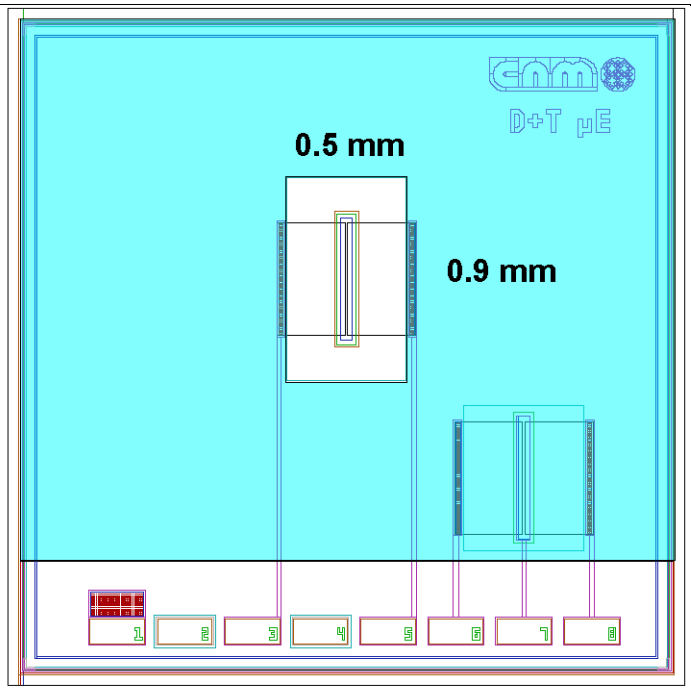

Fig. B.1. ISFET Chip (3mm x 3mm)

ISFET sensors are delivered mounted on a probe-stick with a 5-pin connector and encapsulated by a polymer to guarantee long life-time of a device, as presented in Fig. B.2. It is highly recommended to avoid touching by hand contact pins. The photo of the ISFET is shown in Fig. B.3.

Appendix B Information of ISFET Sensor

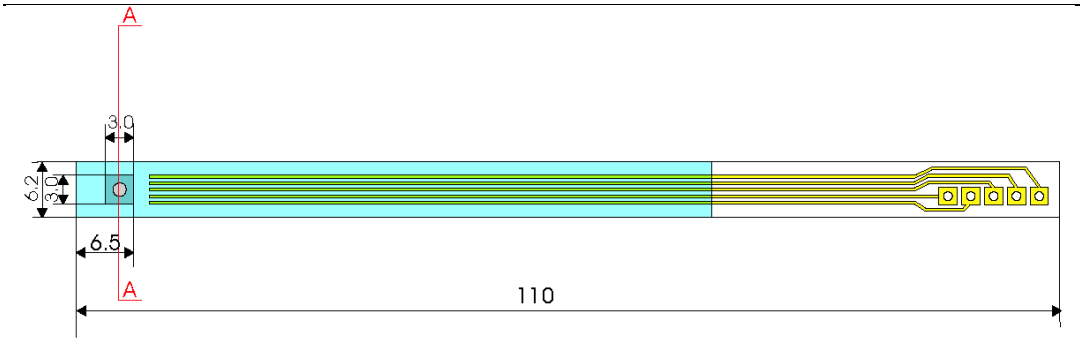

Fig. B.2. ISFET Mounted On A Long Probe Stick (All Dimensions Are in Millimeters)

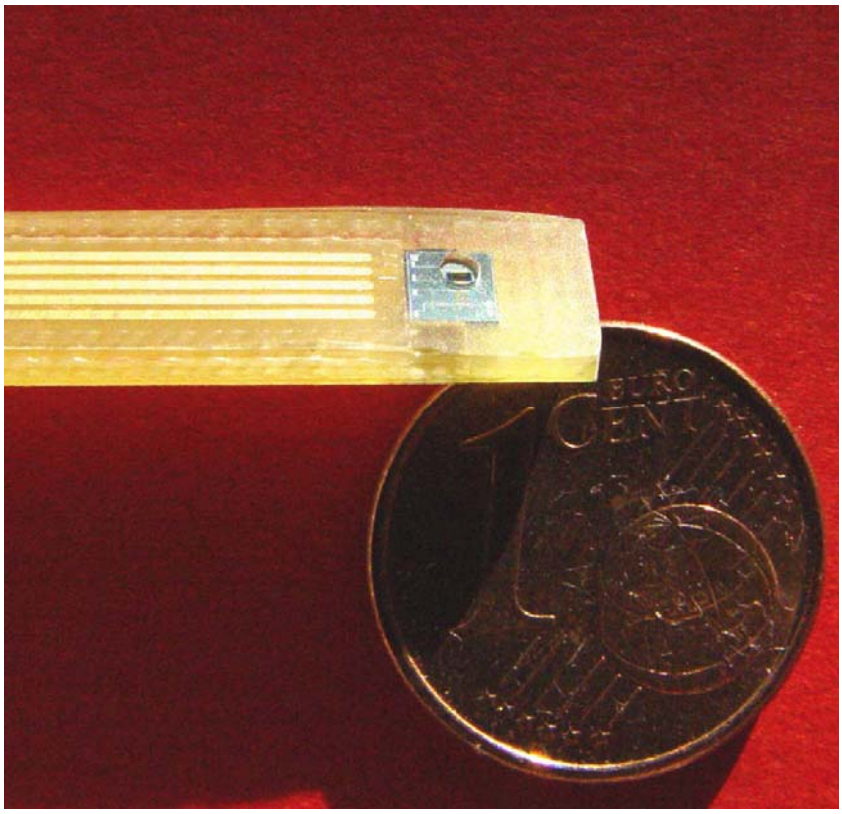

Fig. B.3. Encapsulated ISFET Sensor

Appendix B Information of ISFET Sensor

B. 2. Definition of Oxide Capacitance (C'_{OX}) of the Si_3N_4-gate ISFET Sensor

In MOSFET, the oxide capacitance per unit area is given by [89]:

$$C_{OX} = \frac{\varepsilon_{ox}}{t_{ox}} \tag{B.1}$$

where t_{ox} is the thickness of the insulator (SiO_2) and ε_{ox} is its permittivity, given by [89]

$$\varepsilon_{ox} = k_{ox}\varepsilon_0 \tag{B.2}$$

with ε_0 the permittivity of free space (8.854×10^{-14} F/cm) and k_{ox} the dielectric constant of the insulator; for SiO_2, $k_{ox} = 3.9$.

However, For an ISFET, it is with a dual dielectric composed of a lower layer of SiO_2 and an upper layer of Si_3N_4 [25]. So, the gate capacitance is the effective capacitance of SiO_2 in series with a sensitivity layer of silicon nitride (Si_3N_4). Herewith, the expression of two capacitances in series is given by:

$$C'_{OX} = \frac{\varepsilon_{ox} + \varepsilon_{Ni}}{\varepsilon_{Ni} \times t_{ox} + \varepsilon_{ox} \times t_{Ni}} \tag{B.3}$$

where t_{Ni} is the thickness of the sensitivity layer (Si_3N_4) and ε_{Ni} is its permittivity, given by:

$$\varepsilon_{Ni} = k_{Ni}\varepsilon_0 \tag{B.4}$$

with k_{Ni} the dielectric constant of the Si_3N_4, $k_{Ni} = 7.5$.

Appendix C

Information of Reference Electrode

The reference electrode utilized in this project is the commercially purchased Ag/AgCl reference electrode as shown in Fig. C.1. It is stable and quite robust.

Fig. C.1 Photo of Ag/AgCl Reference Electrode

As shown in the figure, the body of the electrode is made from glass tube. The porous glass serves as the ionic conducting electrical pathway between the inside of the reference electrode and the pH buffer solution. The filling solution in the reference electrode is saturated KCL or 3.5M KCL. KCL has the uncanny ability to “creep” and form a crusty layer of solid KCL where the solution is exposed to the air.

Appendix D

Information of the Process of the Readout Circuit

The ISFET readout circuit has been fabricated in TSMC CMOS 0.25μm process technology. This CMOS process has 5 metal layers and 1 poly layer. The process is for 2.5V applications. A thick oxide layer can be used for 3.3 volt transistors. TSMC CMOS 0.25μm process includes two processes: CL025 process and CR025 (CM025) process. In CL025 process, silicide block (RPO), thick gate oxide (3.3V), ESD 3.3V, and NT_N options are available on multi-project runs. CR025 (CM025) (mixed-mode) offers the above layers of CL025 plus deep n-well, Thick-Top-Metal (inductor) and MiM options. MiM (Cap-Top-Metal, also known as Metal 4 Prime, to Metal 4) provides a capacitance of 1fF/μm^2. This mixed signal/RF process, CR025 (CM025), offers three threshold voltages: nominal, medium and zero. Zero threshold voltage is also called depletion threshold voltage. Nominal is the default.